Microdamage: Its Role in the Mechanical Integrity of Low Bone Mass Diseases and its Treatment Implications

By

Mathieu Scott Davis

A dissertation submitted in partial fulfillment
of the requirements for the degree of
Doctor of Philosophy
(Mechanical Engineering)
in the University of Michigan
2 0 1 3

Doctoral Committee:

Assistant Professor Kenneth M. Kozloff, Co-Chair
Professor Albert J. Shih, Co-Chair
Assistant Professor Michelle S. Caird
Assistant Professor Jianping Fu
Professor David H. Kohn

"*Faith Is The Substance of Things Hoped For, The Evidence Of Things Not Seen" Hebrews 11:1*

"*We Walk In Faith, Not By Sight" 2nd Corinthians 5:7*

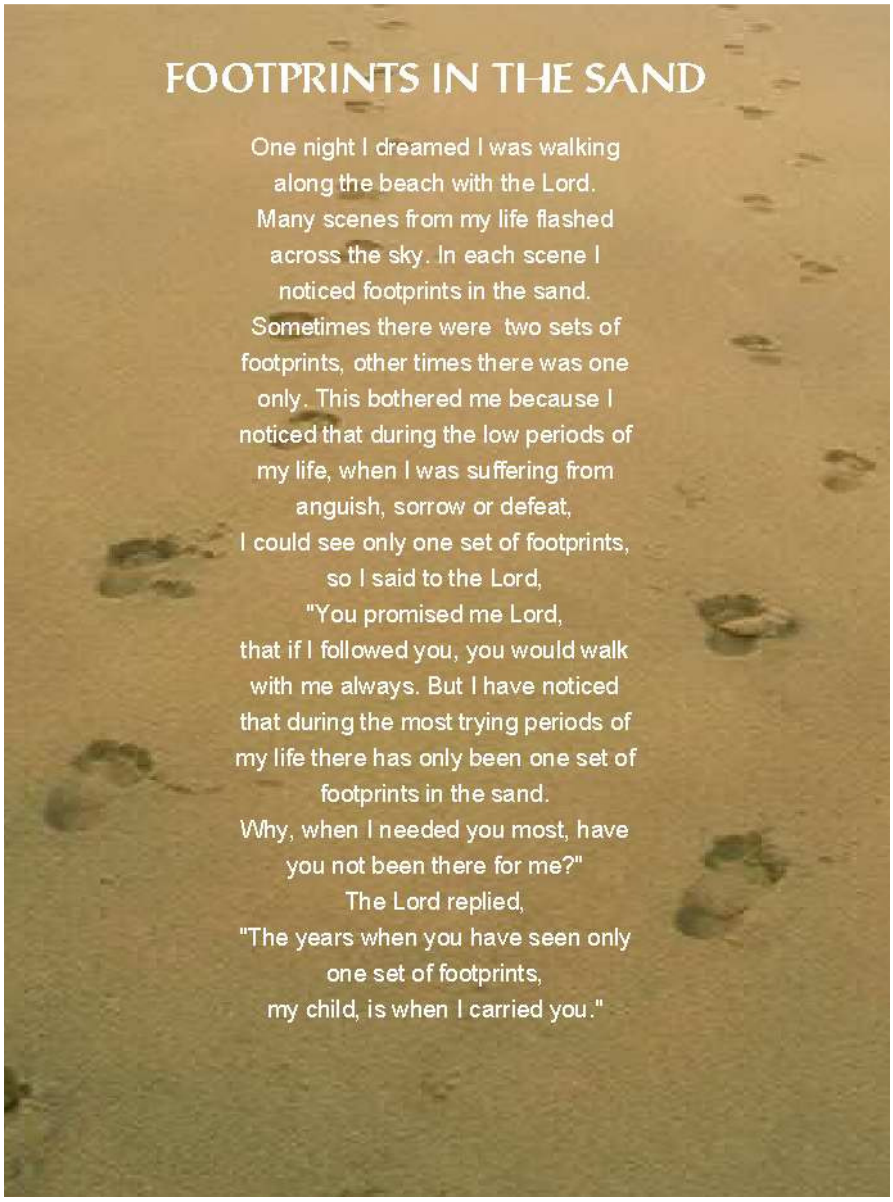


ISSN 8756-3282
Volume 50, Issue 3, March 2012
ELSEVIER
Bone
Official Journal
International Bone
& Mineral Society
IBMS
Available online at www.sciencedirect.com
SciVerse ScienceDirect

Dedication

This thesis is dedicated to my family members and friends who are not here with me physically; my aunt Sandra Morgan, my grandfather Edgar Davis and my grand-aunt Gloria Edwards. My friends Dulani Barrett and Andre Mitchell. I take you with me in everything that I do.

Acknowledgements

I would first like to acknowledge the work of my Lord and savior Jesus Christ for His continued mercies and blessings in my life. Over the past five years I have been faced with many challenges, but He has been my rock whilst I've been away from my close friends and family, and He continues to strengthen me in my daily pursuits.

Like any modern day structure, there are many people that must come together to build a mechanically stable structure. This dissertation is no different as there have been a myriad of people who have played significant roles in helping me to achieve this monumental task.

First off I would like to thank my funding sources over the past 5 years. The National Science Foundation Graduate Research Fellowship and National GEM Consortium have provided me with greatly appreciated external funding. In addition, the Rackham Graduate School, the Department of Mechanical Engineering, Dr. Albert Shih and Dr. Kenneth Kozloff have provided financial assistance for me to pursue my degree. None of this would be possible without your financial support.

Thank you to my research adviser Dr. Kenneth Kozloff for taking me into his research group. I am extremely grateful for his willingness to take on a mechanical engineer with a limited background in bone mechanics and groom him into a competent researcher and bio-mechanist. His patience in answering my questions and allowing me the freedom to explore and learn, have played an integral role in my development as a scientist.

I would like to send a special thank you to my adviser Dr. Albert Shih for believing in me from the start. He took me into his lab as a summer undergraduate student out of Florida and was extremely supportive of my work and my aspirations to attend graduate school. I can sincerely say that he is the primary reason for my enrolling in the University of Michigan, as it was his belief in my ability that persuaded me that I could succeed at this institution. He saw in me something that I did not necessarily see in myself, and his support was paramount in me procuring financial support to attend the University of Michigan.

Thank you to my co-authors, who provided a wealth of knowledge to my first publication. Bethany Kovacic assisted me with structuring the Ritchie fracture toughness protocol and helped me out significantly with the fracture toughness experimental design. Dr. Joan Marini has been a key collaborator and without her Brtl/+ mouse model, none of this research would have been possible. Her clinical

knowledge of osteogenesis imperfecta has proved vital in helping me keep our research in perspective of the people we aim to help.

I would also like to acknowledge my dissertation committee, not only for their willingness to sit on my committee, but for their constructive feedback and support during this process. Dr. Michelle Caird has been a steady presence in our research group and her clinical experience in the operating room has brought great perspective to our meetings. She has always taken the time out of her busy clinical schedule to be there for the students. Dr. Jianping Fu is the other mechanical engineer on the committee and having his pragmatic assessment of my research has brought refreshing and vital perspective to my work. Dr. Michael Morris was willing to provide his numerous resources to our disposal when we attempted to utilize Raman spectroscopy to determine if any compositional differences existed between Brtl/+ mice and WT mice. Having access to the foremost expert in this field was a truly invaluable experience. Dr. David Kohn has brought extremely valuable perspective to my microdamage studies, and has also provided thought provoking insight into analyzing my data.

I've been fortunate to work with talented collaborators out of the Morris Group over the course of my degree. Special thanks to Dr. Mekhala Raghavan and Dr. Katie Cilwa for their assistance in Raman spectroscopy experiments and data

analysis. Thank you both for your patience in answering my questions and I have truly learned a lot from my interactions with both of you.

The members of the Orthopedic Research Laboratories have truly made this experience an unforgettable and enjoyable one. Special thanks to John Foo for teaching me a myriad of histology tricks and for assisting me with the Zeiss confocal and the Zeiss microscope in the early stages of my research. A special thanks goes out to the Microscopy and Imaging Laboratory for helping me with many of my imaging and operational questions over the course of this thesis. Bruce, Sasha and Shelly; you guys are truly appreciated. I would like to give a very special thank you to the late and great Dennis Kayner who built the ulnar loader. He was the guru for strain gauging and troubleshooting the oft temperamental ulnar loader. I am very grateful to have known this amazing man, and I am thankful for the knowledge he passed on to me. A monumental thank you goes out to Charles Roehm a.k.a Big G for his patience with me and assistance with the ulnar loader, strain gauging, and simply saving my projects more times than I can remember. Our conversations in the machine shop were truly enjoyable. I can sincerely say that the lessons I've learned from the "old bull" are lessons I will probably pass on to my kids someday. Also thanks to John Baker for his help in histology and putting up with my basic fuchsin spills. I appreciate you also keeping the fridge stocked with my favorite yogurts and my favorite beverage in the world.

Bonnie Nolan is simply irreplaceable and deserves significant credit for the completion of this dissertation. Enumerating the ways both her and “Big G” have helped me would take up all the pages of this dissertation. Peggy Piech and Sharon Vaassen have been vital safety nets who always have the administrative answers for all my questions. Dr. Robert Goulet has been an amazing IT resource, as has Einor Jacobsen and Edward Sihler. Kathy Sweet has always been there if I needed her to assist me with injections or anesthesia. In addition, I’ve been fortunate to interact and work with some of the smartest students and staff one could ever hope to come across. These comrades include Dana Begun, Ethan Daley, John Foo, Eugene Manley, Kristin Graf, Jason Long, Adrienne Alimasa, Grant Goulet, Neil Halonen, Connie Pagedas, Erik Waldorff, Jeff Meganck, Danese Joiner, Lauren Smith, Erin Bigelow, David Barton, Jacque Cole, and Steve Schlecht. Please forgive me if I’ve forgotten anyone. I appreciate you all.

I have to give special recognition to both Ben Sinder and Joey Perosky. Ben has been there from the very beginning and has been a great asset and knowledge base for me. He’s also been very helpful in assisting me with any injections that I have not been able to perform. Also, as part of the Screaming Banshees he was the second (and arguably better) half of the famous Davis-Sinder connection which resulted in some truly SportsCenter Top 10 worthy indoor goals. I would also like to thank Joey Perosky for his support in mechanical testing and MicroCT scanning.

I will also thank Matthew Sims for helping out with mechanical testing and Basma Khoury for providing a major assist in MicroCT analysis. Your help truly expedited the process and allowed me to worry about one less thing in my experiments.

Last but not least, I would like to thank all my family and friends around the world for their love, support and prayers. To my mother, who continues to be an I-Beam of support in my life. I would need to write another thesis just to explain her influence in my life. To my dad, my sisters, grandma, Althia, Uncle Junior, Aunty Sandra, Aunty Judy and Uncle Paul who make up the core of my familial support. Thank you all for being there for me and for never being more than a phone call away. Thanks to all my friends who have made life outside of lab enjoyable. Jenahvive, Jason, Rebecca, Tomi O, Amanda, Angie and TJ; you've all formed a solid crew that I can depend on. Special thanks to Jenahvive for being so patient and supportive during the last few months leading up to this point. Thank you also to the Bethel AME church community for your continued support. Last, but certainly not least, a very special thank you to Rev. Yolanda Whiten for being my spiritual mentor here in Ann Arbor. Knowing that she is an arm's length away has provided me with so much security. Much love and many thanks to you all.

Table of Contents

Dedication ii

Acknowledgements iii

List of Figures xiii

List of Tables xv

Chapter 1. Introduction 1

1.1 Background 1

1.2 Thesis Overview 6

1.3 Societal Impact 10

Chapter 2. Increased Susceptibility to Microdamage in Brtl/+ Mouse Model for Osteogenesis Imperfecta 13

2.1 Introduction 13

2.2 Materials and Methods 16

2.2.1 Murine Models 16

2.2.2 In-Situ Strain Measurements 17

2.2.3 Cyclic Loading 19

2.2.4 Microdamage Quantification 22

2.2.5 Fracture Toughness 23

2.2.6 Statistics 28

2.3 Results 29

2.3.1 Brtl/+ ulnae demonstrate lower stiffness loss during loading ..29

2.3.2 Brtl/+ ulnae have more microdamage than WT 29

2.3.3 Brtl/+ femora display a moderate trend toward reduced fracture toughness compared to WT 30

2.3.4 Microdamage is differentially regulated by fracture toughness in loaded vs. unloaded ulnae.....32

2.4 Discussion 33

Chapter 3. The Effect of Bisphosphonate Therapy on Microdamage Accumulation in the Brtl/+ Mouse Model.....56

3.1 Introduction.....56

3.2 Materials and Methods.....59

3.2.1 Murine Model 59

3.2.2 Bisphosphonate Treatment.....60

3.2.3 In-Situ Strain Measurements.....61

3.2.4 Cyclic Loading in Untreated Animals 65

3.2.5 Cyclic Loading in Treated Animals.....68

3.2.6 Confocal Microscopy Parameters 69

3.2.7 Microdamage Quantification 70

3.2.8 Fracture Toughness 71

3.2.9 Statistics 76

3.3 Results.....77

3.3.1 WT and Brtl/+ treated specimens underwent premature fracture 77

3.3.2 Brtl/+ ulnae demonstrate lower stiffness loss during loading ..78

3.3.3 Unloaded and loaded Brtl/+ ulnae have more microdamage than WT counterparts....79

3.3.4 Cyclic loading resulted in increased levels of damage....79

3.3.5 5 weeks of Alendronate treatment did not impact microdamage content in unloaded limbs....80

3.3.6 Despite loading to a lower surface strain, treated limbs attained similar levels of microdamage....81

3.3.7 Brtl/+ femora display a reduced fracture toughness compared to WT....81

3.3.8 Bisphosphonate treatment results in a trend towards reduced fracture toughness in both Brtl/+ and WT....83

3.3.9 Fracture toughness correlations with microdamage....84

3.4 Discussion....85

Chapter 4. Visualization of Bisphosphonate Binding to Bone Microcracks, Surrounding Osteocyte Lacunae, and Osteocyte Apoptosis Spatial Distribution Using Near-Infrared Optical Imaging....106

4.1 Introduction....106

4.2 Materials and Methods....111

4.2.1 Murine Models....111

4.2.2 Bisphosphonate Treatment....111

4.2.3 Cyclic Loading....112

4.2.4 Fluorescent Bisphosphonate (FRFP) Administration....113

4.2.5 In-Vivo Apoptosis Marker (AV750) Administration....113

4.2.6 Verification of In-Vivo Apoptosis Marker....114

4.2.7 FRFP Imaging Protocol....116

4.2.8 FRFP Image Analysis and Staining Thresholds....118

4.2.9 FRFP Co-Localization Assessment 119

4.2.10 Annexin-Vivo Confocal Microscopy Parameters.....120

4.2.11 Apoptosis Image Analysis 121

4.2.12 Gray Value Threshold Affirmation and Distinguishing of Osteocyte Lacunae.....123

4.2.13 Apoptosis Quantification 124

4.2.14 Statistical Analysis.....125

4.3 Results.....126

4.3.1 Brtl/+ microcracks demonstrate higher affinity for FRFP.....126

4.3.2 WT osteocyte lacunae demonstrate high affinity for FRFP near damaged regions 127

4.3.3 WT and Brtl/+ display similar levels of FRFP o-localization in non-damaged regions.....127

4.3.4 WT and Brtl/+ display similar vascular and osteocyte lacunae densities.....128

4.3.5 Osteocyte apoptosis spatial distribution around peri-damaged regions 129

4.3.6 Apoptosis spatial distribution around non-damaged regions .130

4.4 Discussion.....131

Chapter 5. Conclusion 160

References.....182

List of Figures

Figure 2-1: Typical linear regression force-strain curve 44

Figure 2-2: Sinusoidal loading pattern 45

Figure 2-3: MicroCT image of starter notch 46

Figure 2-4: SEM image of notched surface.....47

Figure 2-5: Half-Crack angle determination 48

Figure 2-6: Schematic of fracture surface 49

Figure 2-7: Average stiffness loss for each phenotype 50

Figure 2-8: Microdamage levels in Brtl/+ and WT specimens 51

Figure 2-9: Confocal images of microdamage 52

Figure 2-10: Fracture toughness values for WT and Brtl/+ specimens.....53

Figure 2-11: Pooled fracture toughness correlations.....54

Figure 3-1: Typical fracture position seen in treated forearm failure 98

Figure 3-2: % stiffness loss in treated and untreated loaded specimens 99

Figure 3-3: Crack surface and numerical density comparisons 100

Figure 3-4: Fracture toughness comparisons.....101

Figure 3-5: Morphological images of fracture sites 102

Figure 3-6: Crack numerical density vs. fracture toughness correlations ...103

Figure 3-7: Crack surface density vs. fracture toughness correlations 104

Figure 4-1: Annexin-Vivo 750 apoptosis verification 150

Figure 4-2: Local co-localization of FRFP and basic fuchsin.....151

Figure 4-3: Excitation and emission spectra for basic fuchsin

and FRFP 152

Figure 4-4: % co-localized crack lengths in WT and Brtl/+ 153

Figure 4-5: % co-localized osteocytes in both WT and Brtl/+.....154

Figure 4-6: Blood vessel vs. osteocyte lacunae.....155

Figure 4-7: Microdamage and osteocyte apoptosis co-localization 156

Figure 4-8: Spatial distribution of osteocyte apoptosis 157

List of Tables

Table 2-1: Comparison of fracture toughness data 55

Table 3-1: Theoretical critical buckling loads.....105

Table 4-1: Data showing co-localization of FRFP stained cracks and osteocytes as well as combined effects.....158

Table 4-2: Osteocyte apoptosis data.....159

Chapter 1.

Introduction

1.1 Background

The 213 bones in the adult body together form a protective network that serves a myriad of functions including calcium homeostasis, blood production through our marrow in the medullary cavity, as well as important protective and structural responsibilities. Bone is similar to any other engineering material in that it is susceptible to damage accumulation through fatigue loading. However, as bone itself is a "living material," it can adapt, sense and repair itself based on cellular signals. Under normal circumstances in a healthy patient, damage is repaired through a process where osteoclasts, specialized cells that destroy bone, target areas of damage for removal, and are followed spatially and temporally by osteoblasts, the

bone forming cells which can refill excavated sites with new, healthy bone. In a condition where repair of this damage is inhibited, patients may accumulate large amounts of damage in their bones, which if allowed to proceed unchecked, can progress to catastrophic failure. Recent clinical reports have suggested that bisphosphonates, one of the most common drugs used to treat low bone mass diseases like osteoporosis have also been associated with a small but significant number of low trauma, atypical femoral fractures with features that suggest damage accumulation in bone [1-6].

Bisphosphonates are a class of anti-resorptive drugs which are used to target osteoclast destruction of bone in diseases where too much osteoclast activity leads to a reduced bone mass and increased risk of fragility fracture. Over the past 10 years, millions of osteoporotic women have taken these drugs for their condition [7]. Despite widespread clinical success, the impact of bisphosphonate use on repair vs. accumulation of damage in bone

tissue has not fully been determined [8]. Our ongoing research efforts seek to define the role of bisphosphonates on microdamage accumulation in the skeleton, and determine how bisphosphonate use may interfere with the natural tissue repair required to maintain a healthy skeleton capable of withstanding loads associated with activities of daily living.

While rooted in fundamental principles of fracture mechanics and materials testing, the results of our studies will have broad clinical impact for diseases like osteoporosis, where bone structure deteriorates with patient age, as well as genetic diseases like osteogenesis imperfecta (OI), where mutations in proteins associated with bone adversely impact bone mass and fragility. Osteoporosis results in a decrease in bone mass, which in turn leads to an increase in fracture risk. This disease affects over 10 million Americans, with an additional 34 million more estimated to have osteopenia or low bone mass on the verge of osteoporosis [9, 10] . Bone mineral density (BMD) naturally decreases with age, with the onset of osteoporosis

impacting those over 50 years of age. With the baby boomer generation continuing to have a strong impact on many of today's policy decisions, the attention paid to osteoporosis will continue to increase. In women over 45, osteoporosis is responsible for more hospital stays than diabetes, cancer, or heart attack, with an estimated $20 billion spent on direct health care services related to osteoporotic fractures [10]. As one can imagine, this will only continue to grow as people are living longer and remaining more active in their later lives.

While osteoporosis is widespread throughout our aging population, OI typically affects approximately 1 in 20,000 young children [11], and the severity ranges from lethality in the perinatal stage to a barely detectable form of connective tissue disorder [12]. In both diseases, a disproportionate increase in osteoclast and osteoblast activity results in an overall imbalance favoring osteoclast destruction of bone [13, 14]. Thus, patients with osteoporosis or osteogenesis imperfecta are often treated with

bisphosphonate drugs to prevent the high bone destruction responsible for increased skeletal fragility and high fracture rates. Using animal models representative of osteoporosis and osteogenesis imperfecta, our ongoing research seeks to determine 1) the impact of disease on the fracture toughness of bone material, 2) the effect of bisphosphonate therapy on the generation of bone microdamage and potential increase in bone brittleness following therapy and, 3) investigate the spatial distribution of bisphosphonates in proximity to microdamage as well as investigate the osteocytic response to extended bisphosphonate treatment. Findings from these studies will impact the potential management of diseases of low bone mass, and may lead to alternative prevention strategies to reduce fracture susceptibility without potential long term side effects of accumulated microdamage.

1.2 Thesis Overview

To accomplish these research goals, we have utilized a specific mouse model to replicate the material properties associated with low bone mass and collagen characteristics consistent with osteogenesis imperfecta. The Brittle IV (Brtl/+) mouse model for OI contains an identical mutation present in a type IV OI patient, and replicates the disease in the form of bone fragility, moderately deformed skeleton, and high tissue brittleness [15]. Furthermore, Brtl/+ replicates many of the cellular features characteristic of OI [16]. Wild-type animals are used as controls, to replicate bone with normal material properties unaffected by the collagen mutations present in OI, but likely susceptible to the effects of aging over time.

As summarized below, the thesis was broken down into three parts. In our first study (Chapter 2), using linear elastic fracture mechanics principles, we established that Brtl/+ has a moderately reduced fracture toughness compared to WT animals, consistent with findings of bone

brittleness using traditional four-point bending techniques. Then, using an in vivo model of forearm limb loading, we were able to determine that Brtl/+ was highly susceptible to the generation and accumulation of skeletal microcracks under normal ambulation and during high applied load. Our findings were featured on the cover of *Bone* [17] and were recognized by a Young Investigator award at the 2011 International Society of Biomechanics meeting.

Given these findings of increased microdamage in models of OI, along with associations between microdamage accumulation and bisphosphonate usage, our second study (Chapter 3) aimed to assess the impact on bone mechanical integrity and the resulting fracture toughness following extended bisphosphonate treatment during the growing phase of the mouse. The use of bisphosphonates could ultimately lead to the prevention of damage repair, thus leading to decreased mechanical integrity in bone, and may further implicate bisphosphonates in observances of

increased fractures in certain sub-populations of treated patients. We noted that bisphosphonates appear to impact the bone's durability as indicated by matching microdamage and stiffness loss levels despite loading to a lower surface strain. This adverse result at high strains was countered with the positive result of no additional damage in unloaded treated limbs. Additionally, we noted a moderate decrease in fracture toughness following treatment. These findings suggest that bisphosphonates may have adverse effects at higher strains and may not be as detrimental at lower strains.

Having established the impact of bisphosphonate therapy on the Brtl/+ mouse, we wanted to determine how bisphosphonates are spatially distributed within the bone tissue. This would help us to determine the cellular and local bisphosphonate delivery to microcracks and their surrounding cellular components following long term bisphosphonate treatment during the growing phase of the mouse. Chapter 4 has focused on using a fluorescence molecular imaging strategy to identify the precise

localization of bisphosphonate delivery in bone. Using fluorescent analogs to bisphosphonates given to mice immediately following a bout of fatigue loading, we were able to demonstrate that these anti-resorptive drugs localize directly to bone microcracks themselves, as well as some of the surrounding cellular structures. Additionally using a fluorescent apoptosis marker we monitored the local cellular response to microdamage to determine whether the cells responsible for signaling local bone repair are affected by local bisphosphonate delivery. Interference with this signaling could potentially inhibit the needed repair of microdamage at the cellular level, as well as interfering with repair at the site of microdamage itself. We observed a decrease in osteocyte apoptotic signals in regions around microdamage in extended bisphosphonate treated bones. These findings may suggest multiple levels of regulation of microdamage repair, and the portion of the findings relating to fluorescent bisphosphonate binding to microcracks

and osteocyte lacunae was recently presented at the 2013 Orthopaedic Research Society meeting.

1.3 Societal Impact

The efficacy of bisphosphonates in treating bone fragility [18-23] cannot be ignored. However, there is a prudent concern about the long-term effects of bisphosphonates on the inhibition of targeted repair of skeletal microdamage. Extended bisphosphonate treatment has been correlated with observations of increased skeletal microdamage in animal models [24-27], which may in turn have detrimental effects on the bone's mechanical integrity [24-26, 28]. To date, there has been no direct relationship to link extended bisphosphonate therapy with atypical, low-energy subtrochanteric femoral fractures observed in osteoporotic patients undergoing treatment [29, 30]. The results of this thesis suggest that the binding of bisphosphonates to microdamage and the surrounding osteocyte lacunae

may lead to arrested microdamage repair and could represent a contributing factor toward these femoral fractures.

Furthermore, these observations could also have strong implications for bisphosphonate treatment of fracture-prone osteogenesis imperfecta (OI) patients, since animal models suggest they have increased susceptibility to microdamage accumulation [17, 31]. With both OI and osteoporosis patients being increasingly susceptible to critical bone failure, treatment modalities need to be carefully assessed for their potential to affect damage repair.

This thesis demonstrates that bisphosphonates may interfere with targeted microdamage repair directly by binding to microcrack surfaces and interfering with osteoclast repair at the site that needs it most. Our results also suggest that bisphosphonates could interfere with targeted repair indirectly, because binding to surrounding osteocyte lacunae might interfere with the apoptotic signal required to induce targeted remodeling. Since

decreased fracture incidence is the critical rationale for treatment of patients with bisphosphonates, the implications of arrested microdamage repair for their quality of life are significant.

Additionally, the potential of adverse mechanical effects of bisphosphonates are important to consider, since they are still the most common treatment modality prescribed to low bone mass patients. The moderately reduced fracture toughness properties measured in this work suggests that dosage as well as treatment duration still remains an important consideration when administering treatment to these patients. While bisphosphonates may improve bone mass, any adverse impact to bone on a microscopic level may inadvertently lead to increased fractures. Further studies are needed to determine ideal bisphosphonate treatment protocols that can be safely administered throughout growth and development, yet still maintain the positive benefits that bisphosphonates bring to the table.

Chapter 2.

Increased Susceptibility to Microdamage in Brtl/+ Mouse Model for Osteogenesis Imperfecta

2.1 Introduction

Osteogenesis Imperfecta (OI) is a genetic disease that adversely impacts bone mass and fragility, and produces other connective tissue manifestations in bone. It typically affects young children [11], and the severity ranges from lethality in the perinatal stage to a barely detectable form of connective tissue disorder [12]. OI is identified in approximately 1 in 20,000 births and affects between 20,000 to 50,000 individuals in the United States [32]. Patients who suffer from OI typically have a mutation in either COL1A1 or COL1A2, which encode the α chains of type I collagen

[33]. Although most forms of OI are autosomal dominant, about 10% of cases have autosomal recessive inheritance of mutations in proteins responsible for post-translational modification of collagen, resulting in similar changes in the skeletal composition, structure and morphology to classical OI [34-36].

Studies have demonstrated a disproportionate up-regulation of osteoclast and osteoblast activity in OI patients, with an overall imbalance favoring osteoclast resorption [13, 14]. The mechanical and physiologic mechanisms responsible for this phenomenon are not fully understood. Increased bone turnover and fragility inherent to OI may be related to targeted repair of elevated levels of bone microdamage resulting from the brittle properties of OI. However, there has been limited investigation on the presence and impact of microdamage in OI patients. Animal models representing OI suggest that OI bone may be more susceptible to microdamage accumulation during cyclic loading [31, 37]. This study uses

the Brittle IV (Brtl/+) mouse model for OI to determine the impact of an OI-causing collagen mutation on the generation and accumulation of bone microdamage. Brtl/+ has a Gly349→Cys (G349C) substitution in one col1a1 allele, reproducing the genetic mutation found in a Type IV OI patient [38]. Brtl/+ demonstrates bone fragility, a moderately deformed skeleton, and a low ductility phenotype, accurately representing the biomechanical phenotype of the disease [15]. Furthermore, Brtl/+ features an up-regulation of osteoclast and osteoblast activity consistent with observations found in OI patients [16]. The direct cause of this upregulation has yet to be described.

The primary goal of this study is to determine whether the Brtl/+ mouse is more susceptible to microdamage accumulation compared to wild type (WT) controls and to determine the correlation between fracture toughness and propensity to accumulate microdamage. We propose that a propensity to accumulate damage is directly correlated with reductions in

fracture toughness found in Brtl/+. Understanding the role of this inherent bone matrix property will help elucidate the role of collagen mutations in governing susceptibility of OI bone to microdamage.

2.2 Materials and Methods

2.2.1 Murine Models

A total of 18 male Brtl/+ and wild type WT (n=9 each) mice were bred from our colony and used in this study. Brtl/+ mice have a mixed background of Sv129/CD-1/C57BL/6S and are bred by crossing heterozygous Brtl/+ with WT [38]. Mice were euthanized at 8 weeks of age in preparation for all loading experiments. All procedures used in this study were approved by the University Committee on Use and Care of Animals (UCUCA) at the University of Michigan.

2.2.2 *In-Situ Strain Measurements*

The ulnar loading model [39] was used throughout this study to produce compressive loads and induce microdamage. This loading model has been shown to produce loads primarily within the ulna and not the radius, and has been shown to induce microcrack formation within the ulna of rats [40]. The right forearms of mice were exposed to cyclic uniaxial compression loading across the olecranon and carpus process as described by others [40, 41]. Loading was done using a custom built servo-motor loader. Force-controlled, haversine, cyclic loading was performed at 1 Hz frequency while force and strain voltages were recorded using Labview 7.1 software (National Instruments, U.S.A.).

Six cadaver mice (n=3 Brtl/+ and n=3 WT) were used to record ulnar strains during loading in order to assess the level of force required to induce strains that would produce linear microdamage in compression (estimated at 4000 micro strain) [40, 42]. A 5 mm incision was made at the mid-diaphysis

of the left forearm and the bones were further prepared using prescribed techniques [43] and commercial reagents (Vishay Micro-Measurements, U.S.A.) for the placement of strain gauges. Briefly, 100% ethanol followed by acetone was applied to the exposed ulna surface using a cotton tip applicator. A catalyst (Catalyst-C) was then applied followed by a drop of adhesive (M-Bond 200). Single element strain gauges (EA-06-015DJ-120, Vishay Micro-Measurements, U.S.A.) were placed longitudinally as close to the lateral surface as possible of the ulna of both Brtl/+ and WT mice, near the mid-diaphysis. It has been confirmed experimentally [41], as well as through finite element modeling [44], that due to the geometry of the ulna, this area is the region of highest compressive strain and deformation during axial ulnar loading.

Cyclic loading was performed continuously, and several rounds of data were collected for each mouse and analyzed using linear regression in order to determine the load-strain relationship for both Brtl/+ and WT

genotypes **(Figure 2-1)**. From these regressions it was noted that the loads that induced approximately 4000 micro strain were 2.71 ± 0.35 N for the Brtl/+ and 4.92 ± 0.04 N for the WT mice.

2.2.3 Cyclic Loading

A total of 12 cadaver mice (n=6 Brtl/+ and n=6 WT) were used for cyclic loading. To induce microdamage, a similar loading construct and data recording protocol was used as described for in-situ strain gauging, with the exception that force and actuator displacement were recorded using Labview 7.1 software. Cyclic loading was performed in situ in order to accurately simulate future in-vivo experiments involving sedated animals. The contralateral forelimbs were not loaded and were used as controls to assess baseline levels of microdamage in the bone matrix. Each specimen was allowed a 5 minute (300 cycles) period of dynamic pre-conditioning in order to mitigate the effects of soft tissue compliance and thus isolate and account for the effects of the actuator displacement to that of solely bone matrix

degradation [44]. This time also afforded the opportunity to gradually ramp up the force amplitudes for each forearm to produce the required range of strains, as necessitated by the intrinsic differences in bone size between animals. Bones were then cyclically loaded for 30 minutes (1800 cycles) at force-controlled loads that produced approximately 4000 microstrain (με) based on data collected in the in situ strain gauge experiments **(Figure 2-2)**. Minimal compressive loads on the reversal phase of loading of approximately 2.45 N and 1.34 N for WT and Brtl/+ mice, respectively, were used to ensure that platens remained in contact with the bone during the unloading segment. Post hoc calculations showed that WT mice displayed compressive strains ranging between a minimum of approximately 418.4 με during the unloading segment and approximately 4010.8 με (approximately 5N) at maximum loading, whereas Brtl/+ exhibited strains of 541.7 and 4039.1 με (approximately 3N) during unloading and loading segments, respectively. The displacement of the ulna during cyclic loading

was recorded for each bone using a linear variable differential transformer (LVDT). Loss of stiffness for each bone was determined using Eq. (1), which was previously used by Bentolila et al. [40] as a surrogate for effective stiffness loss.

Equation 2-1

$$\text{Stiffness Loss} = \frac{L_o - L}{L_o}$$

where L_o is the initial length of bone and L is the final length of the bone. The initial length was always measured at the end of the dynamic pre-conditioning period (300 cycles) while L was measured when loading was complete. Both L_o and L were measured using the calibrated external LVDT during loading, while the forearm was still within the platens.

2.2.4 Microdamage Quantification

After loading, the loaded (right) and unloaded (left) forelimbs were excised and stained with 1% basic fuchsin using an established protocol [45] and rinsed in 100% ethanol. Samples were subsequently embedded undecalcified in poly methyl methacrylate (PMMA) for histology. Using a Buehler Isomet diamond-blade saw, 400 µm sections were then cut transverse to the longitudinal axis of the ulna. These sections were mounted on a plastic microscope slide and polished to a final thickness of 100 µm. Sections were cover slipped and examined with a confocal microscope (Zeiss LSM 510-META Laser Scanning Confocal Microscope, Carl Zeiss MicroImaging, Inc., Thornwood, NY, U.S.A.) at 63x magnification using a Helium Neon 1 (HeNe1) laser (543 nm) with a Texas red/rhodamine filter. Slides from the mid-diaphyses of each ulna were analyzed to quantify microdamage. Images were taken for the entire 100 µm thick cortical region and subsequently analyzed using the Zeiss LSM Image Browser (Version

4.2.0.121, Carl Zeiss Micro Imaging, Inc.) to quantify linear microdamage within the cortical region. Cracks that were positively labeled with basic fuchsin dye were deemed as damage-induced during loading. Diffuse damage was not assessed in this study. The following parameters were measured throughout the entire cortical bone region of each section: number of microcracks (#), bone cortical volume (B.Vol., mm^3), microcrack numerical density (Cr.Dn., $\#/mm^3$) and microcrack surface density (Cr.S.Dn., mm/mm^3).

2.2.5 Fracture Toughness

To correlate microdamage with fracture toughness, femurs from each mouse were prepared and tested according to techniques established by Ritchie [46]. This technique utilizes linear elastic fracture mechanics (LEFM) principles and a self-induced starter notch to measure the bone's resistance to fracture (fracture toughness). For regular mechanical testing of engineering materials, ASTM standards require that a sharp starter notch be

the initiation point of fracture [47]. This starter notch is typically induced by a fatigue loading technique; however, due to the small geometry of mouse bones, this procedure is not optimum. Studies have shown that accurate fracture toughness data can be attained from razor sharpened micronotches [48] and this technique has been deployed for small animal studies [46] **(Figure 2-3)**. Using this technique will provide us with a true mechanical measure of the bone's inherent fracture toughness, without the viscoelastic influence of soft tissue.

The left femora of Brtl/+ (n=6) and WT (n=6) were harvested, cleaned of soft tissue, and stored frozen at -20°C in gauze soaked in Lactated Ringer's Solution (LRS) until testing. Bones were machine-notched through the posterior cortex at the mid-shaft using a micro milling device with a cutting radius of 0.01 inches. Notches were then sharpened using a custom rigged mounted razor blade, pasted with 1 μm diamond polish (Struers). Bone diameters were measured with electronic calipers and notch depths

were made using a micro mill to approximately 1/3 of the bone diameter. This notching procedure typically produces a reproducible sharpened notch root radius of approximately 10 μm [46, 48] .

In preparation for three-point mechanical bend testing, the femoral heads were removed, while the condyles were left intact. This was done to maintain stability within the three-point bending apparatus. Femurs were thawed in LRS soaked gauze at room temperature to preserve moisture content until they were ready for testing. Specimens were loaded to failure in three-point bending at 0.001 mm/s using a servohydraulic testing machine equipped with a 220N load cell (858 MiniBionixII Material Test System; MTS Systems Corporation, Eden Prairie, MN, USA) in accordance to ASTM standards [47, 49] and other established protocol [46]. During three-point bending, the specimens were placed such that the posterior surface was in tension and the anterior surface was in compression with the top loading point oriented directly above the notch on the anterior surface. A span

length of 4.5 mm was used in testing. Load and displacement values were recorded throughout the experiment using integrated Material Test System data acquisition software (858 MiniBionixII Material Test System; MTS Systems Corporation, Eden Prairie, MN, USA).

After mechanical testing, fractured bone specimens were fixed in 70% ethanol, defatted in toluene under vacuum for 24 hours, and cleared of soft tissue with 2% potassium hydroxide for 12 hours. The specimens were dehydrated by immersion in a graded series of alcohols (50%, 70%, 95% and 100%) and coated with carbon [37]. Specimens were imaged by SEM to determine the transition from stable to unstable crack growth (**Figure 2-4**). Fracture toughness, K_c, was measured using solutions for circumferential through-wall cracks established for cylindrical pipes [46, 50, 51]. Both the maximum load and the crack instability techniques were used to determine fracture toughness values [46]. All measurements used in the LEFM calculations, such as specimen width and thickness, were taken from

SEM images of fracture sites using the public domain software ImageJ (National Institutes of Health).

All measurements of thickness and radii were measured on the fracture surface of each specimen i.e. the non-notched surface as previously instructed by Ritchie [46]. Cortical thickness was taken as an average measurement of 6 different thicknesses measured at different points along the fracture surface. The centroid for each specimen was determined by drawing a line parallel to the notch that was half the bone's diameter. This line represented the major axis. Another axis that was rotated 90 degrees to the first was also placed at half the bone diameter. This line represented the minor axis. The intersection of these perpendicular lines represented the centroid of the bone **(Figure 2-6)**. In determining the stable to unstable transition region, the SEM was used in backscatter mode. The difference in morphology was used to determine the transition. The stable region is typically described as having a darker appearance with linear groves,

whereas the unstable region has a more spongy appearance. Half-crack angles (2θ) were determined by measuring the included angle (maximum load technique) which is formed from the centroid to the notched surface, and with the excluded angle (instability technique) which is formed from the centroid to the stable to unstable transition region **(Figure 2-6)**.

2.2.6 Statistics

Effect of genotype on percent stiffness loss, crack numerical density, crack surface density, and fracture toughness values calculated using either the maximum load or instability technique were compared using a non-parametric Mann-Whitney test (GraphPad Prism 4.0) to account for small samples sizes. Linear regression between microdamage data and fracture toughness data was performed across genotypes and loading conditions. In all tests, significance was attributed to $p<0.05$. All data is presented as mean ± SD.

2.3 Results

2.3.1 Brtl/+ ulnae demonstrate lower stiffness loss during loading

Whole bone loss of stiffness for each forearm was measured via LVDT during cyclic loading according to Equation (1). While Brtl/+ and WT ulnae were loaded with matching surface strains, Brtl/+ demonstrated a lower percentage stiffness loss (1.77 ± 0.84%) compared to WT (3.56 ± 1.29%) over the 35 minute load period **(Figure 2-7)**.

2.3.2 Brtl/+ ulnae have more microdamage than WT

Non-loaded control limbs from Brtl/+ demonstrate significantly increased linear microcrack numerical density (217%) and microcrack surface density (354%) compared to their WT counterparts **(Figure 2-8A,B)**. In loaded limbs, Brtl/+ demonstrates a 220% increase in crack numerical density and 331% increases in crack surface density over WT **(Figure 2-**

8A,B). Linear microdamage was observed on the tensile and compressive (medial and lateral) sides of the ulnar cortices. While some cracks were oriented circumferentially, others ran through the cortex and spanned multiple lacuno-canalicular structures **(Figure 2-9)**.

2.3.3 Brtl/+ femora display a moderate trend toward reduced fracture toughness compared to WT

Femora paired with loaded ulnae from within the same animal were tested for fracture toughness. During sample preparation and testing, 2 Brtl/+ and 2 WT specimens were lost due to errors in the notching process or due to premature fracture during three-point bending. Using the maximum load technique, which assesses fracture toughness based on the initial notch geometry and the maximum load encountered during three-point bending, WT femora displayed average K_c values of 3.36 Mpa$\sqrt{m}$ whereas Brtl/+ specimens had K_c values of 2.73 Mpa$\sqrt{m}$ ($p=0.486$) **(Figure 2-10A)**. The instability technique relies on identification of the transition between

unstable and stable crack growth, and showed a more sensitive 35.4% difference in K_c values between genotypes (WT 3.79 Mpa√m; Brtl/+ 2.44 Mpa√m) (p=0.057) **(Figure 2-10B)**. During crack instability calculations, four cases (3 WT and 1 Brtl/+) demonstrated half-crack angles that exceeded the range of values deemed valid ($\Theta/\pi = 0.611$) for thick wall cylindrical pipe circumferential analysis ($\Theta/\pi = 0.663, 0.645, 0.707, 0.756$) [46]. These represent specimens that are more ductile than the equation allows for accurate calculation. In those cases, by setting Θ/π to 0.611 for these specimens, an additional lower bound estimation of instability fracture toughness was estimated, resulting in a 31.4% difference in fracture toughness between Brtl/+ (2.44 Mpa√m) and WT (3.56 MPa√m) **(Table 2-1)**.

2.3.4 *Microdamage is differentially regulated by fracture toughness in loaded vs. unloaded ulnae*

The inability of maximum load fracture toughness values to be predictive of genotype precluded it from regression analysis. Fracture toughness measured by the instability technique was only predictive of crack numerical density and crack surface density when genotypes were pooled into separate regression models for loaded and unloaded ulnae (**Figure 2-11**). Brtl/+ and WT ulnae showed a negative correlation between instability fracture toughness and crack surface density ($R=-0.85$, $p=0.01$) and instability fracture toughness and crack numerical density ($R=-0.72$, $p=0.04$). Brtl/+ and WT unloaded ulnar instability fracture toughness also showed a strong negative correlation with crack surface density ($R=-0.72$, $p=0.04$) and with crack numerical density ($R=-0.87$, $p=0.01$). While there was no significant difference between the regression slopes of unloaded and loaded crack numerical density ($p=0.4$, **Figure 2-11A**), the relationship

between instability fracture toughness and crack surface density varied depending on whether ulnae were loaded or unloaded (p=0.02, **Figure 2-11B**).

2.4 Discussion

Currently, little is known about OI regarding the susceptibility of bones to produce and accumulate microdamage compared to bone with normal collagen. High propensity to form and accumulate microdamage may play a role in the inherent fragility and remodeling behavior seen in OI patients. This study utilized the Brtl/+ mouse to investigate the correlation between propensity to form microdamage and the inherent fracture toughness of bone formed with an OI-causing mutation.

Brtl/+ ulnae subject to normal cage activity demonstrated a larger amount of cortical microdamage than WT controls. Furthermore, following 35 minutes of axial compressive loading matched for bone surface strains between genotypes, Brtl/+ ulnae were more prone to damage than WT

despite a greater resistance to whole-bone deformation. Femoral fracture toughness tests show a trend toward differences in K_c values between Brtl/+ and WT, although these differences were not statistically significant. These fracture toughness values correlate well with levels of microdamage quantified in intact and mechanically-loaded limbs.

The moderate reductions in fracture toughness found in Brtl/+ are consistent with reductions found in other mouse models of matrix insufficiency. Osteopontin deficient mice have reduced work to fracture (59%) and post-yield deformation (39.6%) compared to WT controls [52], and 8 week OPN -/- mice show a corresponding 30% decrease in instability fracture toughness compared to WT [53]. Brtl/+ has shown similar reductions in work to failure (59%) and post-yield displacement (42%) [15] and a 35% decrease in fracture toughness in the present study.

The amount of energy that a material can withstand before the onset of a critical microcrack is an important parameter to consider in fracture

mechanics [54] [55]. In the present study, instability fracture toughness from Brtl/+ showed a strong trend, but not statistically significant reduction compared to WT. This suggests that the lower work to failure and post-yield energy associated with Brtl/+ may represent both an inability to prevent onset of critical microcracking, as well as a reduced resistance to crack growth toughness which was not directly measured in this study. Crack growth appeared to be differentially regulated by instability fracture toughness between loaded and unloaded limbs in this study, whereas crack number had a similar relationship to instability fracture toughness whether limbs were loaded or not. Other OI models have implicated collagen integrity as a potential cause for OI bone's inability to withstand damage accumulation. Oim mice have demonstrated low work to failure and require fewer cycles to generate equivalent amounts of microdamage compared to WT counterparts [31]. The Mov 13 mouse displays a purely quantitative COL1A1 mutation with a 50% decrease in type 1 collagen content [56], and

demonstrates a 61% decrease in post-yield displacement [37]. Furthermore, the cortical tissue components integral in the prevention of damage accumulation are severely compromised in Mov 13, leading to increased rate of damage accumulation and a decrease in the number of cycles to failure when compared to WT [57]. It is evident that mutations involving type 1 collagen production have significant impact on the microdamage accumulation, fatigue strength and overall mechanical properties of bone.

Our in-situ strain gauge data shows that the Brtl/+ ulnae required 45% less load to induce the prescribed 4000 με. This is likely due to the geometric differences in bone sizes reported in other load bearing bones such as the femur [13]. X-ray images of ulnae demonstrated a small decrease in Brtl/+ lengths compared to WT (1.8%) but a 25% decrease in diameter (data not shown). However, during loading, Brtl/+ ulna showed a greater resistance to whole-bone deformation, likely due to previously observed increases in tissue mineral density associated with the collagen mutation,

[58] thus leading to a less compliant bone compared to its wildtype counterpart. This increase in tissue mineral density is in line with the more brittle phenotype, that has been previously displayed in Brtl/+ [15] and in humans [11, 59, 60]. Our observance of higher linear microcracks in Brtl/+ is supported by numerical probabilistic models, that show that higher mineralization in bone will facilitate the formation of linear microcracks [61]. This is further supported by experimental studies on dogs treated with bisphosphonates, which demonstrate bones had increased tissue mineralization with treatment but became more prone to a concomitant increase in microcracks and reduced energy absorption [62]. Despite Brtl/+ specimens displaying a lower loss of stiffness, we still observe higher levels of microdamage. Previous studies have shown that there appears to be a difference in the surrounding bone matrix mineral composition between microdamaged areas and undamaged areas [63, 64]. These studies provide evidence that there may be differences in the way energy from a microcrack

is released to the surrounding bone matrix of Brtl/+ and WT specimens, thus potentially explaining our high microdamage but low stiffness loss observations in Brtl/+ specimens.

A significant amount of linear damage was observed at the tensile and compressive (medial and lateral) sides of the samples cortices and were oriented circumferentially. Previous studies of rat bone cyclically induced crack numerical densities ranging from 0.2 to 4.0 /mm^2 and crack surface densities of approximately 0.2 mm/mm^2 [40, 65]. In the present study, crack numerical densities ranged from 20 to 300/mm^3, while surface densities were between 1 and 34 mm/mm^3. The volumetric approach used in the present study accounts for these differences, as crack size and length were quantified through a 100 μm volume thickness, rather than a single section from the mid-span of the specimen. This volumetric approach minimizes the influence of surface polishing artifacts on the overall results, and quantifies damage through a larger segment of the tissue. As a means of

verifying this approach, crack surface densities of several samples were analyzed on single optical slices. Results demonstrate that values from a single slice approach are within range of those observed by previous studies (data not shown).

Differences in fracture toughness were observed in our study, and were more noticeable using the instability technique. These differences reflect changes in half-crack angles between Brtl/+ and WT, where, on average, Brtl/+ specimens had smaller half-crack angles closer to the original starter notch, while WT specimens, with a more ductile fracture, had stable crack propagation further away from the starter notch. During these calculations, there were 4 cases (3 WT and 1 Brtl/+) where the half crack angles exceeded the range of angles deemed valid for accurate assessment of fracture toughness [46], indicating specimens that were more ductile than the equations can accurately calculate. To assess any potential error associated with these specimens, calculations were repeated using the maximum

permissible half crack angle of 1.9195 radians as an upper limit estimate. As such, the determined value of K_c for these re-calculated toughness values effectively represents a lower bound estimation of instability fracture toughness for ductile specimens. In this case, a 31.4% difference between Brtl/+ and WT K_c values remained (Brtl/+ 2.44 Mpa√m and WT 3.56 Mpa√m) despite these estimated parameters. Furthermore, similar correlations between microdamage and instability fracture toughness were observed regardless of whether the original or re-calculated data was used, suggesting a minimal effect of these outliers on our conclusions. The lack of significance in our fracture toughness data may also suggest that a lower resistance to crack growth toughness, and not crack initiation as measured, may be the more prevalent underlying difference between Brtl/+ and WT fracture toughness.

This study aimed to investigate the susceptibility of OI bone to microdamage accumulation and to explicate any role that microdamage may

play in the inherent fragility and remodeling behavior seen in these patients. Although both osteoblast and osteoclast activity is increased in these patients, there is an imbalance in bone remodeling in favor of osteoclast activity [11], which ultimately leads to a compromised bone structure. It is unknown however as to what is the cause for this up-regulation in remodeling behavior seen in OI patients.

As microdamage levels increase in a healthy individual, the inherent remodeling processes of bone are activated for microdamage repair [66]. The increased remodeling activity seen in OI patients may be related to the extent of microdamage present in their bones, resulting from the compromised collagen inherent to the disease. Brtl/+ mice demonstrate an increase in osteoclast number and function compared to WT [16], and the current findings demonstrate a correlative increase in propensity to generate and accumulate microdamage in the bone. While the cellular asynchrony favoring osteoclast formation and activity in Brtl/+ is a result of an increase

in osteoclast precursors in Brtl/+ marrow [16], the RANKL/OPG ratio is unchanged and the factors regulating increased osteoclasts have yet to be described. Further *in vivo* loading experiments will determine whether generation and accumulation of skeletal microdamage in Brtl/+ is responsible for these increased remodeling rates.

A widespread treatment for the high turnover and low bone mass condition of OI is bisphosphonate therapy. Bisphosphonates function by reducing bone turnover and increasing skeletal mass, but do not target the underlying genetic abnormalities associated with the disease [58]. While the intention for OI treatment with bisphosphonates is to increase skeletal mass, they may concomitantly prevent targeted repair from occurring. It has been shown that downregulation of bone remodeling with bisphosphonate therapy results in an increased accumulation of skeletal microdamage in other models [24-27], subsequently resulting in a reduction of skeletal mechanical integrity [24-26, 28]. The long-term implications for bisphosphonate

therapy in a low-fracture toughness skeleton prone to the generation of microdamage have not yet been described.

In conclusion, our studies have shown that the Brtl/+ mouse model for OI is more susceptible to microdamage accumulation than age-matched WT. These data suggest the possibility that OI patients may engender larger degrees of damage due to the inherent collagen mutation. With the increase in damage comes an additional risk of lowered resistance to bone fracture. Increased microdamage and reduced fracture toughness observed in the Brtl/+ model for osteogenesis imperfecta suggests that microdamage may play a significant role in contributing to bone fragility and increased remodeling associated with OI. These findings have strong clinical implications for explaining increased fragility and remodeling activity in OI patients.

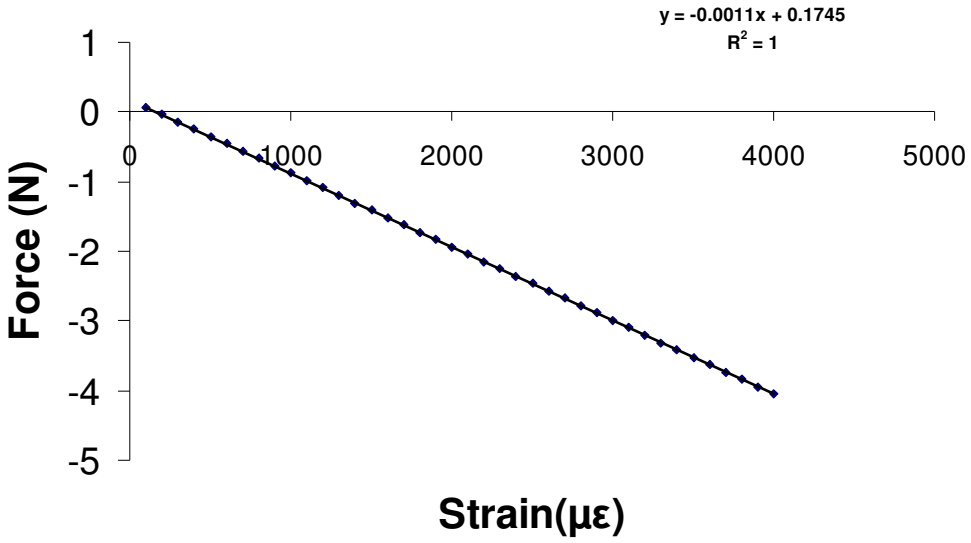

Figure 2-1: Typical linear regression force-strain curve

Graph showing the loading portion of the force-surface strain relationship for a WT specimen being monotonically tested in compression**.**

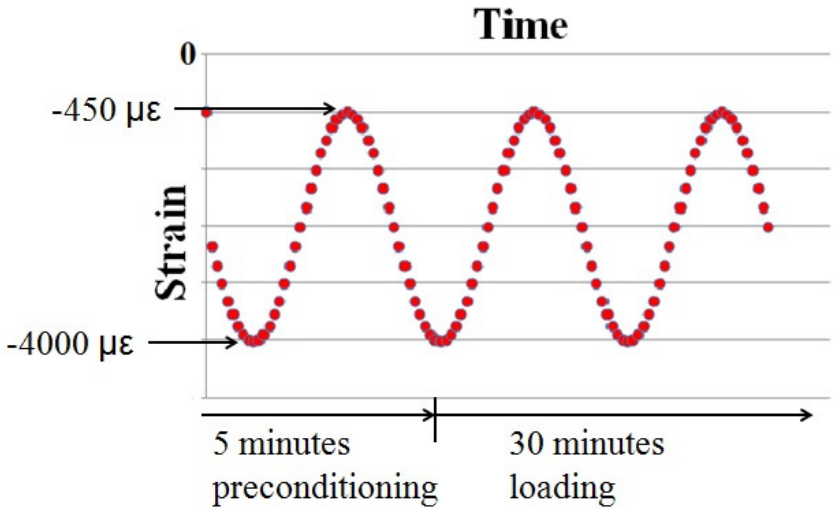

Figure 2-2: Sinusoidal loading pattern

Figure representing the sinusoidal cyclic loading pattern that bones were exhibited to. Strains oscillated between minimum compressive strains of approximately 450 microstrain and 4000 microstrain for 35 minutes of loading, including a 5 minute preconditioning period.

Figure 2-3: MicroCT image of starter notch

MicroCT image showing the starter notch at mid-diaphysis necessary for fracture toughness calculations.

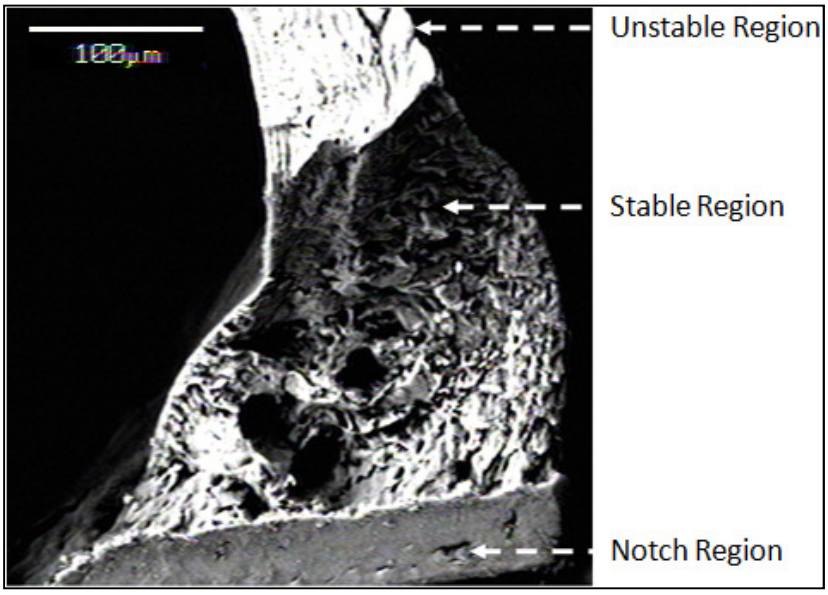

Figure 2-4: SEM image of notched surface

SEM image showing the notch, stable crack growth and unstable crack growth region used to determine the half-crack angles for assessing the instability fracture toughness.

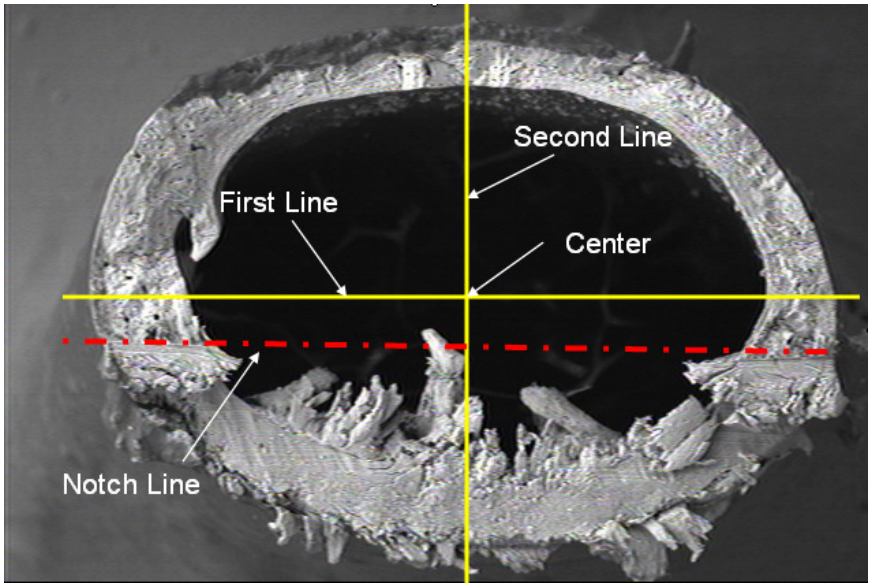

Figure 2-5: Half-Crack angle determination

SEM image showing the method used to determine the centre of images. The first line was drawn parallel to the notch at about half the thickness of the bone. The second line was drawn 90 degrees at about half the thickness in the other direction.

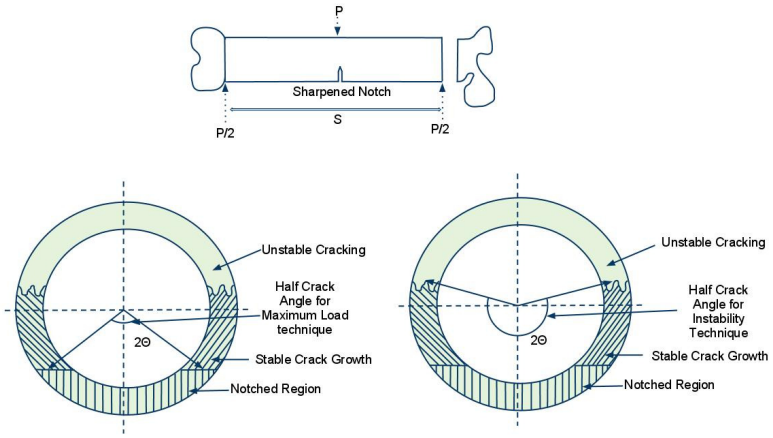

Figure 2-6: Schematic of fracture surface

The top schematic displays the setup of the femur for 3-point bend testing where S represents the span of the bottom anchors (4.5 mm) and P represents the applied load. Notice that the femoral head has been cut off and the sharpened notch is placed at the mid-diaphysis. The bottom schematic represents a cross-section of the femoral cortex, which displays the measurement of the half-crack angle for determining the fracture toughness K_c using the maximum and instability methods. The displayed included and excluded angles represent 2x the half crack angle. Figure adapted from Ritchie et al [46]

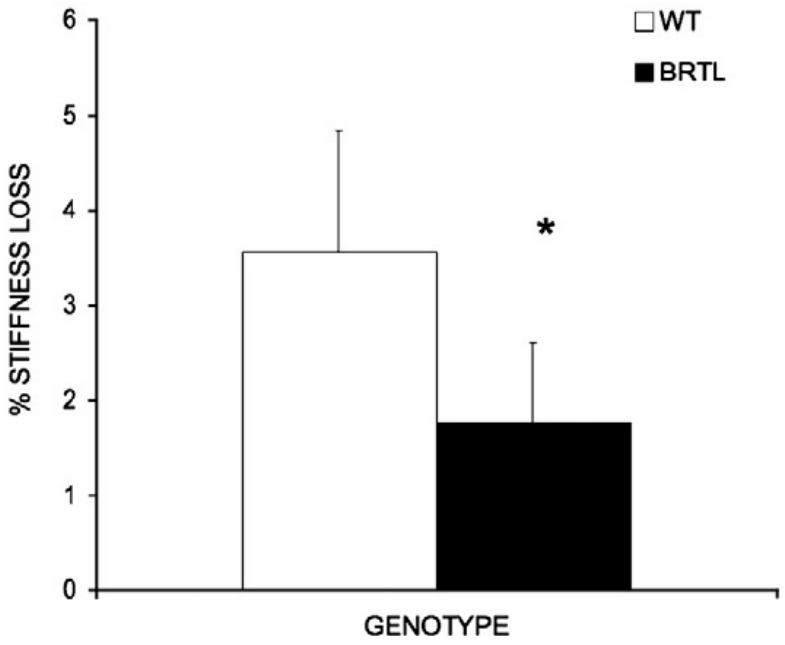

Figure 2-7: Average stiffness loss for each phenotype

Average stiffness loss for each phenotype after 5 minutes of 1Hz cyclic pre-conditioning loading and 30 minutes of 1Hz cyclic loading. Brtl/+ specimens display lower loss of stiffness (1.77%) when compared to their WT counterparts (3.56%) under cyclic loading. * $p < 0.05$

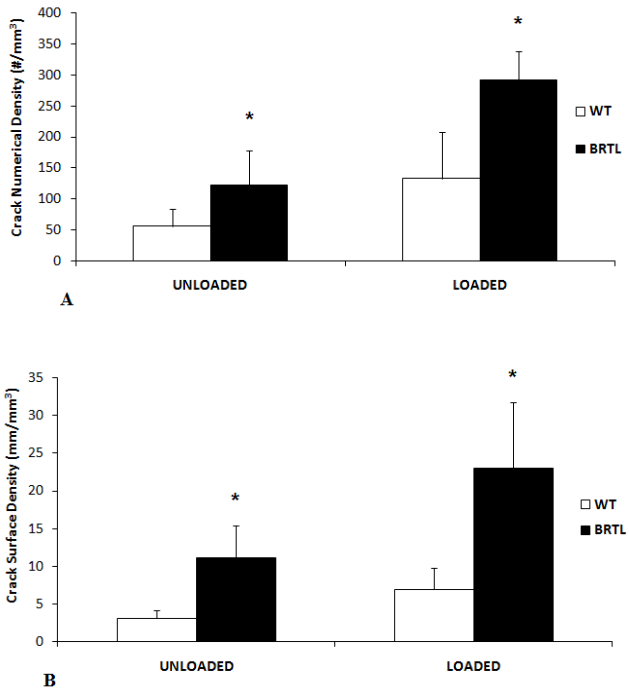

Figure 2-8: Microdamage levels in Brtl/+ and WT specimens

Summary data quantifying the amount of microdamage seen in both loaded and unloaded Brtl/+ and WT specimens. The crack numerical density (Cr.Dn), which measures the number of individual linear microcracks along the specimen surface area for both loaded and unloaded Brtl/+ and WT specimens, can be seen in **(A)**. The crack surface density (Cr.S.Dn) which measures the amount of damaged tissue across the specimen surface area, can be seen in **(B)**. * $p < 0.05$ vs. WT within loading condition.

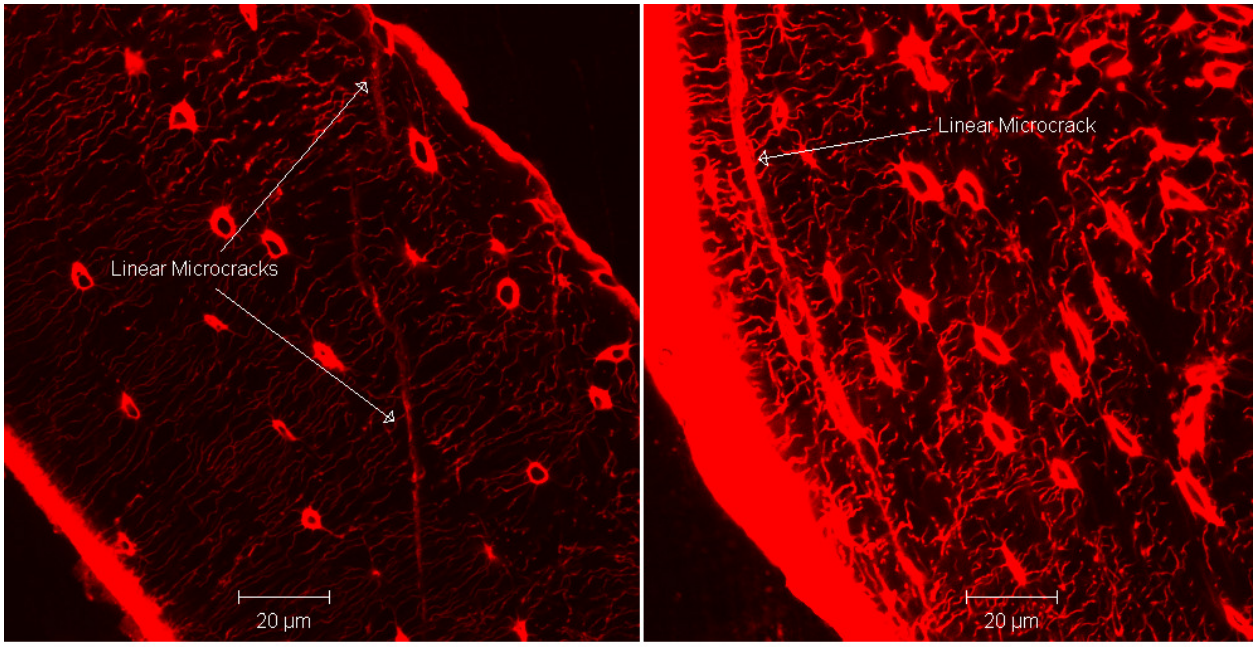

Figure 2-9: Confocal images of microdamage

Confocal photomicrographs of basic fuchsin stained cross sections obtained from the ulna mid-diaphysis of an unloaded Brtl/+ specimen (A) and a loaded Brtl/+ specimen (B). Linear microcracks in the cortex are stained with basic fuchsin. Scale bar 20 µm with a photomicrograph field width of 128 µm.

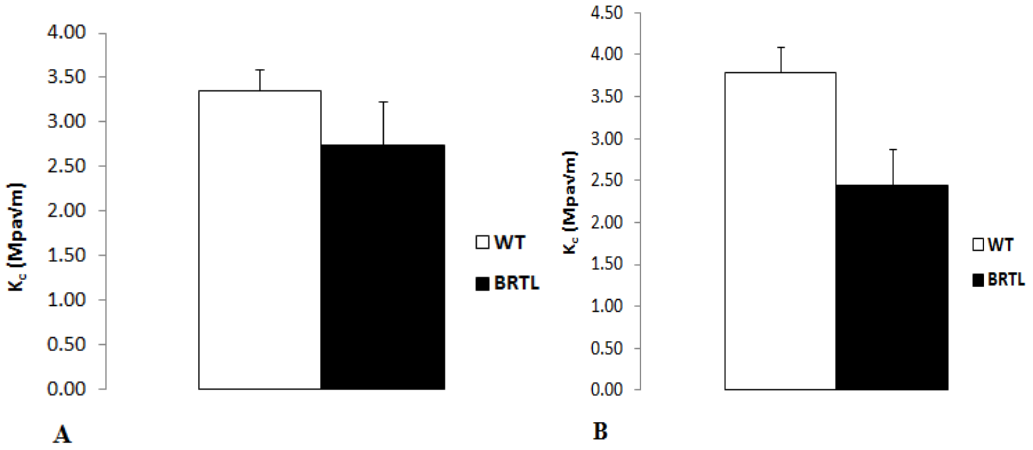

Figure 2-10: Fracture toughness values for WT and Brtl/+ specimens

Graph showing the average fracture toughness values for WT and BRTL/+ specimens tested using the maximum load(A) and instability techniques(B) described by Ritchie [46]). There was an 18.6% difference noted with the maximum load technique (p=0.486) whereas as 35.4% difference was noted with the instability technique (p=0.057).

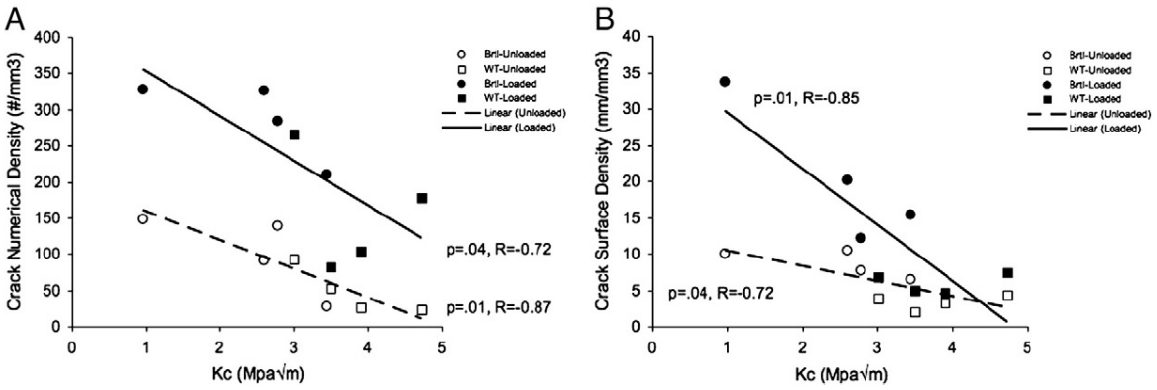

Figure 2-11: Pooled fracture toughness correlations

Correlations between instability fracture toughness values and crack numerical density (A) and crack surface density (B). Instability fracture toughness was negatively correlated with loaded and unloaded ulnar CND and CSD. Whereas the slopes governing this relation between Kc and CND were the same between loaded and unloaded limbs (p=0.4), the slopes were significantly different in the relationship governing Kc and CSD between loaded and unloaded ulnae (p=0.02)

Table 2-1: Comparison of fracture toughness data

Method	Brtl/+ K_c (Mpa√m)	WT K_c (Mpa√m)	% Difference
Crack Instability	2.44	3.79	35.4
Worst Case Crack Instability	2.44	3.56	31.4
Maximum Load	2.73	3.36	18.8

Chapter 3.

The Effect of Bisphosphonate Therapy on Microdamage Accumulation in the Brtl/+ Mouse Model

3.1 Introduction

Bisphosphonates are a potent anti-resorptive drug commonly used to treat diseases of low bone mass or high bone turnover such as osteoporosis [67], Paget's disease [68], and most recently osteogenesis imperfecta (OI)[69]. Since its introduction as a treatment option for pediatric OI patients, there has been an increased interest in our understanding of their effects in the growing skeleton. OI, which is commonly known as "brittle bone disease", is a heritable connective tissue disorder that is attributed to mutations in type I collagen or collagen-associated proteins [70] which in

turn impacts the skeleton structurally and morphologically. Common traits of the disease include decreased bone fragility, increased brittleness and fracture incidence, and an up-regulation in bone remodeling [11, 14, 71].

Bisphosphonates aim to improve bone mass, and strength, but do not affect the defective type I collagen. Instead, bisphosphonates increase bone mass by inhibiting osteoclast-mediated bone resorption through decreased osteoclast recruitment, promotion of apoptosis of mature osteoclasts [72, 73], and possible inhibition of apoptosis of osteocytes and osteoblasts [74]. Treatment of OI patients with bisphosphonates has shown to be especially promising in reducing vertebral fracture rates [75, 76] but has not demonstrated a notable functional improvement in long bones [75, 77, 78]. Animal studies have played a key role in determining the effects of bisphosphonates on skeletal integrity. While bisphosphonates are used to increase bone mass, there have been reports in several animal models that indicate an increase in skeletal microdamage after extended treatment [79-

81], which subsequently leads to a decrease in mechanical integrity of the bone [80-82]. Although there have been studies that have investigated the effects of long term bisphosphonate treatment in OI mouse models [58, 83, 84], none have presently looked at microdamage levels following treatment.

For the purposes of this study, we used the Brtl/+ mouse to investigate the effects of bisphosphonates in a model of OI. Brtl/+ is heterozygous for a Gly349→Cys substitution in *col1a1*, reproducing the genetic mutation found in a type IV OI child [85]. Brtl/+ mice have a moderately affected skeletal phenotype, with long bone deformities and fragility. In addition, Brtl/+ demonstrates post-pubertal adaptations to improve mechanical integrity with age, which is similar to the clinical observations of decreased fractures in human OI patients after skeletal maturity [15]. Moreover, we have shown in our earlier studies that the Brtl/+ mouse is more susceptible to microdamage accumulation during normal ambulation, and externally applied loading when compared to their WT counterparts. [86]. This study aims to identify

the effect of a 5 week bisphosphonate treatment protocol during the growing phase of the Brtl/+ mouse. We hypothesize that treatment with bisphosphonates will have an adverse effect on the mechanical integrity of bone which will be manifested through an increase in microdamage and a reduction in fracture toughness properties.

3.2 Materials and Methods

3.2.1 Murine Model

A total of 38 male Brtl/+ and wild type WT (n= 19 each) mice were bred from our colony and used in this study. 8 week old male mice were assigned to 4 groups, which included bisphosphonate treated WT and Brtl/+ groups, as well as WT and Brtl/+ untreated groups with n=8/group. Brtl/+ mice have a mixed background of Sv129/CD-1/C57BL/6S and are bred by crossing heterozygous Brtl/+ with WT [38]. Animals were genotyped at between 14 and 21 days of age using polymerase chain reaction (PCR) and

DNA from mouse tails. Mice were allowed a regular diet of rodent chow and water ad libitum. All procedures used in this study were approved by the University Committee on Use and Care of Animals (UCUCA) at the University of Michigan.

3.2.2 Bisphosphonate Treatment

For this study, the effects of bisphosphonate treatment were compared between treated and untreated groups in Brtl/+ and WT mice. For the WT and Brtl/+ treated groups, the bisphosphonate Alendronate (Aln) (Sigma-Aldrich) was injected subcutaneously at 0.219 mg/kg in PBS, once per week from 3 to 8 weeks of age. We chose this dosage to match earlier Alendronate treatment studies in the Brtl/+ mouse, to compare and contrast observations [58]. Earlier studies in the oim mouse demonstrated that this dosage was the lowest concentration required to increase mineralization and prevent resorption [87]. Untreated mice received no injections at any time point.

3.2.3 In-Situ Strain Measurements

The ulnar loading model [39] was used throughout this study to produce compressive loads and induce microdamage. This loading model has been shown to produce loads primarily within the ulna and not the radius, and has been shown to induce microcrack formation within the ulna of rats [40]. The right forearms of mice were exposed to cyclic uniaxial compression loading across the olecranon and carpus process as described by others [40, 41]. Loading was done using a custom built servo-motor loader. Force-controlled, haversine, cyclic loading was performed at 1 Hz frequency while force and strain voltages were recorded using Labview 7.1 software (National Instruments, U.S.A.).

To measure strains in treated mice, 6 cadaver mice (n=3 Brtl/+ and n=3 WT) which were treated with Alendronate using the above mentioned treatment protocol, were used to record ulnar strains during cylic loading to assess the level of force required to induce strains that would produce linear

microdamage in compression (estimated at 4000 micro strain) [40, 42]. Earlier studies in the Brtl/+ mouse demonstrated that 4000 micro strain was sufficient to generate damage in both Brtl/+ and WT untreated bone [86]. The strain gauge technique was described in earlier studies [86]. Briefly, a 5 mm incision was made at the mid-diaphysis of the right forearm and the bones were further prepared using prescribed techniques [43] and commercial reagents (Vishay Micro-Measurements, U.S.A.) for the placement of strain gauges. 100% ethanol followed by acetone was applied to the exposed ulna surface using a cotton tip applicator. A catalyst (Catalyst-C) was then applied followed by a drop of adhesive (M-Bond 200). Single element strain gauges (EA-06-015DJ-120, Vishay Micro-Measurements, U.S.A.) were placed longitudinally as close to the lateral surface as possible of the ulna of both Brtl/+ and WT mice, near the mid-diaphysis. It has been confirmed experimentally [41], as well as through finite element modeling [44], that due to the geometry of the ulna, this area

is the region of highest compressive strain and deformation during axial ulnar loading.

Cyclic loading was performed continuously, and several rounds of data were collected for each mouse and analyzed using linear regression in order to determine the load-strain relationship for both Brtl/+ and WT genotypes. From these regressions it was noted that the loads that induced approximately 4000 micro strain were 7.16 ± 0.71 N for the WT and 6.75 ± 1.24 N for the Brtl/+ treated mice. Strain gauge data from our earlier studies showed that 4000 microstrain would be attained at 2.71 ± 0.35 N for Brtl/+ and 4.92 ± 0.04 N for the WT untreated mice [86].

Table 3-1 represents data collected from a small sample of untreated and treated animals using micro computed tomography (MicroCT). Using Euler's Column Formula **Eqn. (3-1)**, the theoretical critical buckling load was calculated assuming an effective length factor (K) of 1, to roughly determine how geometric differences and material differences impact the

load required to initiate critical buckling. The I_{min} value used was the lowest bending moment of inertia for each specimen, as it was assumed that failure would occur in the plane with the lowest bending moment of inertia. Using Young's Modulus values from Kozloff et al. [15] and Uveges et al.[88] as references, (Brtl/+ untreated at 8 weeks old =862.44 MPa, WT untreated at 8 weeks old=645.24 Mpa, Brtl/+ treatment for 6 weeks with Alendronate at 8 weeks old =4319.4 Mpa and WT treatment for 6 weeks with Alendronate at 8 weeks old=3306.8 MPa) the theoretical critical buckling loads were calculated. Despite the small number of animals analyzed, it does appear that the critical loads do in fact increase with treatment, which corresponds with the increased loads to engender 4000 microstrain in our treated specimens.

Equation 3-1:

$$P_c = \frac{\pi^2 E I_{min}}{(KL)^2}$$

P_c = Critical buckling load
E = Young's Modulus (MPa)
I_{min} = Minimum bending moment of inertia (mm^4)
K = column effective length factor
L = length of bone (mm)

3.2.4 Cyclic Loading in Untreated Animals

A total of 32 mice (n=16 Brtl/+ and n=16 WT) were used for cyclic loading. To induce microdamage, a similar loading protocol (1 Hz sinusoidal wave pattern) and data recording protocol was used as described for in-situ strain gauging, with the exception that force and actuator displacement were recorded using Labview 7.1 software. The contralateral forelimbs were not loaded and were used as controls to assess baseline levels of microdamage in the bone matrix. Each specimen was allowed a 5 minute (300 cycles) period of dynamic pre-conditioning in order to mitigate the effects of soft tissue

compliance and thus isolate and account for the effects of the actuator displacement to that of solely bone matrix degradation [44]. This time also afforded the opportunity to gradually ramp up the force amplitudes for each forearm to produce the required range of strains, as necessitated by the intrinsic differences in bone size between animals. Bones were then cyclically loaded for 30 minutes (1800 cycles) at force-controlled loads that produced approximately 4000 microstrain (με) based on data collected in the in situ strain gauge experiments. Minimal compressive loads on the reversal phase of loading of approximately 2.45 N and 1.34 N for WT and Brtl/+ mice, respectively, were used to ensure that platens remained in contact with the bone during the unloading segment. Post hoc calculations showed that WT mice displayed compressive strains ranging between a minimum of approximately 100.5 με during the unloading segment and approximately 3870 με (approximately 5N) at maximum loading, whereas Brtl/+ exhibited strains of 70.3 and 3905.3 με (approximately 3N) during unloading and

loading segments, respectively. The displacement of the ulna during cyclic loading was recorded for each bone using a linear variable differential transformer (LVDT). Loss of stiffness for each bone was determined using **Eqn. (3-2)**, which was previously used by Bentolila et al. [40] as a surrogate for effective stiffness loss.

Equation 3-2:

$$\text{Stiffness Loss} = \frac{L_o - L}{L_o}$$

where L_o is the initial length of bone and L is the final length of the bone. The initial length was always measured at the end of the dynamic pre-conditioning period (300 cycles) while L was measured when loading was complete. Both L_o and L were measured using the calibrated external LVDT during loading, while the forearm was still within the platens.

3.2.5 Cyclic Loading in Treated Animals

Treated animals were loaded using the same protocol as untreated specimens and their stiffness loss was calculated similarly. However, during the initial stages of testing these animals, some WT (n=2) and Brtl/+ (n=2) animals underwent premature fracture of the ulnas during testing. A representative image displaying where most fractures occurred in treated specimens is shown in **Figure 3-1**. These animals were dropped from the study and as a result of this observation, subsequent treated animals were loaded to a reduced load that induced approximately 3000 με in order to ensure successful completion of the 35 minute loading protocol. Minimal compressive loads on the reversal phase of loading of approximately 2.43 N and 2.24 N for WT and Brtl/+ mice, respectively, were used to ensure that platens remained in contact with the bone during the unloading segment. Post hoc calculations showed that WT treated mice displayed compressive strains ranging between a minimum of approximately 46.9 με during the

unloading segment and approximately 2800.6 με (approximately 5N) at maximum loading, whereas treated Brtl/+ specimens exhibited strains ranging from 63.6 and 2743.4 με (approximately 4.5N) during unloading and loading segments, respectively. Under these revised testing protocols, treated specimens were able to complete the full 35 minute loading protocol as their untreated counterparts.

3.2.6 Confocal Microscopy Parameters

After euthanasia both loaded and unloaded forelimbs were excised and fixed in 10% neutral buffered formaldehyde. Bones were then stained with 1% basic fuchsin using an established protocol [45] and rinsed in 100% ethanol. Samples were subsequently embedded undecalcified in poly methyl methacrylate (PMMA) for histology. Using a Buehler Isomet diamond-blade saw, 400 μm sections were then cut transverse to the longitudinal axis of the ulna. These sections were mounted on a plastic microscope slide and polished to a final thickness of 100 μm. Sections were cover slipped and

viewed using a 2-Photon Leica confocal inverted microscope system (SP5X Zeiss Confocal Microscope, Carl Zeiss MicroImaging, Inc., Thornwood, NY, U.S.A.), to identify bone areas stained with basic fuchsin. A 40X oil immersion objective was used to capture images. In order to image the basic fuchsin, an excitation of 543nm was used, with an emission range of 553-613nm.

3.2.7 Microdamage Quantification

Images were taken for the entire 100 μm thick cortical region and subsequently analyzed using the Leica LAS AF Image Browser (Version 2.6.0 Build 7266, Leica Microsystems CMS, Inc.) to quantify linear microdamage within the cortical region. Cracks that were positively labeled with basic fuchsin dye were deemed as damage-induced during loading. Diffuse damage was not assessed in this study. The following parameters were measured throughout the entire cortical bone region of each section: number of microcracks (#), bone cortical volume (B.Vol., mm^3), microcrack

numerical density (Cr.Dn., #/mm^3) and microcrack surface density (Cr.S.Dn., mm/mm^3).

3.2.8 Fracture Toughness

To correlate microdamage with fracture toughness, right femurs from each mouse were prepared and tested according to techniques established by Ritchie [46]. This technique utilizes linear elastic fracture mechanics (LEFM) principles and a self-induced starter notch to measure the bone's resistance to fracture (fracture toughness). For regular mechanical testing of engineering materials, ASTM standards require that a sharp starter notch be the initiation point of fracture [47]. This starter notch is typically induced by a fatigue loading technique; however, due to the small geometry of mouse bones, this procedure is not optimum. Studies have shown that accurate fracture toughness data can be attained from razor sharpened micronotches [48] and this technique has been deployed for small animal studies [46] **(Figure 2-3)**. Using this technique will provide us with a true mechanical

measure of the bone's inherent fracture toughness, without the viscoelastic influence of soft tissue.

The right femora from each group were harvested, cleaned of soft tissue, and stored frozen at -20°C in gauze soaked in Lactated Ringer's Solution (LRS) until testing. Bones were machine-notched through the posterior cortex at the mid-shaft using a micro milling device with a cutting radius of 0.01 inches. Notches were then sharpened using a custom rigged mounted razor blade, pasted with 1 μm diamond polish (Struers). Bone diameters were measured with electronic calipers and notch depths were made using a micro mill to approximately 1/3 of the bone diameter[86]. This notching procedure typically produces a reproducible sharpened notch root radius of approximately 10 μm [46, 48] .

In preparation for three-point mechanical bend testing, the femoral heads were removed, while the condyles were left intact. This was done to maintain stability within the three-point bending apparatus[86]. Femurs were

thawed in LRS soaked gauze at room temperature to preserve moisture content until they were ready for testing. Specimens were loaded to failure in three-point bending at 0.001 mm/s using a servohydraulic testing machine equipped with a 220N load cell (858 MiniBionixII Material Test System; MTS Systems Corporation, Eden Prairie, MN, USA) in accordance to ASTM standards [47, 49] and other established protocol [46]. During three-point bending, the specimens were placed such that the posterior surface was in tension and the anterior surface was in compression with the top loading point oriented directly above the notch on the anterior surface. A span length of 4.5 mm was used in testing. Load and displacement values were recorded throughout the experiment using integrated Material Test System data acquisition software (858 MiniBionixII Material Test System; MTS Systems Corporation, Eden Prairie, MN, USA).

After mechanical testing, fractured bone specimens were fixed in 70% ethanol, defatted in toluene under vacuum for 24 hours, and cleared of soft

tissue with 2% potassium hydroxide for 12 hours. The specimens were dehydrated by immersion in a graded series of alcohols (50%, 70%, 95% and 100%) and coated with carbon [37]. Specimens were imaged by SEM to determine the transition from stable to unstable crack growth (**Figure 2-4**). Fracture toughness, K_c, was measured using solutions for circumferential through-wall cracks established for cylindrical pipes [46, 50, 51]. Both the maximum load and the crack instability techniques were used to determine fracture toughness values [46]. All measurements used in the LEFM calculations, such as specimen width and thickness, were taken from SEM images of fracture sites using the public domain software ImageJ (National Institutes of Health).

All measurements of thickness and radii were measured on the fracture surface of each specimen i.e. the non-notched surface as previously instructed by Ritchie [46]. Cortical thickness was taken as an average measurement of 6 different thicknesses measured at different points along

the fracture surface. The centroid for each specimen was determined by drawing a line parallel to the notch that was half the bone's diameter. This line represented the major axis. Another axis that was rotated 90 degrees to the first was also placed at half the bone diameter. This line represented the minor axis. The intersection of these perpendicular lines represented the centroid of the bone **(Figure 2-5)**. In determining the stable to unstable transition region, the SEM was used in backscatter mode. The difference in morphology was used to determine the transition. The stable region is typically described as having a darker appearance with linear groves, whereas the unstable region has a more spongy appearance. Half-crack angles (2θ) were determined by measuring the included angle (maximum load technique) which is formed from the centroid to the notched surface, and with the excluded angle (instability technique) which is formed from the centroid to the stable to unstable transition region.

3.2.9 Statistics

Effect between loaded and unloaded limbs within each group (WT treated, WT untreated, Brtl/+ untreated and Brtl/+ treated) on percent stiffness loss, crack numerical density, and crack surface density, were compared using a paired Student's t-test (Microsoft Excel 2010). Effects between treatment groups on the same limbs (loaded or unloaded) within the same genotype were performed using unpaired t-test (Microsoft Excel 2010). Effects of treatment within the same genotype on fracture toughness values calculated using either the maximum load or instability technique were compared using unpaired t-tests. The overall effect of genotype, loading or treatment was compared using linear mixed models with repeated measures within the subject (IBM SPSS Statistics v. 20) In all tests, significance was attributed to $p<0.05$. All data is presented as mean ± SD.

3.3 Results

3.3.1 WT and Brtl/+ treated specimens underwent premature fracture

During the early stages of loading treated specimens at loads required to induce 4000 με, 4 animals (2 WT and 2 Brtl/+) suffered premature fracture during loading at the metaphyseal regions in both ulna and radius **(Figure 3-1)**. **Figure 3-5** shows the bone architecture at the typical regions of fracture. The radius fracture occurred in predominantly cortical bone while the ulnar fracture occurred in the trabecular region at the proximal metaphyseal region. This observation could possibly indicate weaker trabeculae in treated specimens as opposed to untreated specimens. As a consequence of this observation, loads were adjusted to produce approximately 3000 με in order for treated specimens to complete the 35 minute loading protocol as their untreated counterparts. Upon this adjustment, no further issues of premature critical fractures occurred.

3.3.2 Brtl/+ ulnae demonstrate lower stiffness loss during loading

Whole bone loss of stiffness for each forearm was measured via LVDT during cyclic loading according to **Equation (2-1)**. While Brtl/+ and WT untreated ulnae were loaded with matching surface strains (~4000 με), Brtl/+ demonstrated a significantly lower percentage stiffness loss compared to WT (5.65 ± 1.15% and 9.41 ± 1.41% respectively; $p<0.05$) over the 35 minute load period. Interestingly, despite both Brtl/+ and WT treated specimens being loaded to similar (~3000 με), yet lower surface strains than their untreated counterparts they both attained similar stiffness losses as their untreated counterparts at the end of the loading protocol (Brtl/+ treated = 6.02 ± 2.78% vs. WT treated = 9.19 ± 2.68%; $p<0.05$) **(Figure 3-2)**. When treated limbs were pooled together and compared to untreated groups, no significant differences were seen.

3.3.3 Unloaded and loaded Brtl/+ ulnae have more microdamage than WT counterparts

Both unloaded treated and untreated control limbs from Brtl/+ demonstrate significantly increased linear microcrack numerical density (85.0% (p=0.040) and 124.9% (p=0.044) respectively) and microcrack surface density (72.5% (p=0.032) and 81.8% (p=0.053)) compared to their WT counterparts **(Figure 3-3 A,B)**. Similarly, both loaded treated and untreated limbs from Brtl/+ demonstrate significantly increased linear microcrack numerical density (75.2% (p=0.011) and 103.9% (p=0.015) respectively) and microcrack surface density (75.1% (p=0.052) and 136.9% (p=0.003)) compared to their WT counterparts **(Figure 3-3 A,B)**.

3.3.4 Cyclic loading resulted in increased levels of damage

In general, loaded limbs for both WT and Brtl/+ had significantly more microdamage than their unloaded contralateral limbs in both treated and untreated groups. This trend achieved significance in all groups with the

exception of the WT treated group, which saw a trend towards an increase in both crack numerical density and crack surface density following cyclic loading, but did not achieve significance ($p=0.076$ and 0.105 respectively). Despite this, cyclic loading globally resulted in an increase in microdamage when compared to unloaded limbs in both crack surface density and crack numerical density ($p<0.05$ for both measures)

3.3.5 5 weeks of Alendronate treatment did not impact microdamage content in unloaded limbs

There were no significant differences observed in damage content in unloaded limbs for either genotype when comparing treated to untreated groups. Similar observations were seen in both crack numerical and crack surface density calculations **(Figure 3-3 A,B)**.

3.3.6 *Despite loading to a lower surface strain, treated limbs attained similar levels of microdamage*

There were no significant differences observed between treated loaded limbs and untreated loaded limbs. This occurred despite the fact that treated limbs were loaded approximately 1000 με less than their untreated counterparts. Similar trends were seen in both crack numerical and surface density calculations **(Figure 3-3 A,B)**. This observation suggests that loading at 3000 με in treated specimens produces as much damage content as loading at 4000 με in untreated specimens. When pooling all treated limbs and comparing them to untreated limbs, 5 weeks of Alendronate treatment did not result in an increase in microdamage content ($p=0.134$ for crack numerical density and $p=0.680$ for crack surface density).

3.3.7 *Brtl/+ femora display a reduced fracture toughness compared to WT*

Using the maximum load technique, which assesses fracture toughness based on the initial notch geometry and the maximum load

encountered during three-point bending, WT untreated femora displayed average K_c values of 3.94 Mpa√m whereas Brtl/+ untreated specimens had K_c values of 3.17 Mpa√m (p=0.062) **(Figure 3-4)**. The instability technique relies on identification of the transition between unstable and stable crack growth, and showed a more sensitive difference in K_c values between genotypes (WT 3.96 Mpa√m; Brtl/+ 2.79Mpa√m) (p=0.014) **(Figure 3-4)**.

Similar trends were seen when comparing treated to untreated specimens in WT and Brtl/+ specimens. Brtl/+ treated demonstrated a significant decrease in maximum load fracture toughness when compared to their WT treated counterparts (WT = 3.43 Mpa√m; Brtl/+ = 2.66Mpa√m) (p=0.025) whereas instability fracture toughness values showed a trend towards a decrease in Brtl/+ treated femora when compared to WT treated femora (p= 0.113).

3.3.8 Bisphosphonate treatment results in a trend towards reduced fracture toughness in both Brtl/+ and WT

When comparing treated to untreated groups in both Brtl/+ and WT, we observe a general trend of reduced fracture toughness. WT treated was 12.9% lower (p=0.168) than WT untreated maximum load fracture toughness, while Brtl/+ treated was 16.0% (p=0.155) lower than Brtl/+ untreated.

Similar trends were seen when analyzing the instability fracture toughness values. WT treated was 21% (p=0.03) lower than WT untreated fracture toughness, while Brtl/+ treated was 11.8% lower than Brtl/+ untreated, however this difference was not statistically significant (p=0.469) **(Figure 3-4)**.

After combining all treated limbs and comparing them to untreated limbs, bisphosphonates had a trending but not quite significant decrease in

fracture toughness (p=0.061 for maximum load fracture toughness and p=0.063 for instability fracture toughness)

3.3.9 Fracture toughness correlations with microdamage

In order to determine if there were any correlations between crack numerical density and crack surface density and fracture toughness, loaded and unloaded specimens were pooled together into separate linear regression models (**Figures 3-6 and 3-7).** In loaded treated limbs, Brtl/+ and WT showed negative correlations in crack numerical density (CND) versus instability fracture toughness (R=-0.66 and p=0.005), crack surface density (CSD) versus maximum load fracture toughness (R=-0.472 and p=0.065), CSD versus instability fracture toughness (R=-0.409 and p=0.116), as well as CND versus maximum load fracture toughness (R=-0.610 and p=0.012) (**Figures 3-6 and 3-7)**

It appears that unloaded limbs are weakly correlated with fracture toughness, as neither the instability fracture toughness nor the maximum

load fracture toughness showed any strong correlations with either CND or CSD (**Figures 3-6 and 3-7**)

3.4 Discussion

Bisphosphonates have been a popular treatment option for patients suffering from low bone mass diseases. They have been used in the osteoporosis community for over 40 years and more recently in the treatment of osteogenesis imperfecta patients. While there has been marked improvement in vertebral strength and structure, a growing concern with bisphosphonates are reports in animal models that they may adversely impact mechanical integrity of bone by reducing toughness and by preventing the repair of microdamage. This study utilized the Brtl/+ mouse as a model to investigate the impact of a 5 week (3-8 weeks of age) bisphosphonate (Alendronate) treatment protocol on microdamage content

and the resulting fracture toughness properties of bone formed with an OI-causing mutation.

Both treated and untreated Brtl/+ ulnae subject to normal cage activity demonstrated significantly higher levels of microdamage than their WT counterparts. Extended bisphosphonate treatment did not seem to impact the levels of microdamage in unloaded limbs in either Brtl/+ or WT specimens. However, loading produced equivalent levels of microdamage and stiffness loss in treated animals compared to untreated animals despite loading to 25% reduced surface strain. This decrease in durability is supported by a trending decrease in femoral fracture toughness properties of both WT and Brtl/+ treated animals compared to untreated mice.

In mechanics, fracture toughness serves as an inherent material property that measures a material's ability to resist damage. In this study, there were moderate reductions in fracture toughness observed following treatment with bisphosphonate in both WT and Brtl/+ groups, and instability

fracture toughness showed a significant decrease in WT treated femurs when compared to WT untreated femurs. This decrease in fracture toughness is supported by other studies which demonstrate a decrease in whole bone toughness with extended bisphosphonate treatment [80, 82, 89, 90]. Toughness or work to failure, is a common mechanical parameter measured in the mechanical testing of bone that can somewhat serve as a surrogate indicator of a material's ability to resist fracture. The decreased toughness or work to failure associated with bisphosphonate treatment suggests that bisphosphonate treatment may compromise the bone's ability to prevent the onset of critical failure microcracking.

Our moderate differences in fracture toughness could have been caused by a structural change in the material that could lead to a reduction in the material's ability to resist crack initiation or could result from some other morphological change such as altered collagen crosslinking, increased mineralization, or altered bone architecture. Our results suggest that

treatment does not appear to affect Brtl/+ or WT's ability to resist crack initiation as crack numerical density (the number of cracks) is similar in both unloaded limbs of treated and untreated Brtl/+ and WT specimens. However this does not dismiss the possibility of macroscopic morphological changes. Bisphosphonates have been shown to increase the levels of non-enzymatic cross-linking (pentosidine), as well as altering the ratio of enzymatic cross-links (pyridinoline/deoxypridinoline), and increasing collagen isomerization (tissue age) which could explain our observed trends in reduced fracture toughness [91, 92].

When looking at fracture toughness correlations, we generally saw negative correlations in loaded limbs regardless of whether they were treated or not when comparing damage metrics (CND and CSD) to fracture toughness values. These correlations were weaker in unloaded limbs. It appears that loaded limbs have the more profound correlations, quite possibly because of the greater amount and variation in damage produced in

loaded limbs as opposed to unloaded limbs. Despite the general observation that microdamage increases as fracture toughness decreases in both loaded and unloaded limbs, it appears that fracture toughness variations have more profound effects when limbs are loaded at high strains as opposed to undergoing ambulatory loading.

In our previous study involving the Brtl/+ mouse and microdamage, we demonstrated similar results in untreated mice as the current study, including decreased loss of stiffness in Brtl/+ as well as increased levels of microdamage in loaded limbs [86]. In the current study, we noted an increase in load required to induce 4000 με in both Brtl/+ and WT treated specimens when compared to their untreated counterparts. However, the technicalities involved when collecting strain gauge data must be noted. Several rounds of cylic loading strain-load data were collected and curves of best fit for each were calculated. It was from these curves that strains were calculated to determine the loads that would induce 4000 με. Even though

experimentally we were able to attain loads of 4000 με in both treated Brtl/+ and WT ulnas, these loads were not maintainable for the course of 2100 cycles. This issue was not observed in untreated specimens.

Both crack numerical density (CND) and crack surface density (CSD) showed significant increases in loaded limbs when compared to their unloaded limbs in both treated and untreated groups. The only exception to this trend was the WT treated group, which showed a trend towards an increase in CND ($p=0.076$) and CSD ($p=0.105$). Additionally, we observed both WT and Brtl/+ specimens suffering whole bone failure when loaded at 4000 με **(Figure 3-1).** This observation promoted the reduction to 3000 με in surface strain used for the treated specimens which enabled the treated specimens to complete the same number of cycles as their untreated counterparts. A similar observation was seen in oim mice that demonstrated low work to failure and required fewer cycles to generate equivalent amounts of microdamage compared to WT counterparts [31], albeit without

any pharmacological treatment. Both of these observations combined with the above mentioned matching stiffness loss, suggest that the treated bone has a decreased ability to resist the onset of critical microcracking and perhaps decreased whole bone durability in repetitive high strain loading conditions. Again, we suspect that altered collagen cross-linking may play a role in these observations. Increased cross-linking (measured through pentosidine concentrations) has been shown to reduce ultimate strain [93] and the amount of post-yield deformation [94-96], which are both characteristics of a brittle material. It has been proposed that the increased cross-linking through non-enzymatic processes that result from bisphosphonate treatment results in a more brittle tissue through either the prevention of stress relaxation that normally occurs with crack initiation or by allowing generated cracks to propagate more easily [97, 98]. Thus, we suspect the high strains exerted during loading in concert with the moderately reduced fracture toughness properties of treated specimens, may

have contributed to both the observed premature fractures at 4000 με as well as the increased levels of microdamage despite loading at a decreased surface strain.

Another potential area in which bisphosphonates could adversely the whole bone fatigue durability is through the retention of calcified cartilage. This phenomenon is seen clinically as sclerotic bands, which are typically located in the metaphyseal regions of bones in bisphosphonate treated patients [69, 99-101]. These sclerotic bands tend to occur during the fast paced growth phase of patients, and the distance between the bands are considered times during which normal osteoclastic activity has resumed[99]. Sclerotic bands have been associated with timing of bisphosphonate treatment, and correspond with times of decreased osteoclastic activity [102, 103]. Sclerotic bands have been speculated to result in decreased mechanical integrity [104]. Clinical observations suggest that areas in the metaphysis that do not undergo normal ossification, are at an increased likelihood to

undergo fractures [105]. The occurrence of retained mineralized cartilage is not unique to humans, but has also been observed in murine models treated with bisphosphonates [84, 87, 106, 107]. Work done by Uveges et al. showed the retention of calcified cartilage in the femora of Alendronate treated mice [58]. Incidentally, this metaphyseal area where sclerotic bands are prominent corresponds with the region of premature forearm fractures observed in this study. It is possible that the reason for our observations of fractures at this site could be due to the presence of mineralized cartilage that could serve as a weak spot for the global structural integrity of the bone.

In unloaded limbs, there was no difference in microdamage content in either treated or untreated limbs. We suspect that the low strains exerted during regular ambulation (~1000 με) [41, 108, 109] are not large enough to generate significant increases in microdamage content between treated and untreated limbs. If increased damage content is to be taken as an indicator of the increased chances of undergoing a fracture then our current data showing

no significant changes in damage content in treated versus untreated loaded limbs would support the clinical observations of no significant improvement in long bone fracture rates observed in bisphosphonate treated patients [69, 75, 77, 78, 110]. The observations of this study can be further extended to the clinical postulations that extended bisphosphonate therapy is associated with atypical, low-energy subtrochanteric femoral fractures observed in osteoporotic patients undergoing treatment [29, 30]. The results of the present study support the notion that either slightly reduced fracture toughness, or the high strains seen at the hip [111], could be a contributing factor toward these subtrochanteric femoral fractures. Furthermore, these observations could also have strong implications for fracture prone osteogenesis imperfecta (OI) patients on bisphosphonates who may be more susceptible to microdamage accumulation as suggested by animal models [17, 31]. With both OI and osteoporosis patients being increasingly

susceptible to critical bone failure, any treatment modalities that potentially affect damage repair needs to be carefully assessed.

Bisphosphonates are used clinically to improve bone integrity by increasing bone mass, and their efficacy in improving vertebral bone mineral density and geometry as well as decreasing vertebral fracture rates have been well documented in the osteoporosis community [112-114] . However, there have been reports in several animal models that indicate an increase in skeletal microdamage after extended treatment [79-81], which subsequently leads to a decrease in mechanical integrity of the bone [80-82]. It is proposed that the inhibition of bone remodeling by bisphosphonates could be a key factor that results in the accumulation of microdamage over time [115, 116]. The relatively short term treatment utilized in this study may further explain the lack of differences observed in microdamage in unloaded limbs. It is possible that if extended further, more significant fracture toughness and microdamage differences may be observed in both WT and

Brtl/+ specimens. Indeed, Uveges et al. saw more significant mechanical differences at 12 weeks of Alendronate treatment than at 6 weeks of treatment, including decreased predicted strength and modulus [58]. While we are not directly implicating Alendronate with our observations, it must be noted that Alendronate is a highly potent bisphosphonate that has been implicated in reduced material properties [117, 118], increased levels of microdamage [119], as well as increased non-enzymatic glycations[120]. Further studies investigating the role of other bisphosphonates on fracture toughness and microdamage in the Brtl/+ mouse would prove useful.

In conclusion, this study shows that 5 weeks of bisphosphonate treatment in the Brtl/+ mouse model for osteogenesis imperfecta results in a moderate trend towards a decrease in fracture toughness and no significant differences in microdamage levels in unloaded limbs. Additionally, less force is required to induce similar levels of stiffness loss as well as similar levels of microdamage in treated specimens. The results of this study

suggest that bisphosphonates may not be detrimental at lower strains such as those exhibited in normal ambulation, but may result in compromised mechanical integrity at higher strains. Longer treatment with bisphosphonate is needed to determine if these differences are more pronounced. The findings of this study suggest that the efficacy of bisphosphonates is still open for debate, in particular the duration of treatment.

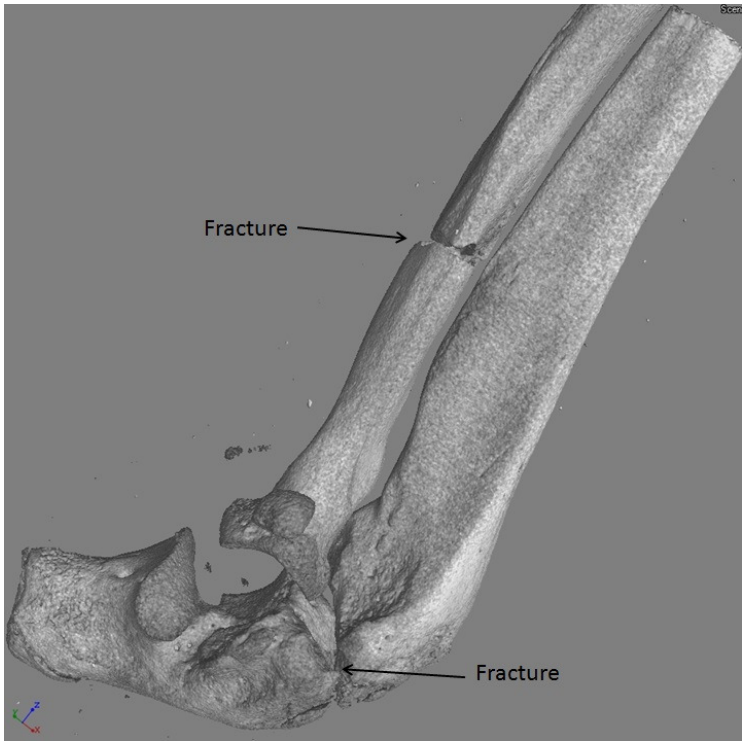

Figure 3-1: Typical fracture position seen in treated forearm failure

A Nano-CT image demonstrating the typical regions of observed failure during cyclic fatigue loading. Fractures occurred at the proximal forearm of the mouse.

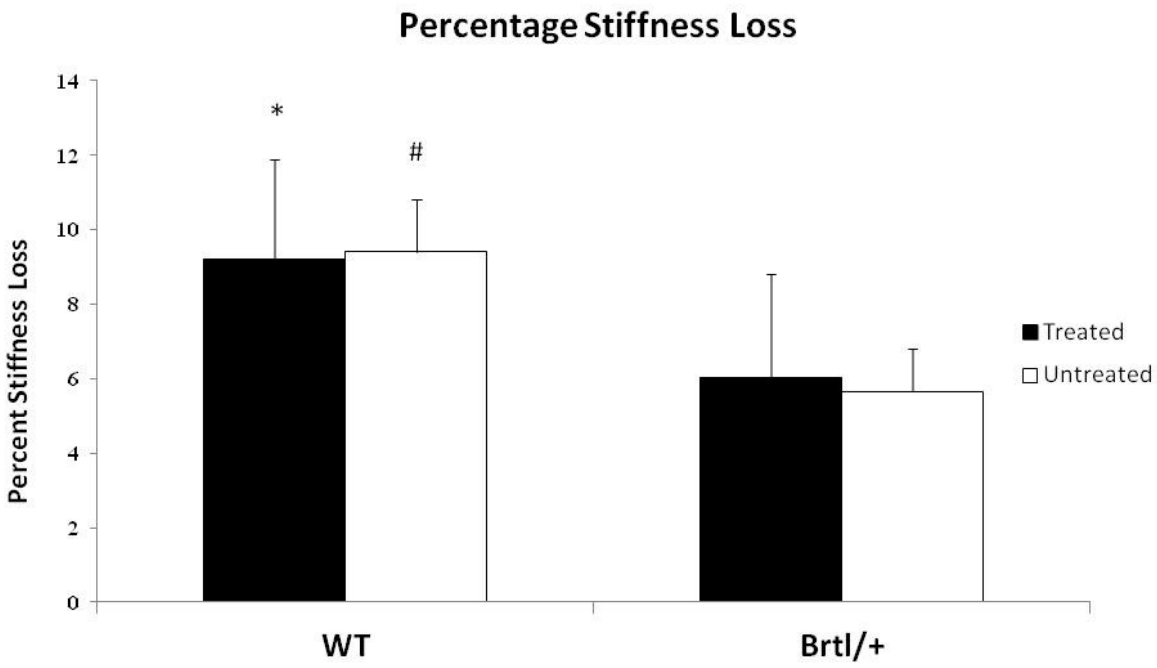

Figure 3-2: % stiffness loss in treated and untreated loaded specimens

Percent stiffness loss between WT and Brtl/+ in treated and untreated specimens. Despite loading to different surface strains based on treatment, similar stiffness losses were reached in both WT and Brtl/+ specimens.
* $p<0.05$ between treated WT and treated Brtl/+; # $p<0.05$ between untreated WT and untreated Brtl/+

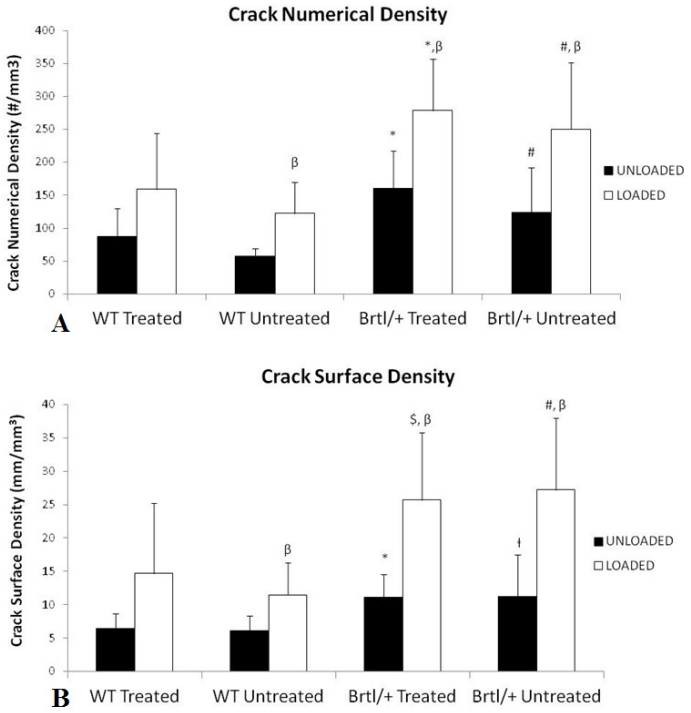

Figure 3-3: Crack surface and numerical density comparisons

Chart representing the degree of microdamage in treated and untreated limbs as measured by crack surface density (A) and crack numerical density (B). * $p<0.05$ between treated WT and treated Brtl/+; # $p<0.05$ between untreated WT and untreated Brtl/+. β: $p<0.05$ between loaded and unloaded limbs in that treatment group. $: $p=0.0515$ between Brtl treated loaded limbs and WT treated loaded limbs.
ł: $p=0.052$ between Brtl untreated unloaded limbs and WT untreated unloaded limbs.

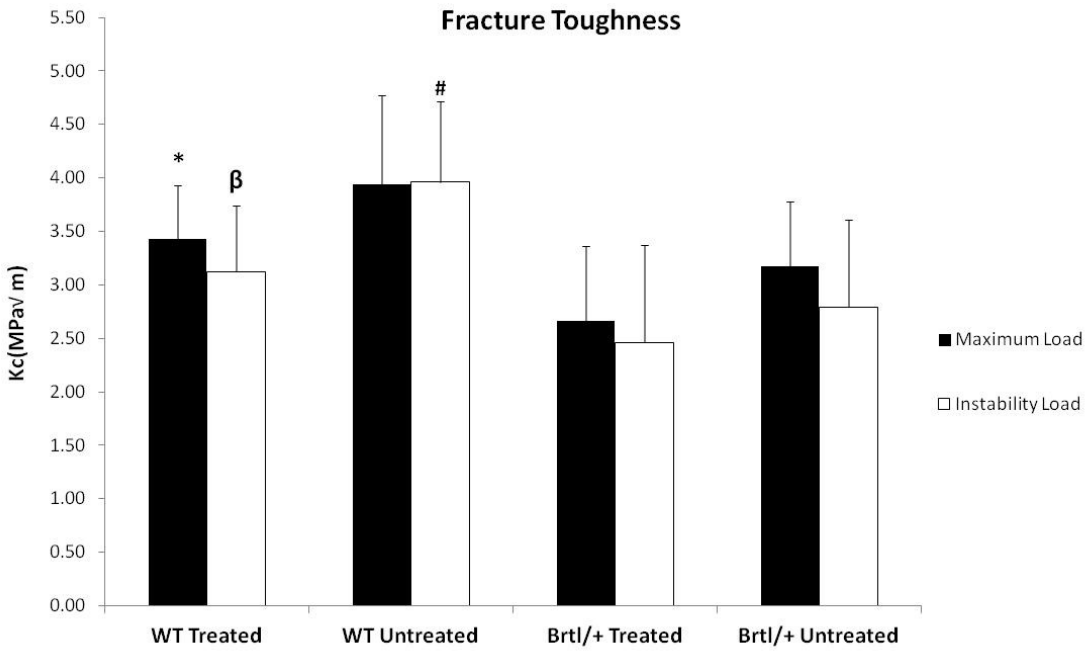

Figure 3-4: Fracture toughness comparisons

Figure representing the fracture toughness as represented by instability fracture toughness and maximum load fracture toughness. *: $p<0.05$ WT treated vs. Brt/+ Treated. β: $p<0.05$ WT Treated vs. WT untreated. #: $p<0.05$ WT untreated vs. Brtl/+ untreated.

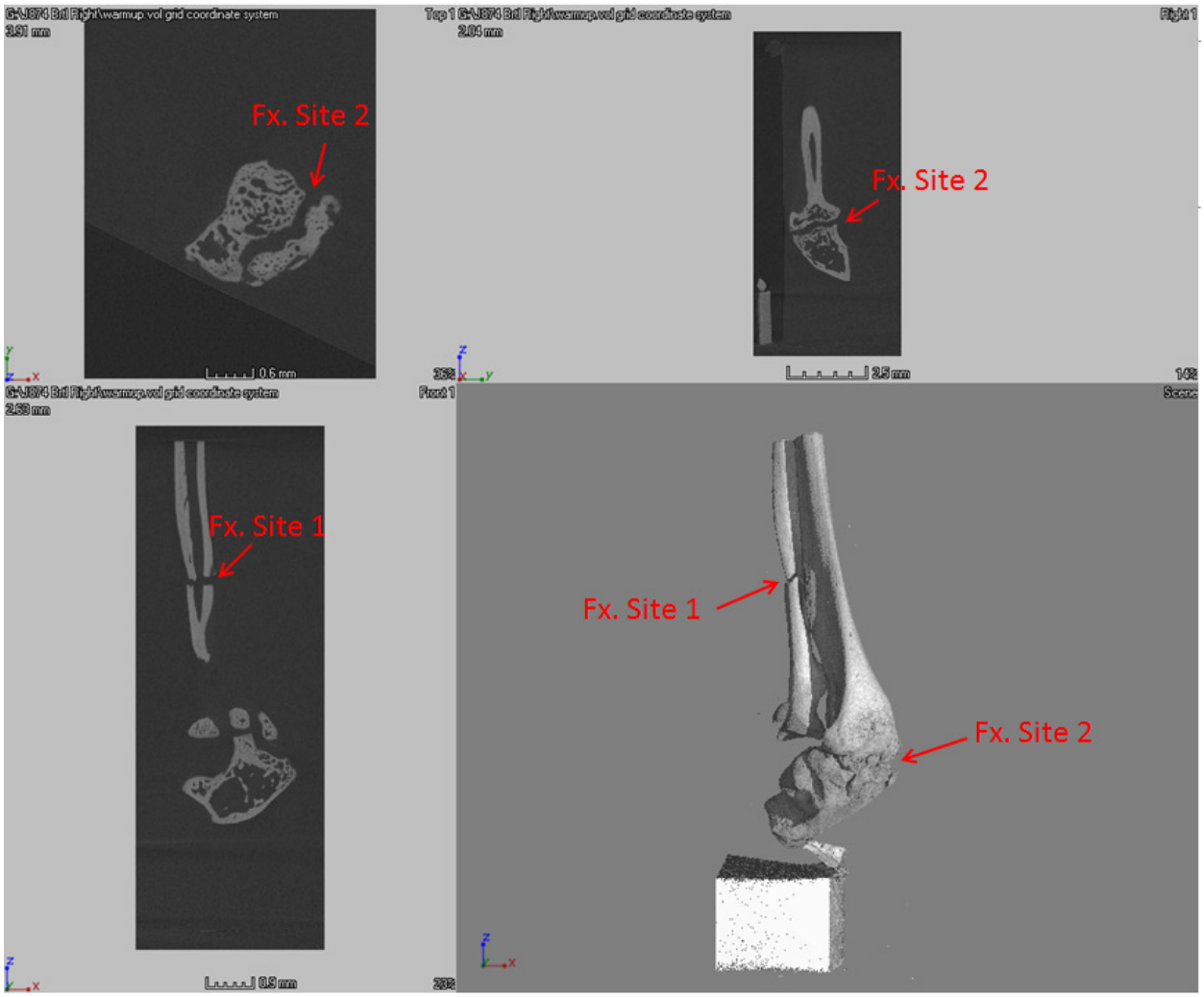

Figure 3-5: Morphological images of fracture sites

Figure shows the bone structure in the regions where fracture typically occurred. The radial fracture occurred in the cortical region of the proximal metaphyseal area. The ulna fracture occurred in trabecular bone at the proximal metaphyseal region.

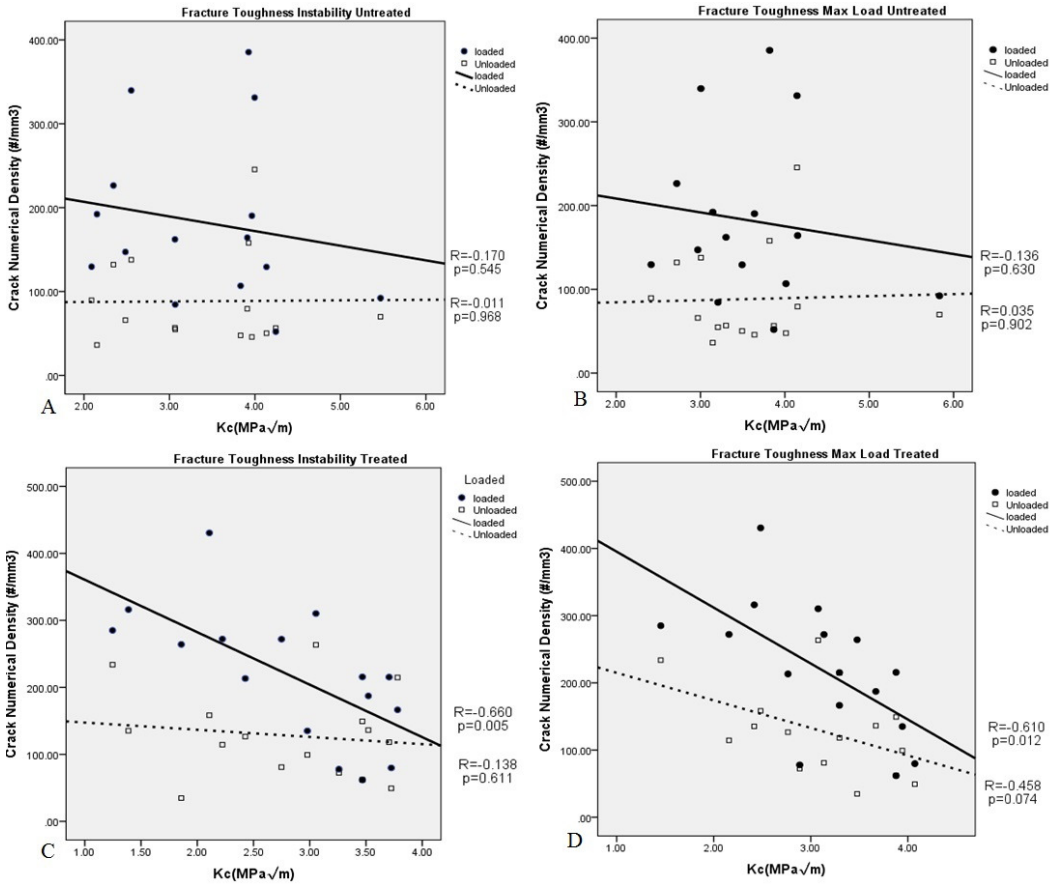

Figure 3-6: Crack numerical density vs. fracture toughness correlations

Correlations between instability fracture toughness values and crack numerical density in pooled untreated (A) and pooled treated (C) animals as well as maximum load fracture toughness and crack numerical density in pooled untreated (B) and pooled treated (D) animals. Fracture toughness was generally negatively correlated with loaded and unloaded CND. There were no significant differences in the slopes in figures B-D,

however, the slopes were significantly different in the relationship governing instability K_c and CND (p=0.009) in treated animals (figure C).

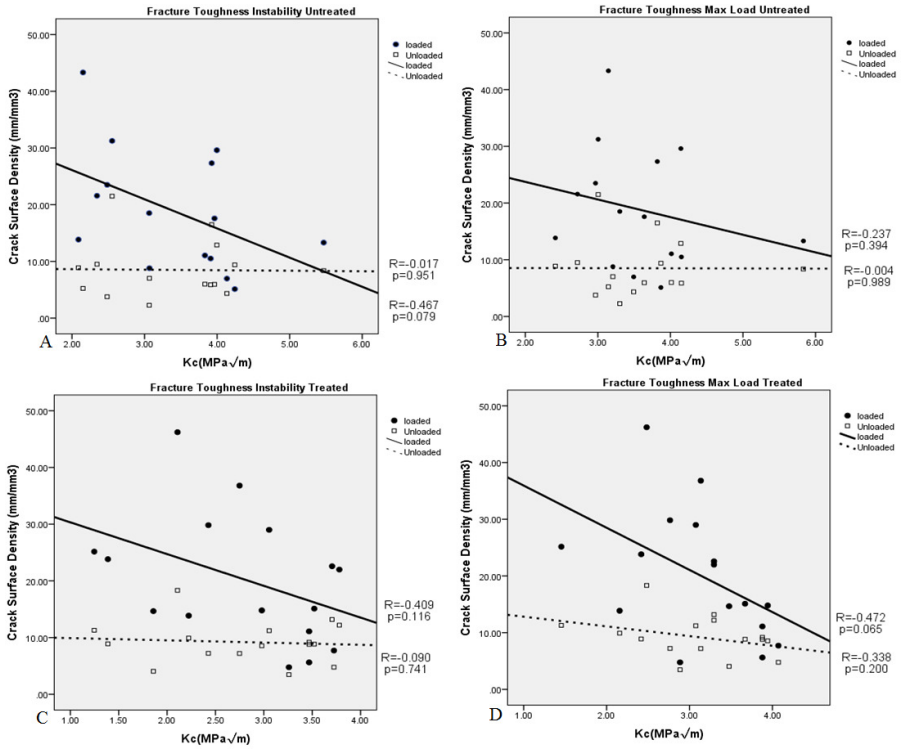

Figure 3-7: Crack surface density vs. fracture toughness correlations

Correlations between instability fracture toughness values and crack surface density in pooled untreated (A) and pooled treated (C) animals as well as maximum load fracture toughness and crack numerical density in pooled untreated (B) and pooled treated (D) animals. Fracture toughness was generally negatively correlated with loaded and unloaded CND. There were no significant differences in the loaded or unloaded slopes in figures B or D, however, the slopes were approaching a significance in different in the relationships governing instability K_c and CSD in untreated animals (p=0.080)

(figure A) as well as that governing instability K_c and CSD (p=0.103) in treated animals (figure C).

Table 3-1: Theoretical critical buckling loads

Genotype	Treatment	Length (mm)	Cortical Area (mm^2)	Total Area (mm^2)	TMD (mg/cc)	Imin (mm^4)	Pcr/E	Pcr (kN)
Brtl/+	No	13.4	0.1962	0.2313	979.27	0.0032	0.000176	0.152
WT	No	14.121	0.3138	0.3872	1012.46	0.0083	0.000411	0.265
WT	No	14.409	0.2867	0.3528	1012.51	0.0088	0.000418	0.270
WT	No	14.841	0.2966	0.3579	976.42	0.0087	0.000390	0.252
WT	yes	14.319	0.3169	0.4004	1014.88	0.0079	0.000380	1.258
Brtl/+	yes	13.096	0.2314	0.2552	1049.73	0.0038	0.000219	0.945

Chapter 4.

Visualization of Bisphosphonate Binding to Bone Microcracks, Surrounding Osteocyte Lacunae, and Osteocyte Apoptosis Spatial Distribution Using Near-Infrared Optical Imaging

4.1 Introduction

Bisphosphonates are a potent anti-resorptive drug commonly used to treat diseases of low bone mass or high bone turnover such as osteoporosis [67], Paget's disease [68], and osteogenesis imperfecta [121]. These drugs reduce bone turnover through the inhibition of osteoclast activity, thereby increasing bone mass and reducing bone fragility. Despite strong clinical findings supporting the use of bisphosphonates in treating bone fragility, [18-23] concern has been raised about the long-term effects of

bisphosphonates on the inhibition of targeted repair of skeletal microdamage. Extended bisphosphonate use has been correlated with observations of increased microdamage accumulation in animal models [24-27], and this may have detrimental effects on bone toughness and increased fragility with long-term use [24-26, 28]. Furthermore, while a causative relationship has not been proven, the association between bisphosphonate therapy and atypical, low-energy subtrochanteric femoral fractures has led to suggestions that long-term bisphosphonate use may indeed have a negative clinical indication in a sub-population of patients undergoing therapy [29, 30].

Several mechanisms governing the accumulation of bone microdamage under extended bisphosphonate therapy have been proposed. Reduced bone remodeling and the associated effects of increased bone age may lead to alterations in both collagen and mineral which could predispose the bone to greater formation of microdamage. Reduced turnover has been associated

with accumulation of altered collagen cross-linking [122-124], increased tissue mineralization [125, 126], and reduced microstructural interfaces [127, 128], all of which may make the skeleton more prone to the generation or propagation of tissue damage. Alternatively, direct interference with osteocyte apoptosis induction [129-132], apoptotic activation of osteoclast-stimulating pathways [133, 134], or the targeting and repair of damage by osteoclasts themselves [40] will likely lead to the accumulation of damage in the skeleton. Bisphosphonates not only inhibit osteoclast activity directly, but also inhibit osteocyte apoptosis in the presence [27, 135] and absence [132, 136, 137] of microdamage, thus potentially modulating microdamage repair at multiple levels.

A direct localization of bisphosphonates at the site of microdamage has not yet been visualized. Vascular perfusion studies have shown that fluorescent contrast agents can pool at microcracks and nearby surrounding osteocytes [138, 139]. However, it has not been shown whether these sites

are permissible for local bisphosphonate binding. If this were the case, this would suggest a potential for both direct and indirect effects of bisphosphonates on modulating targeted microdamage repair. Recently, we have demonstrated the use of bisphosphonates labeled with near-infrared fluorophores for the local detection and quantification of bisphosphonates in vivo, ex vivo, and in histologic sections [140, 141]. The purpose of this study is to visualize local bisphosphonate binding to bone microdamage and surrounding osteocyte lacunae as well as to investigate the impact of extended bisphosphonate treatment on osteocyte apoptosis in a model of bone microdamage. In particular, we have chosen to apply this in normal bone as well as bone that is susceptible to the generation and accumulation of bone microdamage via a collagen mutation resulting in a brittle, osteogenesis imperfecta-like phenotype [15, 86]. We hypothesize that microcracks and their surrounding osteocyte lacunae are particularly prone to direct bisphosphonate binding. Additionally we will test whether or not

extended treatment with bisphosphonates will lead to a suppression of osteocyte apoptosis around areas of microdamage. We further seek to determine whether the alterations in collagen composition characteristic of osteogenesis imperfecta can alter the distribution of drug to microcracks and their surrounding osteocytes. If successful, these findings may have implications for understanding the association of bisphosphonates and microdamage with the emerging findings of atypical fractures in osteoporotic patients treated with bisphosphonates, as well as have potential implications for OI patients who may be particularly susceptible to the generation of microdamage due to matrix alterations in collagen and mineral.

4.2 Materials and Methods

4.2.1 Murine Models

A total of 17 Brtl/+ and 20 WT mice were used for this study. Brtl/+ mice have a mixed background of Sv129/CD-1/C57BL/6S and are bred by crossing heterozygous Brtl/+ with WT [38]. All procedures used in this study were approved by the University Committee on Use and Care of Animals (UCUCA) at the University of Michigan. Three additional Brtl/+ mice were used as staining controls to determine threshold levels for imaging.

4.2.2 Bisphosphonate Treatment

For the WT and Brtl/+ treated groups investigating the effects of bisphosphonate treatment on osteocyte apoptosis, the bisphosphonate Alendronate (Aln) was injected subcutaneously at 0.219 mg/kg in PBS, once per week from 3 to 8 weeks of age. We chose this dosage to match earlier

Alendronate treatment studies in the Brtl/+ mouse [58]. Earlier studies in the oim mouse demonstrated that this dosage was the lowest concentration required to increase mineralization and prevent resorption [87]. Untreated mice received no injections at any time point.

4.2.3 Cyclic Loading

Mouse ulnae were loaded according to a previously established protocol [86] with the aim of generating microdamage. Earlier measurements were taken to attain the strains of treated and untreated specimens. Treated specimens were loaded to approximately 3000 microstrain on the mid-diaphyseal ulna, while untreated specimens were loaded to approximately 4000 microstrain. At 8 weeks of age, animals were anesthetized with 2% isoflurane and prepared for loading. The right forearms of Brtl/+ and WT mice were cyclically loaded across the olecranon and carpus [40, 41] at 1 Hz for 1800 cycles (30 minutes) following a 300 cycle (5 minute) preconditioning phase. During the unloading segment, a

minimum compressive load of approximately 400-500 micro strain was maintained to preserve limb orientation within the loading device.

4.2.4 Fluorescent Bisphosphonate (FRFP) Administration

Upon the conclusion of loading, a cohort of mice untreated with bisphosphonate (n=6 WT and n=6 Brtl/+) were administered a single dose of the far-red fluorescent pamidronate (FRFP) Osteosense 680 (Perkin Elmer, U.S.A.) while still under general anesthesia. The administered dosage was 4nmols of FRFP per 20 grams body mass buffered in PBS in a total injection volume of 150 μL via tail vein injection. Mice were then allowed to recover and resume normal ambulation. Food and water was administered ad libitum. Mice were then subsequently euthanized 24 hours after loading.

4.2.5 In-Vivo Apoptosis Marker (AV750) Administration

In order to measure apoptosis levels in bones, the in-vivo apoptosis marker Annexin-Vivo 750 (AV750) (PerkinElmer) was tail-vein injected in

a cohort of treated (n=6 WT and n=4 Brtl/+) and untreated (n=8 WT and n= 7 Brtl/+) mice immediately after loading was completed while under anesthesia. These mice were a separate cohort than the mice injected with FRFP in the previous section. AV750 solution was pre-mixed by PerkinElmer, and was administered unadulterated using the recommended dosage of 100 μL per mouse. AV750 is supplied in 1000 μL of 25 mM Hepes/NaOH, 140 mM NaCl at a molecular weight of 35kg/mol^{-1}. Mice were then allowed to recover and ambulate but were euthanized 2 hours later using CO_2 based on manufacturer suggested protocols.

4.2.6 Verification of In-Vivo Apoptosis Marker

In order to ensure that the in-vivo apoptosis marker AV750 is in fact staining apoptotic regions, an adult mouse was injected with AV750 and then euthanized 2 hours later. Briefly, tibias were excised, fixed in 10% NBF, dehydrated in a graded series of alcohol and subsequently embedded undecalcified in poly methyl methacrylate (PMMA) for histology. Using a

Buehler Isomet diamond-blade saw, 400 µm sections were then cut parallel to the longitudinal axis of the tibia. These sections were mounted on a plastic microscope slide and polished to a final thickness of 100 µm. Sections were cover slipped and viewed using a 2-Photon Leica confocal inverted microscope system (SP5X Zeiss Confocal Microscope, Carl Zeiss MicroImaging, Inc., Thornwood, NY, U.S.A.), at 40X objective to identify hypertrophic chondrocytes at the proximal tibial growth plate. The AV750 was imaged using an excitation laser of 670nm with an emission range of 700-790 nm. **(Figure 4-1 G-I).** Control images were also taken to ensure limited auto fluorescence and signal bleed through **(Figure 4-1 J-L).**

Annexin-Vivo 750 signals at the tibial growth plate region were compared against tibial growth plate sections stained with a terminal deoxynucleotidyl transferase-dUTP nick end labeling (TUNEL) assay, which is the gold-standard for *in situ* apoptosis signaling and imaging **(Figure 4-1 A-C)**. Briefly, the tibias of an adult mouse were excised, fixed

in 10% NBF, decalcified and embedded in paraffin. Longitudinal 7 μm sections of the tibia were subsequently taken using a Reichert-Jung microtome. Sections were then de-parrafinized and stained with TUNEL/Hoechst using the Click-iT TUNEL Alexa Fluor Imaging Assay (Molecular Probes, Invitrogen Detection Technologies, Eugene, OR U.S.A). Specimens were then imaged using the above mentioned 2-Photon Leica confocal using Invitrogen's recommended excitation of 590nm and emission of 670nm. Control images were taken to ensure limited auto fluorescence and signal bleed through **(Figure 4-1 D-F)**

4.2.7 FRFP Imaging Protocol

Loaded forelimbs were excised and stained with 1% basic fuchsin using an established protocol [45] and rinsed in 100% ethanol. Samples were subsequently embedded undecalcified in poly methyl methacrylate (PMMA) for histology. Using a Buehler Isomet diamond-blade saw, 400 μm sections

were then cut transverse to the longitudinal axis of the ulna. These sections were mounted on a plastic microscope slide and polished to a final thickness of 100 µm. Sections were cover slipped and viewed using a 2-Photon Leica confocal inverted microscope system (SP5X Zeiss Confocal Microscope, Carl Zeiss MicroImaging, Inc., Thornwood, NY, U.S.A.), to identify bone areas stained with FRFP and basic fuchsin. A 40X oil immersion objective was used in this study. To determine an approximation of the excitation and emission curves for both dyes, lambda scans were performed on cortical control specimens using the white light laser of the 2-Photon microscope. The first scan was performed on a specimen stained with basic fuchsin only, whilst the second scan was done on a FRFP stained sample. Excitation scans were performed in increments of 5nm between 480 nm and 670 nm whilst emission scans were performed in increments of 5nm between the range of 500 nm and 800 nm. In order to image the basic fuchsin, an excitation of 543nm was used, with an emission range of 553-613nm **(Figure 4-3)**. The

FRFP was imaged using an excitation laser of 670nm with an emission range of 700-750 nm **(Figure 4-3)**. These parameters were held constant for all images and ensured limited signal bleed through to the opposing channels.

4.2.8 FRFP Image Analysis and Staining Thresholds

All images were scored using the pixel intensity tool provided by the public domain software ImageJ (National Institutes of Health). In order to validate the detected FRFP signal, a basic fuchsin control specimen was imaged under FRFP excitation and emission to determine the degree of crosstalk of basic fuchsin dye into the FRFP channel. It was determined from this analysis that there was a 2.3:1 false signal to background ratio for basic fuchsin bleedthrough. Therefore, in order to deem a region as positively stained for FRFP, a signal to background ratio threshold of 7:1 was applied. When the FRFP only specimen was viewed under the basic fuchsin imaging conditions, it was observed that there was negligible

crossover of FRFP into basic fuchsin images. As a result, a 3:1 signal to background ratio was used to determine a positive staining for basic fuchsin. Any objects of interest that were less than these established signal to background ratios were deemed unstained for their respective dyes.

4.2.9 FRFP Co-Localization Assessment

To determine the degree of FRFP binding to microdamaged regions, the co-localization of FRFP and basic fuchsin to both micro cracks and the surrounding osteocytes were assessed using the following equations:

$$\%\ \text{Co} - \text{Localized Crack Length} = \frac{\text{Length of dual stained crack}}{\text{Length of basic fuchsin stained crack}}$$

$$\%\ \text{Co} - \text{Localized Osteocytes} = \frac{\text{Number of dual stained osteocytes}}{\text{Number of basic fuchsin stained osteocytes}}$$

A 50 micron region of interest was established around each crack to assess osteocytes in the vicinity of microdamage. Regions of interest at least

50 μm away from any microdamage sites were chosen and analyzed to determine the degree of osteocyte co-localization in non-damaged regions.

4.2.10 Annexin-Vivo Confocal Microscopy Parameters

After euthanasia both loaded and unloaded forelimbs were excised and fixed in 10% neutral buffered formaldehyde. Bones were then stained with 1% basic fuchsin using an established protocol [45] and rinsed in 100% ethanol. Samples were subsequently embedded undecalcified in poly methyl methacrylate (PMMA) for histology. Using a Buehler Isomet diamond-blade saw, 400 μm sections were then cut transverse to the longitudinal axis of the ulna. These sections were mounted on a plastic microscope slide and polished to a final thickness of 100 μm. Sections were cover slipped and viewed using a 2-Photon Leica confocal inverted microscope system (SP5X Zeiss Confocal Microscope, Carl Zeiss MicroImaging, Inc., Thornwood, NY, U.S.A.), to identify bone areas stained with AV750 and basic fuchsin. A 40X oil immersion objective was used to capture images. To determine an

accurate imaging protocol, the excitation and emission curves for both dyes were determined. Lambda scans were performed on cortical control specimens using the white light laser of the 2-Photon microscope. The first scan was performed on a specimen stained with basic fuchsin only, whilst the second scan was done on an AV750 stained sample. Excitation scans were performed in increments of 5nm between 480 nm and 670 nm whilst emission scans were performed in increments of 5nm between the range of 500 nm and 800 nm. In order to image the basic fuchsin, an excitation of 543nm was used, with an emission range of 553-613nm. The AV750 was imaged using an excitation laser of 670nm with an emission range of 700-790 nm. These parameters were held constant for all images and ensured limited signal bleed through to the opposing channels.

4.2.11 Apoptosis Image Analysis

All images were scored using the pixel intensity tool provided by the public domain software ImageJ (National Institutes of Health). In order to

validate the detected AV750 signal, a basic fuchsin control specimen was imaged under AV750 excitation and emission to determine the degree of crosstalk of basic fuchsin dye into the AV750 channel. It was determined from this analysis that there was a 2.8:1 false signal to background ratio for basic fuchsin bleedthrough. Therefore, in order to deem a region as positively stained for AV750, a signal to background ratio threshold of 8:1 was applied. When the AV750 only specimen was viewed under the basic fuchsin imaging conditions, it was observed that there was negligible crossover of AV750 signal into basic fuchsin images. As a result, a 3:1 signal to background ratio was used to determine a positive staining for basic fuchsin. Any objects of interest that were less than these established signals to background ratios were deemed unstained for their respective dyes.

4.2.12 Gray Value Threshold Affirmation and Distinguishing of Osteocyte Lacunae

In order to quantify osteocytes in co-localized AV750 and basic fuchsin images, images were analyzed using the Leica LAS AF Image Browser (Version 2.6.0 Build 7266, Leica Microsystems CMS, Inc.) Using only the basic fuchsin channel, this software allows the user to trace out numerous regions of interests (ROI) in the image. Each individual osteocyte lacunae of interest, as identified by basic fuchsin staining around the lacunar wall of small elliptically shaped cells, was traced out in the basic fuchsin channel. A report sheet is then generated by the software that allows the user to see the maximum gray value within each ROI. This analysis is also automatically generated for the AV750 channel. Lacunae that were above the 3:1 threshold were counted as positive ROI's and if the corresponding AV750 ROI surpassed the 8:1 threshold, then it was counted as positively

stained for AV750. Similar techniques were used when analyzing both damage and non-damaged regions.

4.2.13 Apoptosis Quantification

To determine the degree of AV750 binding to osteocyte lacunae surrounding microdamage, the co-localization of AV750 and basic fuchsin to surrounding osteocyte lacunae were assessed using the following equation:

$$\%\ \text{Co} - \text{Localized Osteocytes} = \frac{\text{Number of dual stained osteocytes}}{\text{Number of basic fuchsin stained osteocytes}}$$

A 50 µm region of interest was established around each crack to assess osteocyte lacunae in the vicinity of microdamage. Regions of interest at least 50 µm away from any microdamage sites were chosen and analyzed to determine the degree of osteocyte lacunae co-localization in non-damaged regions. 50 µm was chosen to ensure that both a damaged region, as well as

a non-damaged region could be adequately imaged within the same field of view of the 40X objective, thus minimizing potential artifact from image acquisition parameters between fields.

4.2.14 Statistical Analysis

Differences between Brtl/+ and WT in the percentage of osteocytes co-localized with FRFP and basic fuchsin, and the average percentage of crack lengths co-localized with FRFP and basic fuchsin were assessed by t-test. Fisher's exact test was used to compare genotype differences in the proportion of cracks positively labeled with FRFP. Differences between treated and untreated in average percentages of osteocytes co-localized with AV750 and basic fuchsin were also assessed using t-test. Analyses were performed using GraphPad Prism 4.0. Differences were considered significant at $p<0.05$, and data are presented as mean $\pm$ standard deviation.

4.3 Results

4.3.1 Brtl/+ microcracks demonstrate higher affinity for FRFP

FRFP binds avidly to portions of microcracks and surrounding osteocyte lacunae, with overlapping fluorescence with basic fuchsin at multiple sites **(Figure 4-2)**. Brtl/+ specimens demonstrate a higher percentage of crack length co-localized with FRFP and basic fuchsin (66%), as compared to WT (24%) ($p<0.05$) **(Figure 4-4, Table 4-1)**. One particular Brtl/+ micro crack had a longer FRFP label than its basic fuchsin labeling, leading to a 127% co-localization percentage. Sixteen out of 18 (89%) cracks for Brtl/+ were positively labeled with FRFP (Table 1). In contrast, 12 out of 23 (52%) WT cracks showed positive labeling with FRFP (Table 1). There were, however, two cases in WT where cracks were labeled only with FRFP and were not stained with basic fuchsin. Therefore, these two cases were excluded from our calculations of average percentage of co-

localized crack lengths in WT, as their inclusion would obscure the numerical analysis.

4.3.2 WT osteocyte lacunae demonstrate high affinity for FRFP near damaged regions

WT specimens demonstrate a higher percentage of osteocytes co-localized with basic fuchsin and FRFP (41%) than their Brtl/+ counterparts (20%) ($p<0.05$) **(Figure 4-5, Table 4-1)**. Furthermore, 4 out of 17 cracks analyzed for Brtl/+ (23.5%) had none of their surrounding lacunae stained with FRFP. In contrast, only 1 out of the 23 cracks (4%) for WT showed no binding of FRFP to any of their surrounding osteocytes **(Table 4-1)**.

4.3.3 WT and Brtl/+ display similar levels of FRFP o-localization in non-damaged regions

A region of interest at least at least 50 microns away from any damaged regions was used to analyze non-damaged osteocytes. Analysis of

these osteocytes showed that both WT (n=17 images) and Brtl/+ (n=12 images) specimens displayed similar levels of FRFP binding (29.26% and 29.93% respectively) **(Table 4-1)**.

4.3.4 WT and Brtl/+ display similar vascular and osteocyte lacunae densities

In order to determine if there were any additional factors that could potentially impact drug delivery to microdamage sites, the vascular and osteocyte lacunae densities were calculated for each crack. These densities were assessed within the field of view that the image of the crack was taken. Osteocyte lacunae were defined in basic fuchsin images as small elliptically shaped regions which had void spaces in the middle and had basic fuchsin staining on the perimeter (lacunae wall). Osteocyte lacunae are typically 40μm^2 in cross sectional area. Vascular spaces possessed a more fully rounded structure and had very little if any void spaces. These spaces were typically all stained with basic fuchsin and were about 250 μm^2 in cross

sectional area **(Figure 4-6).** All osteocyte lacunae and vascular supplies were counted and areas were calculated using ImageJ. Results show that there were no significant differences in either osteocyte densities in Brtl/+ versus WT (998.9 ± 290.3 osteocytes/mm^2 and 1119.9 ± 160.2 osteocytes/mm^2 respectively; p = 0.1) or vascular densities in Brtl/+ versus WT (28.1 ± 18.5 vessels/mm^2 and 21.7 ± 9.7 vessels/mm^2 respectively; p = 0.16).

4.3.5 Osteocyte apoptosis spatial distribution around peri-damaged regions

AV750 localized to the regions within the osteocyte lacunae, which suggests that they localized to osteocytes **(Figure 4-7).** When pooled together, treated specimens demonstrate a lower percentage of osteocyte lacunae undergoing apoptosis (22.1%) than their untreated counterparts (35.7%) ($p<0.05$) in regions within 50 μm of a crack **(Figure 4-8 and Table 4-2)**. There is also a significant increase in the amount of osteocyte apoptosis

in Brtl/+ untreated specimens surrounding microdamage (45.3%) when compared to WT untreated specimens (25.8%)($p<0.05$) **(Figure 4-8 and Table 4-2)**. Additionally, there is an increased level of osteocyte apoptosis surrounding Brtl/+ untreated specimens (45.3%) when compared to Brtl/+ treated specimens (26.9%) ($p<0.05$).

4.3.6 Apoptosis spatial distribution around non-damaged regions

Brtl/+ untreated specimens had higher levels of osteocyte apoptosis away from damage (28.17%) than non-damage areas in Brtl/+ treated specimens (19.48%) ($p<0.05$). However, there was no significant difference seen in osteocyte apoptosis levels when comparing WT non-damaged treated regions (10.75%) and WT non-damaged untreated specimens (9.13%).

When comparing across genotypes, there was a significant increase seen in the amount of apoptotic osteocytes away from damage in Brtl/+ untreated specimens versus WT untreated specimens ($p<0.05$). A similar

increase in apoptotic osteocytes was seen in treated Brtl/+ non-damaged regions when compared to treated WT non-damaged regions ($P<0.05$).

When pooled together, there was a significant increase in the amount of osteocyte apoptosis seen near damage in untreated specimens (34.5%) when compared to treated specimens (22.1%) ($p<0.05$). However, there was only a trend towards a decrease in apoptosis in regions away from damage in treated specimens (14.8%) when compared to untreated specimens away from damage (19.0%) ($p=0.153$) **(Figure 4-8 and Table 4-2)**

4.4 Discussion

In this study we demonstrated, using a fluorescent-labeled bisphosphonate, that microcrack surfaces and surrounding osteocytes are prone to local bisphosphonate binding. Additionally, using the in-vivo fluorescent marker Annexin-Vivo 750, we showed that following 5 weeks of treatment with the bisphosphonate Alendronate, apoptosis levels surrounding microdamage were decreased in treated specimens as compared

to untreated specimens. Annexin-Vivo 750 has been used in other applications before [142-144], but to our knowledge, this is the first application to bone tissue. Bisphosphonates are commonly used for the treatment of low bone mass. However their use has also been suggested to affect the amount of skeletal microdamage, both by altering the tissue material properties (e.g. through alterations of collagen cross-linking, increased tissue mineralization, and reduced microstructural interfaces), thereby leading to greater microdamage accumulation, as well as by direct interference with osteoclast repair of damaged tissue. This suggests that bisphosphonates could potentially regulate microdamage repair at multiple levels. The current study demonstrates that bisphosphonate may interfere with targeted microdamage repair directly by binding to microcrack surfaces and interfering with osteoclast repair at the site that needs it the most. Additionally, our results suggest that bisphosphonates may interfere with targeted repair indirectly by binding to the surrounding osteocyte lacunae of

microdamage, thus suppressing the apoptotic signal required to induce targeted remodeling. With decreased fracture incidence being a crucial element in the quality of life of bisphosphonate treated patients, the implications of arrested microdamage repair are significant.

In order to prevent detrimental accumulation of microdamage in healthy bone, damage can either be remodeled stochastically or through targeted repair. The effect of bisphosphonates on damage repair is multi-faceted as it affects the induction of osteocyte apoptosis [129-131], the apoptotic activation of the osteoclast-stimulating pathways [133, 134], and the eventual targeting and repair of damage by osteoclasts themselves [40]. The efficacy of bisphosphonates in treating bone fragility [18-23] cannot be ignored, however, there is a concern regarding the long-term effects of bisphosphonates on the inhibition of targeted repair of skeletal microdamage. Extended bisphosphonate treatment has been correlated with observations of increased skeletal microdamage in animal models [24-27],

which may in turn have detrimental effects on the bone's mechanical integrity [24-26, 28]. To date, there has been no direct relationship to link extended bisphosphonate therapy with atypical, low-energy subtrochanteric femoral fractures observed in osteoporotic patients undergoing treatment [29, 30]. The results of the present study suggest that the binding of bisphosphonates to microdamage and the surrounding osteocytes may lead to arrested microdamage repair and could represent a contributing factor toward these subtrochanteric femoral fractures. Furthermore, these observations could also have strong implications for fracture prone osteogenesis imperfecta (OI) patients on bisphosphonates who may be more susceptible to microdamage accumulation as suggested by animal models [17, 31]. With both OI and osteoporosis patients being increasingly susceptible to critical bone failure, any treatment modalities that potentially affect damage repair needs to be carefully assessed.

In this study, we used the Brtl/+ mouse which is a heterozygous model for type IV OI [38]. The genotype arises from a Gly349Cys substitution in COL1A1, and demonstrates a low ductility phenotype [15]. Wild type (WT) specimens were used as a model to determine the effects of bisphosphonate binding in bone with unaffected collagen. Brtl/+ ulnae, subjected to similar strain matched loads as their WT counterparts, demonstrated higher levels of FRFP co-localization to micro cracks. The opposite was true for osteocytes in the immediate surrounding regions of micro cracks, as Brtl/+ specimens had a lower percent FRFP osteocyte co-localization than their WT counterparts. This data suggests that there may be mechanisms that allow Brtl/+ cracks to serve as depositories for FRFP.

Damage to bone tissue has been shown to alter interstitial fluid flow in the surrounding areas and vascular tracer studies have shown that these agents tend to pool in these areas [138, 139]. Tami et al. provided several analytical scenarios to describe the nature of cracks and their effect on

surrounding lacunae [138]. The first of these mechanisms is a crack acting as a reservoir for mass and fluid flow. In this proposed mechanism, a crack serves as an additional fluid space in the lacunocanalicular network, leading to a much slower increase in concentration up-stream from the crack. The second such mechanism is that of a crack serving as a wall. Here, the crack essentially occludes fluid flow to osteocytes down-stream of the crack, whilst regions up-stream experience an increase in concentration. In the third scenario, where a crack can function as a sink, the crack prevents fluid flow to the down-stream osteocytes similar to a wall, with the notable exception that volume flow and the concentration of molecules are decreased up-stream from the crack [138].

In the present study, both WT and Brtl/+ osteocytes exhibit similar degrees of FRFP binding in regions away from damage. However, the introduction of microdamage has contrasting effects on the surrounding osteocytes of both genotypes. When looking at the damaged regions, 24% of

Brtl/+ cracks analyzed functioned as walls for their respective osteocytes, as there was no binding of FRFP to any of the surrounding osteocytes. Conversely, 4% of WT cracks served as walls. Thus the remaining cracks in both WT and Brtl/+ could either function as reservoirs or sinks. We can infer from our data that the majority of these remaining cracks likely served as sinks, as both WT and Brtl/+ showed large percentages of osteocytes that did not express co-localization of FRFP. In these situations, most, but not all of the FRFP was prevented from being delivered to the regions surrounding damage.

When comparing the non-damaged regions of WT specimens to the damaged regions, it appears that there is a spatial preference towards an accumulation of FRFP around regions of cracks. This is seen from the 10% increase in osteocyte co-localization in damaged regions compared to non-damaged regions. The reverse is true for Brtl/+, as there is a 10% decrease in osteocyte co-localization at areas surrounding damage. It is possible that

WT cracks are less permeable than their Brtl/+ counterparts, and may be acting as a wall, thus leading to an increase in FRFP in the surrounding osteocytes. Brtl/+ cracks on the other hand appear to act as depositories and seem to be more permeable, thus showing lower co-localization of FRFP labeling of osteocytes surrounding Brtl/+ microcracks than WT.

These observations pose interesting questions regarding targeted microdamage repair and the role that bisphosphonates play in this repair process. While the intention for treatment with bisphosphonates is to increase skeletal mass, they may concomitantly prevent targeted repair from occurring on two separate fronts. The first of which is the prevention of osteocyte apoptosis [40, 129, 145], which has been proposed as one of the important first steps in the targeted bone remodeling process. It has been shown that a damaged osteocyte-canalicular system (through microcracks for instance) will result in osteocyte apoptosis, followed by the recruitment or activation of osteoclasts. This process would conclude with the eventual

resorption and repair of damaged regions in bone [40]. Prevention of this activating first step by inhibiting osteocyte apoptosis could lead to a decreased rate of repair. The second front on which bisphosphonates potentially affect microdamage repair is through inhibition of osteoclast remodeling. Bisphosphonates bind to bone, and upon uptake by osteoclasts during the resorption process, result in cell toxicity, thus reducing bone turnover and increasing bone mass. While bisphosphonates globally downregulate stochastic bone remodeling across the skeleton, the present results support the notion that bisphosphonates bind directly to microcrack surfaces and may directly inhibit bone turnover at the site of microdamage itself. This could inherently lead to an unrepaired crack that is allowed to propagate without repair, resulting in critical crack length growth and subsequent failure.

When data for WT treated and Brtl/+ treated specimens were pooled together and compared to pooled data for WT untreated and Brtl/+ untreated

specimens, a significant difference was observed in the levels of apoptotic osteocytes surrounding microdamage. Treated microcracks possessed lower levels of apoptotic osteocytes than their untreated counterparts. This data is supported by other studies that have shown Alendronate suppressing osteocyte apoptosis following cyclic fatigue loading [129, 146]. Furthermore, the observation of increased levels of osteocyte apoptosis observed in Brtl/+ untreated specimens both near and away from damage when compared to WT untreated specimens raises a few questions. Studies have demonstrated a disproportionate up-regulation of osteoclast and osteoblast activity in OI patients, with an overall imbalance favoring osteoclast resorption [13, 14]. It is not fully understood the physiological reasons for this, but our observations of increased osteocyte apoptosis surrounding Brtl/+ cracks raises the possibility that osteocyte apoptosis may also be up-regulated concomitantly.

As microdamage levels increase in a healthy individual, the inherent remodeling processes of bone are activated for microdamage repair [66]. The increased up-regulation of osteocyte apoptosis surrounding microcracks in Brtl/+ could be a function of a genetically caused whole body increase, or could be the Brtl/+ mouse's way of trying to repair microdamage through specific targeting of damage. When data for treated specimens was pooled together, it was observed that the amount of osteocyte apoptosis away from damage was only marginally lower than the amount of osteocyte apoptosis in non-damaged regions for untreated specimens (19.0% vs. 14.8%). The amount of osteocyte apoptosis seen away from damage is similar to the levels seen in work done by Verborgt et al. who showed about 15% of osteocytes imaged being TUNEL positive for apoptosis [129]. It is likely, that even though bisphosphonates may inhibit osteocyte apoptosis, the lack of microdamage in these areas would result in a lack of apoptosis of osteocytes. Thus the presence of bisphosphonates under these conditions is

likely to only have marginal effects on preventing any normal apoptosis that would be occurring in the non-damaged bone tissue. This data supports the notion that microdamage is necessary to induce osteocyte apoptosis.

Studies have shown that as the Brtl/+ mouse ages, a cellular uncoupling leads to a decline in bone formation [16]. During this process there is an increase in osteoclast number and function, whilst osteoid production by osteoblasts is reduced. While the cellular asynchrony favoring osteoclast formation and activity in Brtl/+ is a result of an increase in osteoclast precursors in the Brtl/+ marrow [16], the RANKL/OPG ratio is unchanged and the factors regulating increased osteoclasts have yet to be described. However, there have been studies that have postulated and demonstrated that viable osteocytes do in fact play a role in suppressing osteoclastic attack [147-152]. It is possible that the decreased levels of osteocyte viability demonstrated through increased levels of osteocyte apoptosis in the Brtl/+ mouse could result in the increased levels of

osteoclast activity and thus subsequent elevated levels of osteoblast activity. It is unknown whether the increased levels of microdamage seen in the Brtl/+ mouse explains the elevated levels of osteocye apoptosis observed, however it still remains unclear the specific physiological reasons for this. There is evidence in humans that apoptotic osteocytes are more common in young growing bone experiencing a high degree of resorption than in relatively quiescent normal adult human bone [153]. The same could be applicable to the Brtl/+ mouse at 8 weeks of age, but the question as to why apoptosis levels in Brtl/+ is higher than WT remains.

Our data shows that Brtl/+ cracks have significantly more binding of FRFP (66%) than their WT counterparts (24%). It is possible that this may result in a protective mechanism for Brtl/+ bones by preventing the delivery of bisphosphonate to surrounding osteocytes. This could potentially allow osteocyte apoptosis, and thus osteoclast activation, to occur normally, but at the expense of greater inhibition of remodeling downstream. This may only

suffice for short and low dose bisphosphonate treatments as our apoptosis evidence suggests that with extended treatment, bisphosphonates are eventually metabolized by Brtl/+ osteocytes resulting in the prevention of their apoptosis in areas surrounding microdamage. The presence of bone microdamage has been shown to result in a decrease in lacunocanalicular interstitial fluid flow, which over time has been implicated in the increase of remodeling activity [154]. It is unclear whether the increased remodeling activity seen in Brtl/+ [16] is caused by an increase in inherent microdamage [17], but the presence of bisphosphonates could potentially obstruct the natural processes that Brtl/+ deploys to repair its damage.

We observed that treated Brtl/+ cracks had lower levels of osteocyte apoptosis than their untreated counterparts. We suspect that delivery of bisphosphonate to these osteocytes may have increased over time as Brtl/+ cracks quickly became saturated with bisphosphonate. This then likely resulted in osteocytes being the eventual depositories of the bisphosphonate.

Furthermore, we observed an insignificant decrease in osteocyte apoptosis levels between WT treated and WT untreated cracks. It is possible that the WT cracks may have absorbed bisphosphonates during the treatment protocol, thus preventing excessive absorption in the surrounding osteocytes. It is unclear however how much bisphosphonate is actually necessary to initiate an anti-apoptotic response and at what time point this is actually initiated in the treatment protocol. It is apparent however that in the case of Brtl/+, bisphosphonates appear to be potentially suppressing apoptosis of the osteocytes and could be preventing the first step in potential microdamage repair [129]. In fact, in both WT and Brtl/+, treatment with bisphosphonate appears to bring apoptosis levels near damage and away from damage to similar levels, as no significant differences were observed when comparing these two regions in both genotypes. Even though it is unclear whether targeted microdamage remodeling is present in mice, the implications in OI

patients could be significant, as bisphosphonates could be suppressing the body's attempt of damage repair [129, 147].

Studies have shown that bisphosphonate binding and depth of penetration once leaving the vasculature is strongly impacted by the degree of mineralization [155, 156], with lower affinity bisphosphonates penetrating deeper into the cortical bone canalicular network, including the lacunae[157]. Small differences in Brtl/+ and WT mineralization [88] may be responsible for the observed differences in bisphosphonate binding between genotypes. Alternatively, differences in microstructural features such as lacuno-canalicular connectivity or microdamage complexity may alter local availability of surface binding sites. We found no significant differences between osteocyte density and vascular channel density between Brtl/+ and WT in these studies, suggesting minimal effect of these parameters on drug delivery.

The observations of this study pose interesting questions regarding targeted microdamage repair and the role that bisphosphonates play in this process. While the intention of treatment with bisphosphonates is to increase skeletal mass, the current findings suggest that bisphosphonates may have the potential to prevent targeted repair from occurring on two separate fronts. Osteocyte apoptosis, induced following damage to the osteocyte-canalicular system, has been shown to be required for the activation of osteoclasts during targeted microdamage repair [129-131, 158]. However, bisphosphonates have been shown to inhibit osteocyte apoptosis in the presence [27, 135] and absence [132] of microdamage. Our current findings suggest that bisphosphonate delivery to osteocytes near microdamage is consistent with the finding of reduced osteocyte apoptosis, and reduced microdamage repair as shown by others[135]. Secondly, while bisphosphonates globally downregulate stochastic bone remodeling across the skeleton, the present results support the notion that bone turnover may be

directly inhibited at the site of microdamage itself, leading to persistence, and possible propagation of the crack over time.

There were limitations to this study. When looking at a FRFP only specimen, one can discern finer details and more osteocytes than in a dual-stained specimen. Due to the slight overlap in emission spectra of both basic fuchsin and FRFP, a smaller band width had to be used for FRFP to delineate both dyes and prevent nonspecific basic fuchsin bleed through. This resulted in a higher threshold and thus a lower signal observed for FRFP and therefore an underestimation of the fluorescent bisphosphonate binding. It is important to note then, that the co-localization results shown in this study are a conservative representation of the data. Additionally, the fact that analysis of cracks was not confined to any one region of the ulna, but was rather analyzed throughout the cortex based on where damage itself was located, could lead to a spatial bias in results.

In summary, these findings suggest a dual mechanism for bisphosphonates to inhibit targeted microdamage repair, by binding to surrounding osteocyte lacunae, and potentially inhibiting osteocyte apoptosis required for osteoclast signaling, and by binding directly to the microcrack itself, potentially inhibiting bone resorption directly at the site that requires it the most. It remains to be seen whether these findings are associated with emerging evidence of low-trauma, atypical fractures in osteoporotic patients on extended bisphosphonate therapy, or whether the accumulation of microdamage in patients with OI may further facilitate bone fragility in the long run of that disease. The ability of bisphosphonates to bind directly to bone, and not circulate as other anti-resorptives such as calcitonin or denosumab, suggest that they may impart a unique interaction with microdamage that could potentially be avoided using non-matrix binding alternative therapies.

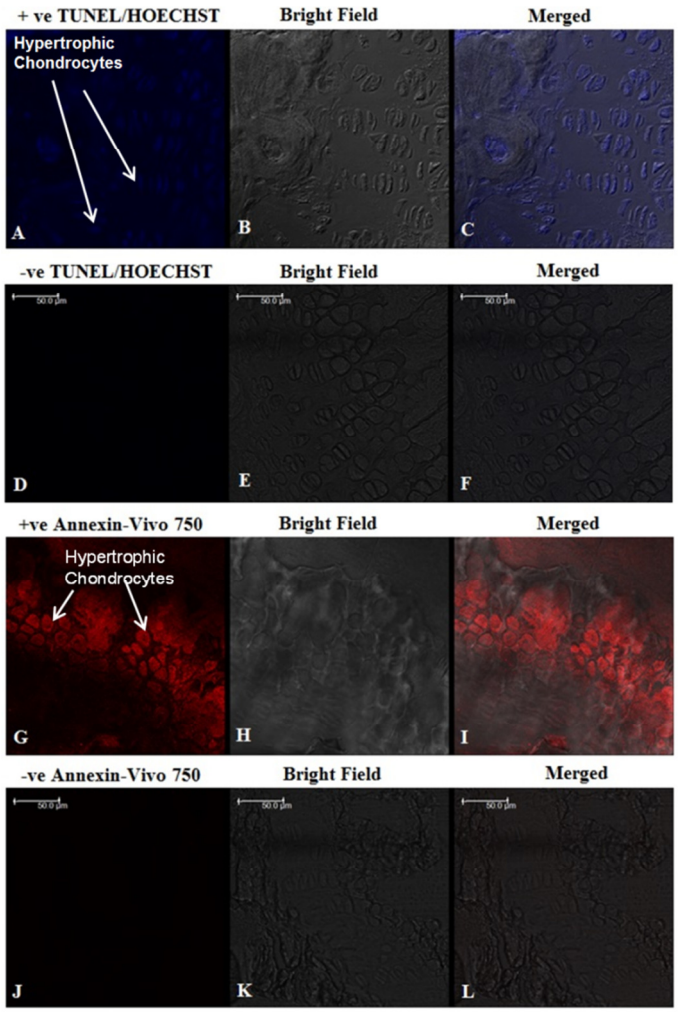

Figure 4-1: Annexin-Vivo 750 apoptosis verification

The signaling of hypertrophic chondrocytes demonstrates that Annexin-Vivo 750 (G-I) is in fact detecting an apoptotic signal. Hypertrophic chondrocytes are known to be apoptotic. This is verified against TUNEL/Hoechst staining which is the gold standard for apoptosis staining (A-C). Corresponding negative controls are attached to demonstrate limited bleed through and auto-fluorescence.

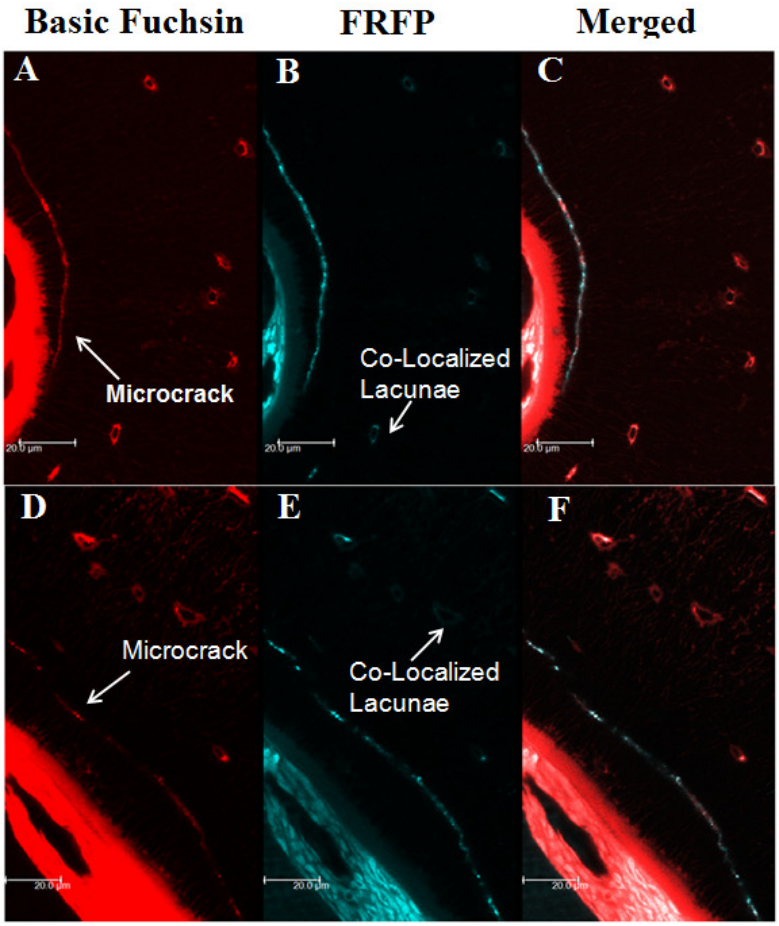

Figure 4-2: Local co-localization of FRFP and basic fuchsin

Image (A,D) showing basic fuchsin labeled crack and surrounding osteocyte lacunae, (B,E) the corresponding FRFP labeled image, and (C,F) a superimposed image of FRFP and basic fuchsin is also illustrated with labeled examples of co-localized osteocyte lacunae and co-localized microdamage. Note the binding of FRFP to the lacunar wall as opposed to the inner space.

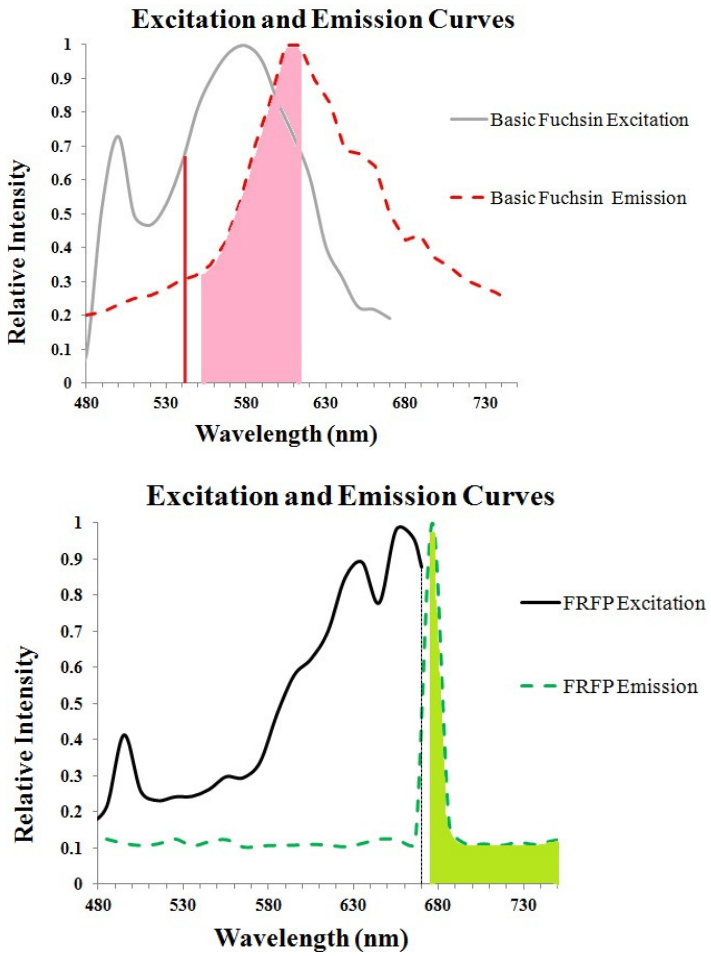

Figure 4-3: Excitation and emission spectra for basic fuchsin and FRFP

Excitation and emission spectra used during imaging of specimens stained with both basic fuchsin and FRFP ensuring limited signal overlap and bleedthrough.

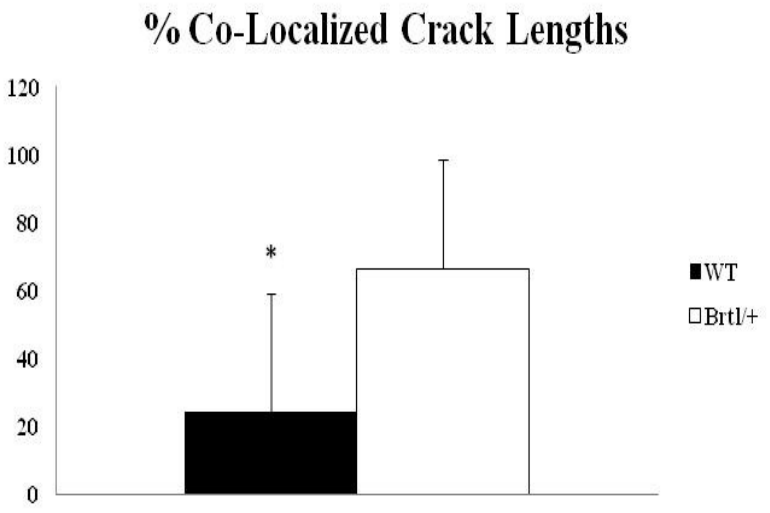

Figure 4-4: % co-localized crack lengths in WT and Brtl/+

Percentage of co-localized crack lengths in both WT and Brtl/+ specimens. $^{*}p<0.05$

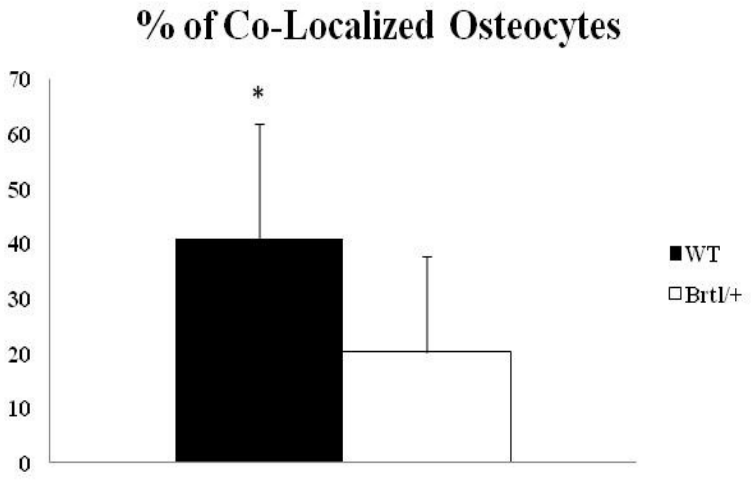

Figure 4-5: % co-localized osteocytes in both WT and Brtl/+

Percentage of co-localized osteocytes in both WT and Brtl/+ specimens near damaged regions. $^{*}p<0.05$

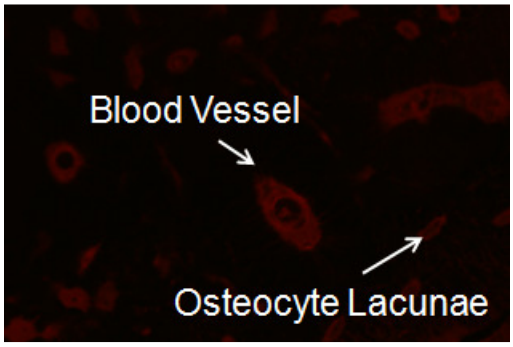

Figure 4-6: Blood vessel vs. osteocyte lacunae

Image showing the size and morphological differentiation between a blood vessel structure and an osteocyte lacunae. Vessel structures are approximately 250μm^2 in area whereas osteocyte lacunae are approximately 40 μm^2

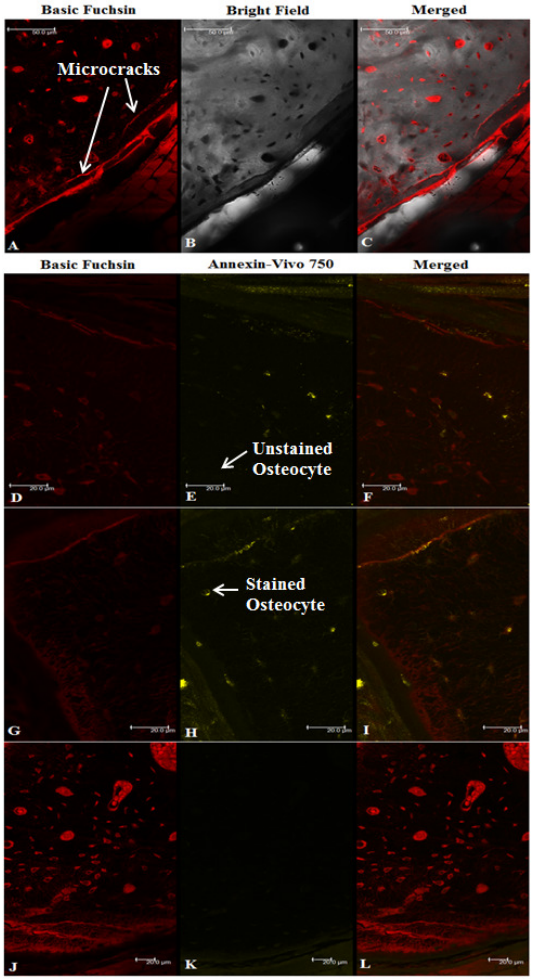

Figure 4-7: Microdamage and osteocyte apoptosis co-localization

Representative image of microdamage stained with basic fuchsin (A) and its corresponding bright field image (B). Panels D-L represent basic fuchsin stained cracks and osteocyte lacunae and Annexin-Vivo stained osteocytes which indicate apoptosis. Note the cellular nature of Annexin-Vivo, as seen by central localization within osteocyte lacunae. Panels J-L shows demonstrates that osteocytes closer to cracks are more stained than those further away.

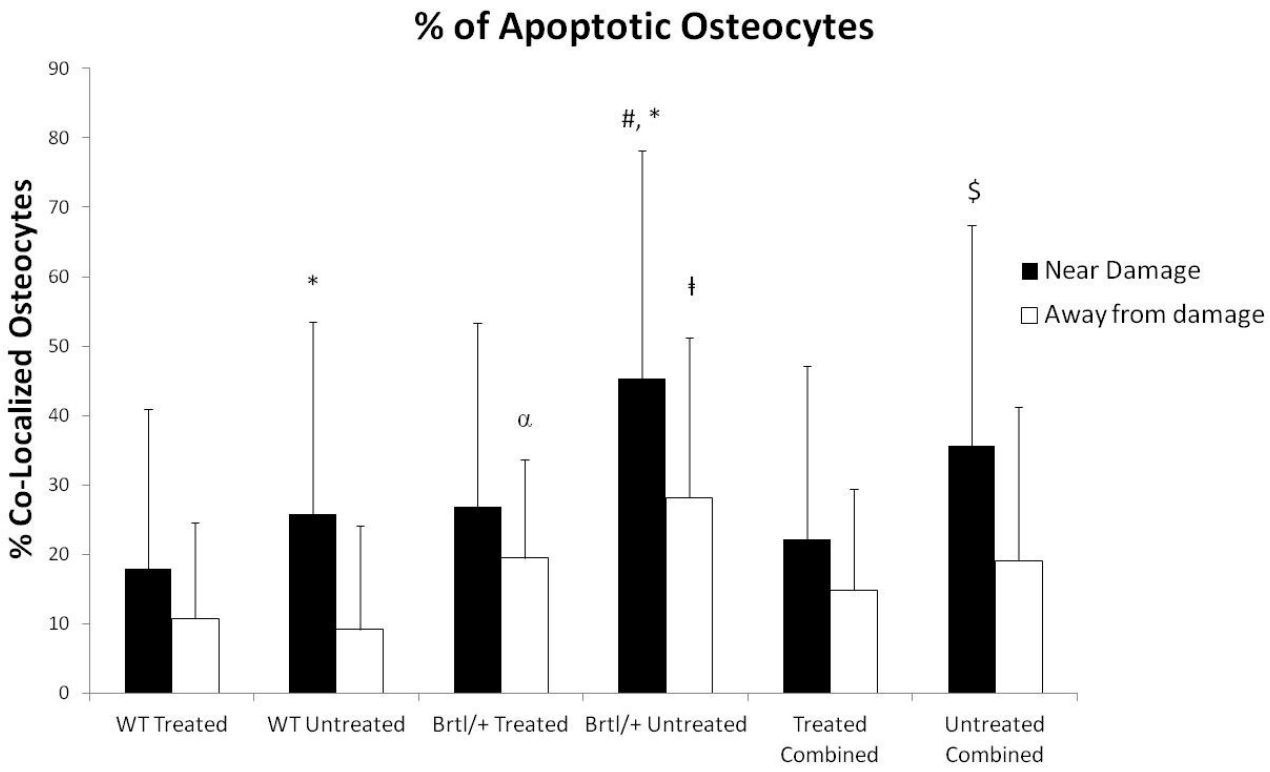

Figure 4-8: Spatial distribution of osteocyte apoptosis

Figure displays the percentage of osteocytes undergoing apoptosis in regions near and away from damage in both treated and untreated genotypes. Pooled values are represented as the last 2 groups. *: $p<0.05$ near damage vs. away from damage within treatment group. α: $p<0.05$ Brtl/+ treated away from damage vs. WT treated away from damage. # : $p<0.05$ Brtl/+ untreated near damage vs. WT untreated near damage. ǂ : $p<0.05$ Brtl/+ untreated away from damage vs. WT untreated away from damage. $: $p<0.05$ Treated combined near damage vs. Untreated combined near damage.

Table 4-1: Data showing co-localization of FRFP stained cracks and osteocytes as well as combined effects

Parameters	Brtl/+	WT	Totals
Total number of cracks assessed	18	23	41
Total number of basic fuchsin stained osteocytes	142	172	314
Total number of FRFP stained osteocytes	31	71	102
Average % of co-localized osteocytes near damage [#]	20.23 ± 17.50 +	40.83 ± 21.04	32.48 ± 21.95
Average % co-localized osteocytes away from damage	29.93 ± 24.47	29.26 ± 26.37	29.54 ± 25.15
Average % of co-localized crack lengths*	66.44 ± 32.35 +	24.46 ± 34.87	43.83 ± 39.47
% of cracks with FRFP label	88.89 +	52.17	68.29
% of cracks with no co-localized FRFP osteocytes[#]	23.53	4.35	12.50

[*] 2 cracks were not included for crack length co-localization calculations in WT. These cracks had no basic fuchsin binding but did show FRFP labeling.

[#] 1 Crack was not included for Brtl/+ osteocyte co-localization calculations. This crack had no basic fuchsin or FRFP stained osteocytes in the surrounding vicinity.

+ $p<0.05$ vs. WT controls

Table 4-2: Osteocyte apoptosis data

	Untreated		
Parameters	**Brtl/+**	**WT**	**Pooled**
Total Number of cracks assessed	44	43	87
Total Number of basic fuchsin stained osteocytes	418	367	785
Total Number of Annexin-Vivo 750 stained osteocytes	194	91	285
Average % of co-localized osteocytes in peri-damaged region	45.29 ± 32.91 *	25.84 ± 27.58 # *	35.68 ± 31.76 $
Average % of co-localized osteocytes away from damage	28.17 ± 23.11	9.13 ± 15.03 ǂ	19.04 ± 22.19
	Treated		
Total Number of cracks assessed	31	35	66
Total Number of basic fuchsin stained osteocytes	230	260	490
Total Number of Annexin-Vivo 750 stained osteocytes	54	56	110
Average % of co-localized osteocytes in peri-damaged region	26.90 ± 26.5	17.92 ± 23.04	22.14 ± 24.94
Average % of co-localized osteocytes away from damage	19.48 ± 14.13 α	10.75 ± 13.83	14.85 ± 14.54

*: $p<0.05$ near damage vs. away from damage within treatment group. α: $p<0.05$ Brtl/+ treated away from damage vs. WT treated away from damage. # : $p<0.05$ Brtl/+ untreated near damage vs. WT untreated near damage. ǂ : $p<0.05$ Brtl/+ untreated away from damage vs. WT untreated away from damage. $: $p<0.05$ Treated combined near damage vs. Untreated combined near damage.

Chapter 5.

Conclusion

Low bone mass diseases such as osteoporosis and osteogenesis imperfecta (OI) are a significant concern in our society today. Osteoporosis affects over 50 million Americans 50 years and older [9] , while OI, despite being rarer, affects around 50,000 people in the United States. Together, these diseases account for the more than 2 million fragility fractures in the United States each year, and account for over $20 billion dollars in health care expenses [10]. A disease such as OI, despite being less common in society, is still very important to investigate clinically as well as in basic science, as the physical and emotional toll of the disease affects not only the patient, but their family and loved ones. Often times, these patients are

children who are wheelchair bound and merely want to enjoy their childhood like anyone would without the worry of suffering the frequent fractures that are known to come with the disease.

Finding an effective solution to alleviate the conditions of OI is a multi-pronged system and many scientists have been investigating these potential solutions. Some are looking at cellular and gene-therapy [159, 160], which is focused on actually targeting the root causes of the disease, while others are looking at drug therapies such as parathyroid hormone (PTH) [161], RANKL inhibitors [162], and sclerostin antibody [163]. However, the most common form of treatment that exists are bisphosphonates which aim to increase bone mass and strength through osteoclast-mediated bone resorption. Despite the clinical success seen in improved vertebral strength, increased BMD, and reduced vertebral fracture rates, there is still no clear improvement seen on fracture rates in the long bones of OI patients.

It is common practice to use animal models as surrogates to investigate the mechanical properties of low bone mass diseases as well as the effects of their treatment modalities. Animal models that have been used to investigate bisphosphonate treatment have shown compromised mechanical integrity with long term treatment. In addition, bisphosphonates have been implicated in preventing microdamage repair through the inhibition of osteoclast targeting mechanisms. In fact, the increased occurrence of sub-trochanteric fractures seen in the past decade after long term bisphosphonate use has been linked to the inhibition of damage repair in this high stress site.

For the duration of this thesis, we used a mouse model for OI, the Brtl/+ mouse which replicates Type IV OI. The use of a mouse model for this study comes with its advantages and disadvantages. The primary advantage of using any animal model is that they serve as good surrogates for assessing issues in humans. For the purposes of our study, the mouse

provided a good starting point model for human bone, without the obvious complications of dealing with human subjects. The mouse allows us to study the developmental changes of bone as it ages much more quickly than other larger animals. The average mouse lives approximately 2 years while the average human lives about 75 years. This translates to quicker turn around in research time. For example, the current study was interested in looking at the potential effects in pediatric patients with OI. The mouse enters full puberty at 8 weeks of age, which is ideal with regards to treatment with bisphosphonate. In 5 weeks of treatment, we are effectively able to treat the mouse from a very young age (3 weeks) until puberty (8 weeks), which approximates the treatment of most pediatric OI patients. In larger animals this would require higher dosages (due to body size) as well as longer treatment durations due to longer maturity times. In addition, mice are significantly cheaper to house and maintain than larger animals, for examples dogs, and produce larger litters through shorter gestation periods

thus allowing for larger numbers to be studied. The mouse also allows us the ability to more cost effectively perform genetic engineering through knock-in and knock-out models, thus allowing us to replicate diseases such as Type IV osteogenesis imperfecta more effectively than in larger animals. Additionally, classical genetics in a mouse has been well established and there is large availability of different genetic strains. The small size of the mouse generally corresponds with less reagents, smaller processing times and is generally better for spatial resolution in fluorescence imaging due to the smaller size of the tissue.

Despite the advantages listed above, there are disadvantages of using the mouse including the obvious observation that mice are not humans. The physiology of the mouse is different from a human. For example, the aspect ratio of vertebrae as well as the functional purpose of the forearm is different in mice when compared to humans. On a macroscopic bone tissue level, the absence of osteons and interstitial bone tissue in mice could have an impact

on the propagation of cracks. It is proposed that in humans, osteons and the lamellar structure of bone can arrest crack growth, thus preventing cracks approaching critical lengths. Additionally, the apparent absence of intracortical remodeling and bone modeling units in the mouse may result in the development of more detrimental cracks, which may otherwise be repaired in human bone. This may raise the question of whether or not microdamage accumulation in the mouse (in the potential absence of repair) is an adequate representation of the potential effects that may or may not arise in humans. Overall, the Brtl/+ mouse is an effective model for use in this study as it demonstrates similar mechanics, post-pubertal adaptations, up-regulation in bone remodeling, and has a genetic mutation that replicates the disease of a Type IV OI patient.

The intention of this thesis was to form a clearer picture of the interplay between microdamage and bisphosphonate therapy, as well as any potential targeting mechanisms that could possibly affect long term repair of

microdamage. As mentioned earlier, OI patients suffer from increased bone fractures. It is not unreasonable to assume that with an increase in fracture propensity, comes an increase in inherent damage in OI bone. Aim 1 of this study looked at whether or not OI bone is more susceptible to microdamage accumulation than a healthy bone. We hypothesized that the Brtl/+ mouse is more susceptible to microdamage accumulation compared to wild type (WT) controls. In this study we found that Brtl/+ is in fact more prone to microdamage accumulation, not only following cyclic loading, but during normal ambulation as well. In addition, we saw good correlations between fracture toughness and propensity to accumulate microdamage in Brtl/+. The outcome of this study highlights the potential that OI patients may possess increased levels of microdamage in their bones, which likely leads to whole bone loss of structural integrity.

Having determined that Brtl/+ does in fact possess more microdamage than a normal healthy bone, we next set out in Aim 2 to investigate the role

of bisphosphonate therapy in the Brtl/+ mouse. In particular we were interested in assessing whether or not an extended treatment protocol would adversely impact the microdamage content as well as fracture toughness properties in the growing phase of the Brtl/+ mouse. As bisphosphonates are regularly administered to children who are rapidly growing, it was important to determine whether treatment could potentially adversely affect the bone negatively. We set out to test the hypothesis that bisphosphonate treatment would lead to an increase in microdamage content and a concomitant decrease in bone material properties in the Brtl/+ mouse.

Aim 2 provided its fair share of unexpected challenges, but at the same time still yielded important results that shed light on some potential effects of bisphosphonate treatment. It is apparent that bisphosphonate treatment in the Brtl/+ mouse may adversely affect the bone's cycle fatigue durability. Although cycle fatigue was not tested directly, the observation of matched stiffness loss and microdamage levels despite loading at lower

surface strains than untreated specimens, suggest that bisphosphonates could possibly be affecting the collagen structure on the microscopic level. We proposed that the increased levels of collagen crosslinking is likely playing a key role in this as well as the moderate trends towards a decrease in fracture toughness observed in treated specimens. It is also possible that the retention of calcified cartilage at the proximal metaphyseal site of the forearm could potentially explain the occurrences of premature fracture at the elbow region. This area could serve as a structural weak point for the entire forearm and may be more prone to fractures.

For future work, the proposed decrease in fatigue durability with bisphosphonate treatment will be investigated, possibly through cyclic fatigue of femurs using 3-point bending. We hypothesize that after 5 weeks treatment, the fatigue life under high strain cyclic loading(~3500 microstrain) will be lower than untreated bones in both Brtl/+ and WT femurs. Additionally, extending the current bisphosphonate treatment study

to 12 weeks would provide some valuable extensive data to the current study. Studies done by Uveges et al. demonstrated more pronounced differences with bisphosphonate treatment after 12 weeks of treatment as opposed to 6 weeks of treatment. We hypothesize that the current trend of decreased fracture toughness will become more significant with extended treatment into adulthood of the mouse. Additionally, we suspect that the level of baseline microdamage in unloaded limbs after 5 weeks of treatment may probably be too short to see any significant differences in microdamage levels when compared to untreated limbs. As such, we hypothesize that there will be more baseline levels of microdamage in the unloaded treated limbs than in the unloaded untreated limbs, following 12 weeks of treatment.

Our current observations of no differences in microdamage in unloaded limbs does suggest that bisphosphonates may work perfectly fine in low strain situations, but the implication of structural integrity does appear to come into question at higher strain levels. Despite the short term

nature of the bisphosphonate treatment study in Aim 2, our data shows that bisphosphonates are having an effect on some inherent material properties and are the likely culprit in comparable microdamage levels observed in Brtl/+ and WT mice despite the application of lower strains in treated specimens. Most clinical uses of bisphosphonates are long term, and with observations that long term use tends to lead to a decrease in bone's mechanical integrity, there is the potential that the long term remodeling of microdamage may also be compromised. This would be somewhat counterintuitive to the notion of bisphosphonates improving whole bone strength. For Aim 3 we wanted to investigate the targeting and spatial distribution of bisphosphonates as well as any potential impacts on osteocyte apoptosis, which has been proposed as a key step in the damage repair process.

This particular study took advantage of fluorescent probes and the imaging power of the Leica Inverted Confocal microscope. Through the use

of an in-vivo fluorescent bisphosphonate and fluorescent apoptosis marker, we were able to co-localize damage with its surrounding osteocyte lacunae. We firstly observed that following cyclic loading, the bisphosphonate fluorophore bound itself not only to osteocyte lacunae, but to the actual microcracks. This observation in both Brtl/+ and WT has significant consequences for the concept of targeted damage repair as bisphosphonates have been implicated as inhibitors of osteocyte apoptosis which is a proposed first step in damage repair.

Our osteocyte apoptosis data provided some interesting possibilities that may play some role in the observed increase in up-regulation of bone remodeling seen in Brtl/+ (and OI). We noted a stark increase in osteocyte apoptosis surrounding microdamage in untreated Brtl/+ specimens when compared to WT untreated specimens. This raises the question of the possibility that the up-regulation of remodeling may happen concomitantly with an increase in osteocyte apoptosis. It is generally understood that viable

osteocytes keep osteoclasts away, but could Brtl/+ be compensating for its increased levels of microdamage by up-regulating all cellular processes including osteocyte apoptosis?

Some burning questions arise from the observations of this study. Firstly, are RANKL expressions decreased in bisphosphonate treated bone in the Brtl/+ mouse? The decrease in osteocyte apoptosis levels suggest that it would be, as it is understood that RANKL triggers osteoclast recruitment. Studies done by Kurata and colleagues indicate that damage to osteocytes does result in the production of RANKL and other soluble factors that are necessary for the initial phase of osteoclastic cell formation [164]. If this observation is indeed somewhat linearly correlated, it would be highly interesting to see if bisphosphonates could be used in a regulatory fashion to lower osteocyte apoptosis levels to “normal” levels. One could then investigate whether other biological markers such as OPG adjusts to reach a

steady state level, or if they remain equally up-regulated regardless of pharmacological intervention.

We hypothesize that the observed increases in remodeling activity seen in the Brtl/+ mouse is partially due to the increased levels of osteocyte apoptosis that we have observed in this thesis. We propose that the increase in osteocyte apoptosis in Brtl/+ results in increased levels of RANKL, and subsequent osteoclast activity. Additionally, we suspect that bisphosphonate treatment will suppress RANKL levels in the Brtl/+ mouse, by suppressing osteocyte apoptosis. To test this hypothesis, baseline RANKL levels in Brtl/+ would be measured using immunohistochemical staining and light microscopy at 8 weeks and 16 weeks of age. These results will be compared to Brtl/+ animals that have been treated with bisphosphonate from 3 weeks of age until 8 and 16 weeks of age. The aim of this experiment would be to determine if bisphosphonates could potentially be used to regulate remodeling activity. Further iterations of this study could demonstrate that at

the correct dosage, clinicians could potentially use bisphosphonates as a regulatory mechanism for patients with high bone turnover diseases.

Several other interesting questions remain to be tested that could shed further light on some of the questions addressed in this thesis. Firstly, attaining microscopy capabilities that can delineate both basic fuchsin, and 2 far-red flourophores such as Annexin-Vivo 750 and FRFP into 3 distinct signals would be an advanced capability. This would enable us to co-localize microdamage, bisphosphonate delivery, as well as osteocyte apoptosis in one scan. This would enable us to determine if bisphosphonate presence strongly correlates with osteocyte apoptosis. We hypothesize that cells which demonstrate bisphosphonate binding (through FRFP localization) will be less likely to undergo apoptosis (indicated by AV750 localization). This study would aim to investigate the direct impact of bisphosphonate treatment and localization on cellular processes such as apotosis.

Additionally, the question of microdamage repair in the mouse still remains somewhat of a white whale. Does it or does it not exist? Firstly it would be interesting to investigate if microdamage accumulates in the Brtl/+ mouse with age. Testing microdamage levels at 3,5,7,9,11 and 13 weeks of age would give us a good idea of whether damage levels increase or simply remain the same over time. Once this is determined, the next logical step would be to determine if remodeling of damage exists. This could be done by having a set of Brtl/+ and WT animals (n=15/group) loaded at 8 weeks of age and a control group of n=15/group left unloaded. Over the course of the next 8 weeks, 3 animals would be sacked every week and the levels of microdamage could be assessed to determine if loaded limbs eventually converged upon the unloaded animals. We hypothesize that microdamage levels will increase linearly over the course of several weeks. This experiment is a very "expensive" experiment however as it would likely require many mice to attain the power necessary to see differences.

Additionally, if remodeling in a mouse does exist, identifying the time point it begins will prove challenging.

Another experiment worth pursuing is investigating whether or not similar levels of microdamage exist in other OI mouse models such as the Mov 13 mouse. The heterozygous Mov 13 mouse is different from the Brtl/+ mouse in that it carries a provirus that prevents the initiation of the transcription of the α1(I) collagen gene [165]. This mutation has been associated with structurally normal type-1 collagen, but at a 50% decrease in quantity [56]. Mechanical tests have verified that Mov 13 in fact replicates Type I OI [56]. Assessing the levels of baseline microdamage and subsequently determining the impact of bisphosphonate therapy in these mice would provide an interesting contrast to the current Brtl/+ mouse observations. The current suggestion that RANKL levels may be associated with increased microdamage and osteocyte apoptosis in Brtl/+ could be tested against the Mov 13 mouse which does not possess the up-regulation in

remodeling activity as the Brtl/+ mouse. We hypothesize that Brtl/+ bones possess more baseline microdamage and higher levels of osteocyte apoptosis than Mov 13. If this observation is correct, it could further support the notion that the high levels of microdamage in Brtl/+ could be partially responsible for the elevated remodeling activity observed in Brtl/+. Also, mechanical effects such as fracture toughness, as well as taking note if similar occurrences of premature fractures occur in the Mov 13 mouse following treatment will be assessed. The results of this study would provide information to aid clinicians in determining whether or not bisphosphonates are differentially better to administer to patients with simply low bone mass (Type I OI) or patients with increased bone turnover corresponding to decreased bone mass (osteoporosis or Type IV OI).

This thesis showed that microdamage content and susceptibility to damage generation may play a role in bone fragility. Additionally, we suggest that treatment with bisphosphonates may hinder damage repair

through several targeting mechanisms and could potentially promote further fractures. Our work specifically focused on Type IV OI and made suggestions that the observations could be translated to other low bone mass diseases. From a clinical perspective, it is important to determine however if this observation of increased microdamage in other low bone mass diseases is an underlying trait of the condition. Hence looking at other models for low bone mass diseases for example Type I OI (Mov 13), Type III OI (oim mouse) and osteoporosis and determining if microdamage is an equal concern is an essential question to answer. We proposed that the binding of bisphosphonates to damage sites is a key way in which bisphosphonates lead to increased fragility. Hence assessing whether the binding characteristics of bisphosphonates are any different in these models will determine if the potential consequences are similar to our current study.

Our current studies serve as a caution to clinicians who use bisphosphonates to approach patients who may have high quantities of

microdamage carefully. Using a RANKL inhibitor such as Denosumab which lowers osteoclast activity but doesn't bind to bone tissue may be the best way to treat these patients. Additionally, patients who have been treated with bisphosphonates who are suspected to have higher levels of inherent damage may need to be placed on a drug holiday and switched off bisphosphonates onto an alternative such as Denosumab. Furthermore, these patients could also potentially benefit from using a treatment such as sclerostin-antibody which would also increase the level of bone mass without bone tissue binding issues.

The results of this thesis and the additionally proposed studies can be used by clinicians in a somewhat precautionary fashion, if the correct information is at their disposal. If clinicians could be provided with iliac crest biopsies of their patients, they could potentially determine the levels of microdamage in their patients before prescribing a treatment option. Bisphosphonate treatment to a patient with high levels of damage in their

bones may not be a prudent decision. With the evidence of bisphosphonate binding to microcracks and surrounding osteocyte lacunae, it is possible that bisphosphonates could prevent the repair of these cracks. This would be a greater concern if the patient had higher levels of baseline damage as you increase the likelihood of the prevention of a critical microcrack being repaired. Additionally, our observations of moderately reduced fracture toughness in concert with high strain loading demonstrating critical failures should prompt clinicians to make their patients aware that despite treatment with bisphosphonates and improved bone mass, there are still risks for fractures. Tempering and strictly monitoring patient's physical activity is crucial to ensure that fractures in potentially weakened sites such as the metaphyseal regions of long bones is avoided.

The above mentioned experiments are some of the unknown questions that would help somewhat close the loop in the OI-microdamage-bisphosphonate-bisphosphonate targeting-long term repair cycle. This thesis

has helped to elucidate a few of these links. Further basic science studies are needed to help close the link. It is important to note however that the purpose of all of these studies is to help the patients who are afflicted with this disease. The findings of this thesis and the others that will subsequently follow will not only help the OI community, but will likely transcend to other low bone mass diseases such as osteoporosis.

References

[1] Odvina CV, Zerwekh JE, Rao DS, Maalouf N, Gottschalk FA, Pak CYC. Severely Suppressed Bone Turnover: A Potential Complication of Alendronate Therapy. Journal of Clinical Endocrinology & Metabolism 2005;90: 1294-1301.

[2] Abrahamsen B, Eiken P, Eastell R. Subtrochanteric and Diaphyseal Femur Fractures in Patients Treated With Alendronate: A Register-Based National Cohort Study. Journal of Bone and Mineral Research 2009;24: 1095-1102.

[3] Giusti A, Hamdy NAT, Dekkers OM, Ramautar SR, Dijkstra S, Papapoulos SE. Atypical fractures and bisphosphonate therapy: A cohort study of patients with femoral fracture with radiographic adjudication of fracture site and features. Bone 2011;48: 966-971.

[4] Lenart BA, Neviaser AS, Lyman S, Chang CC, Edobor-Osula F, Steele B, Meulen MCH, Lorich DG, Lane JM. Association of low-energy femoral fractures with prolonged bisphosphonate use: a case control study. Osteoporosis International 2009;20: 1353-1362.

[5] Park-Wyllie Ly. Bisphosphonate use and the risk of subtrochanteric or femoral shaft fractures in older women. JAMA 2011;305: 783-789.

[6] Schilcher J, Michaëlsson K, Aspenberg P. Bisphosphonate Use and Atypical Fractures of the Femoral Shaft. New England Journal of Medicine 2011;364: 1728-1737.
[7] Whitaker M, Guo J, Kehoe T, Benson G. Bisphosphonates for Osteoporosis — Where Do We Go from Here? New England Journal of Medicine 2012;366: 2048-2051.
[8] Shane E, Burr D, Ebeling PR, Abrahamsen B, Adler RA, Brown TD, Cheung AM, Cosman F, Curtis JR, Dell R, Dempster D, Einhorn TA, Genant HK, Geusens P, Klaushofer K, Koval K, Lane JM, McKiernan F, McKinney R, Ng A, Nieves J, O'Keefe R, Papapoulos S, Sen HT, van der Meulen MCH, Weinstein RS, Whyte M. Atypical subtrochanteric and diaphyseal femoral fractures: Report of a task force of the american society for bone and mineral Research. Journal of Bone and Mineral Research 2010;25: 2267-2294.
[9] Cooper C, Melton LJ. Epidemiology of osteoporosis. Trends in Endocrinology & Metabolism 1992;3: 224-229.
[10] Holroyd C, Cooper C, Dennison E. Epidemiology of osteoporosis. Best Practice & Research Clinical Endocrinology & Metabolism 2008;22: 671-685.
[11] Rauch F, Glorieux F. Osteogenesis imperfecta. The Lancet 2004;363: 1377-1385.
[12] Byers PH, Cole WG. In Connective tissue and its heritable disorders molecular, genetic and medical aspects. . In: Royce PM, Steinmann B, editors. Osteogenesis Imperfecta. 2nd ed. New York: Wiley-Liss; 2002, p. 385–430.
[13] Brenner RE, Vetter U, Bollen A-M, Mörike M, Eyre DR. Bone resorption assessed by immunoassay of urinary cross-linked collagen peptides in patients with osteogenesis imperfecta. Journal of Bone and Mineral Research 2009;9: 993.

[14] Baron R, Gertner JM, Lang R, Vignery A. Increased bone turnover with decreased bone formation by osteoblasts in children with osteogenesis imperfecta tarda. Pediatric research 1983;17: 204.
[15] Kozloff KM, Carden A, Bergwitz C, Forlino A, Uveges TE, Morris MD, Marini JC, Goldstein SA. Brittle IV Mouse Model for Osteogenesis Imperfecta IV Demonstrates Postpubertal Adaptations to Improve Whole Bone Strength. Journal of Bone and Mineral Research 2004;19: 614-622.
[16] Uveges TE, Collin-Osdoby P, Cabral WA, Ledgard F, Goldberg L, Bergwitz C, Forlino A, Osdoby P, Gronowicz GA, Marini JC. Cellular Mechanism of Decreased Bone in Brtl Mouse Model of OI: Imbalance of Decreased Osteoblast Function and Increased Osteoclasts and Their Precursors. Journal of Bone and Mineral Research 2008;23: 1983-1994.
[17] Davis MS, Kovacic BL, Marini JC, Shih AJ, Kozloff KM. Increased susceptibility to microdamage in Brtl/+ mouse model for osteogenesis imperfecta. Bone 2012;50: 784-91.
[18] Liberman UA, Weiss SR, Broll J, Minne HW, Quan H, Bell NH, Rodriguez-Portales J, Downs RW, Jr., Dequeker J, Favus M. Effect of oral alendronate on bone mineral density and the incidence of fractures in postmenopausal osteoporosis. The Alendronate Phase III Osteoporosis Treatment Study Group. N Engl J Med 1995;333: 1437-43.
[19] Harris ST, Watts NB, Genant HK, McKeever CD, Hangartner T, Keller M, Chesnut CH, 3rd, Brown J, Eriksen EF, Hoseyni MS, Axelrod DW, Miller PD. Effects of risedronate treatment on vertebral and nonvertebral fractures in women with postmenopausal osteoporosis: a randomized controlled trial. Vertebral Efficacy With Risedronate Therapy (VERT) Study Group. JAMA 1999;282: 1344-52.
[20] Reid IR, Brown JP, Burckhardt P, Horowitz Z, Richardson P, Trechsel U, Widmer A, Devogelaer JP, Kaufman JM, Jaeger P, Body JJ, Brandi ML, Broell J, Di Micco R, Genazzani AR, Felsenberg D, Happ J, Hooper MJ, Ittner J, Leb G, Mallmin H, Murray T, Ortolani S, Rubinacci A,

Saaf M, Samsioe G, Verbruggen L, Meunier PJ. Intravenous zoledronic acid in postmenopausal women with low bone mineral density. N Engl J Med 2002;346: 653-61.
[21] Bone HG, Hosking D, Devogelaer JP, Tucci JR, Emkey RD, Tonino RP, Rodriguez-Portales JA, Downs RW, Gupta J, Santora AC, Liberman UA. Ten years' experience with alendronate for osteoporosis in postmenopausal women. N Engl J Med 2004;350: 1189-99.
[22] Black DM, Delmas PD, Eastell R, Reid IR, Boonen S, Cauley JA, Cosman F, Lakatos P, Leung PC, Man Z, Mautalen C, Mesenbrink P, Hu H, Caminis J, Tong K, Rosario-Jansen T, Krasnow J, Hue TF, Sellmeyer D, Eriksen EF, Cummings SR. Once-yearly zoledronic acid for treatment of postmenopausal osteoporosis. N Engl J Med 2007;356: 1809-22.
[23] Lyles KW, Colon-Emeric CS, Magaziner JS, Adachi JD, Pieper CF, Mautalen C, Hyldstrup L, Recknor C, Nordsletten L, Moore KA, Lavecchia C, Zhang J, Mesenbrink P, Hodgson PK, Abrams K, Orloff JJ, Horowitz Z, Eriksen EF, Boonen S. Zoledronic acid and clinical fractures and mortality after hip fracture. N Engl J Med 2007;357: 1799-809.
[24] Komatsubara S, Mori S, Mashiba T, Li J, Nonaka K, Kaji Y, Akiyama T, Miyamoto K, Cao Y, Kawanishi J, Norimatsu H. Suppressed bone turnover by long-term bisphosphonate treatment accumulates microdamage but maintains intrinsic material properties in cortical bone of dog rib. J Bone Miner Res 2004;19: 999-1005.
[25] Mashiba T, Hirano T, Turner CH, Forwood MR, Johnston CC, Burr DB. Suppressed bone turnover by bisphosphonates increases microdamage accumulation and reduces some biomechanical properties in dog rib. J Bone Miner Res 2000;15: 613-20.
[26] Mashiba T, Turner CH, Hirano T, Forwood MR, Johnston CC, Burr DB. Effects of suppressed bone turnover by bisphosphonates on microdamage accumulation and biomechanical properties in clinically relevant skeletal sites in beagles. Bone 2001;28: 524-531.

[27] Li J, Mashiba T, Burr DB. Bisphosphonate treatment suppresses not only stochastic remodeling but also the targeted repair of microdamage. Calcif Tissue Int 2001;69: 281-6.
[28] Allen MR, Reinwald S, Burr DB. Alendronate reduces bone toughness of ribs without significantly increasing microdamage accumulation in dogs following 3 years of daily treatment. Calcif Tissue Int 2008;82: 354-60.
[29] Lenart BA, Lorich DG, Lane JM. Atypical fractures of the femoral diaphysis in postmenopausal women taking alendronate. N Engl J Med 2008;358: 1304-6.
[30] Shane E, Burr D, Ebeling PR, Abrahamsen B, Adler RA, Brown TD, Cheung AM, Cosman F, Curtis JR, Dell R, Dempster D, Einhorn TA, Genant HK, Geusens P, Klaushofer K, Koval K, Lane JM, McKiernan F, McKinney R, Ng A, Nieves J, O'Keefe R, Papapoulos S, Sen HT, van der Meulen MC, Weinstein RS, Whyte M. Atypical subtrochanteric and diaphyseal femoral fractures: report of a task force of the American Society for Bone and Mineral Research. J Bone Miner Res 2010;25: 2267-94.
[31] Dong XN, Zoghi M, Ran Q, Wang X. Collagen mutation causes changes of the microdamage morphology in bone of an OI mouse model. Bone 2010;47: 1071-1075.
[32] Avioli LV. Metabolic Bone Disease and Clinically Related Disorders. 3rd ed. San Diego: Academic Press; 1998.
[33] Marini JC, Forlino A, Cabral WA, Barnes AM, Antonio JDS, Milgrom S, Hyland JC, Körkkö J, Prockop DJ, Paepe AD, Coucke P, Symoens S, Glorieux FH, Roughley PJ, Lund AM, Kuurila-Svahn K, Hartikka H, Cohn DH, Krakow D, Mottes M, Schwarze U, Chen D, Yang K, Kuslich C, Troendle J, Dalgleish R, Byers PH. Consortium for osteogenesis imperfecta mutations in the helical domain of type I collagen: regions rich in lethal mutations align with collagen binding sites for integrins and proteoglycans. Human Mutation 2007;28: 209-221.

[34] Morello R, Bertin TK, Chen Y, Hicks J, Tonachini L, Monticone M, Castagnola P, Rauch F, Glorieux FH, Vranka J. CRTAP is required for prolyl 3-hydroxylation and mutations cause recessive osteogenesis imperfecta. Cell 2006;127: 291.
[35] Barnes AM, Chang W, Morello R, Cabral WA, Weis M, Eyre DR, Leikin S, Makareeva E, Kuznetsova N, Uveges TE, Ashok A, Flor AW, Mulvihill JJ, Wilson PL, Sundaram UT, Lee B, Marini JC. Deficiency of cartilage-associated protein in recessive lethal osteogenesis imperfecta. New England Journal of Medicine, The 2006;355: 2757.
[36] Cabral WA, Chang W, Barnes AM, Weis M, Scott MA, Leikin S, Makareeva E, Kuznetsova NV, Rosenbaum KN, Tifft CJ, Bulas DI, Kozma C, Smith PA, Eyre DR, Marini JC. Prolyl 3-hydroxylase 1 deficiency causes a recessive metabolic bone disorder resembling lethal/severe osteogenesis imperfecta. Nat Genet 2007;39: 359-365.
[37] Jepsen KJ, Goldstein SA, Kuhn JL, Schaffler MB, Bonadio J. Type-I collagen mutation compromises the post-yield behavior of Mov13 long bone. Journal of Orthopaedic Research 1996;14: 493.
[38] Forlino A, Porter FD, Lee EJ, Westphal H, Marini JC. Use of the cre/lox recombination system to develop a non-lethal knock-in murine model for osteogenesis imperfecta with an α1(I) G349C substitution. Journal of Biological Chemistry 1999;274: 37923-37931.
[39] Lee KCL, Maxwell A, Lanyon LE. Validation of a technique for studying functional adaptation of the mouse ulna in response to mechanical loading. Bone 2002;31: 407-412.
[40] Bentolila V, Boyce TM, Fyhrie DP, Drumb R, Skerry TM, Schaffler MB. Intracortical remodeling in adult rat long bones after fatigue loading. Bone 1998;23: 275-281.
[41] Torrance AG, Mosley JR, Suswillo RFL, Lanyon LE. Noninvasive loading of the rat ulna in vivo induces a strain-related modeling response

uncomplicated by trauma or periostal pressure. Calcified Tissue International 1994;54: 241.
[42] Boyce TM, Fyhrie DP, Glotkowski MC, Radin EL, Schaffler MB. Damage type and strain mode associations in human compact bone bending fatigue. Journal of Orthopaedic Research 1998;16: 322.
[43] Fritton S, Rubin C. Bone Mechanics Handbook. Boca Raton, FL; 2001.
[44] Tami AE, Nasser P, Schaffler MB, Tate MLK. Noninvasive fatigue fracture model of the rat ulna. Journal of Orthopaedic Research 2006;21: 1018.
[45] Burr DB, Hooser M. Alterations to the en bloc basic fuchsin staining protocol for the demonstration of microdamage produced in vivo. Bone 1995;17: 431.
[46] Ritchie RO, Koester KJ, Ionova S, Yao W, Lane NE, Ager JW. Measurement of the toughness of bone: A tutorial with special reference to small animal studies. Bone 2008;43: 798.
[47] ASTM Standard E-399. Standard test method for linear-elastic plane-strain fracture toughness KIC of metallic materials. In. West Conshohocken, PA: American Society for Testing and Materials:; 2006.
[48] Kruzic JJ, Kuskowski SJ, Ritchie RO. Simple and accurate fracture toughness testing methods for pyrolytic carbon/graphite composites used in heart-valve prostheses. Journal of Biomedical Materials Research Part A 2005;74A: 461-464.
[49] ASTM Standard E-1820. Standard test method for measurement of fracture toughness. In. West Conshohocken, PA; 2006.
[50] Zahoor A. Ductile Fracture Handbook. Palo Alto: Electric Power Research Institute; 1989.
[51] Takahashi Y. Evaluation of leak-before-break assessment methodology for pipes with a circumferential through-wall crack. Part I:

stress intensity factor and limit load solutions. The International journal of pressure vessels and piping 2002;79: 385.
[52] Duvall CL, Taylor WR, Weiss D, Wojtowicz AM, Guldberg RE. Impaired Angiogenesis, Early Callus Formation, and Late Stage Remodeling in Fracture Healing of Osteopontin-Deficient Mice. Journal of Bone and Mineral Research 2006;22: 286-297.
[53] Thurner PJ, Chen CG, Ionova-Martin S, Sun L, Harman A, Porter A, Ager Iii JW, Ritchie RO, Alliston T. Osteopontin deficiency increases bone fragility but preserves bone mass. Bone 2010;46: 1564-1573.
[54] Rajachar RM, Chow, D. L., Curtis, C.E., Weissman, N.A., Kohn, D.H. Acoustic Emission: Standards and Technology Update. In: S.J. V, editor. Use of Acoustic Emission to Characterize Focal and Diffuse Microdamage in Bone. West Conshohocken; 1999.
[55] Zioupos P, Currey JD. Changes in the Stiffness, Strength, and Toughness of Human Cortical Bone With Age. Bone 1998;22: 57-66.
[56] Bonadio J, Saunders TL, Tsai E, Goldstein SA, Morris-Wiman J, Brinkley L, Dolan DF, Altschuler RA, Hawkins JE, Bateman JF. Transgenic mouse model of the mild dominant form of osteogenesis imperfecta. Proceedings of the National Academy of Sciences of the United States of America 1990;87: 7145.
[57] Jepsen K, Schaffler MB, Kuhn JL, Goulet RW, Bonadio J, Goldstein SA. Type I collagen mutation alters the strength and fatigue behavior of Mov13 cortical tissue. Journal of Biomechanics 1997;30: 1141.
[58] Uveges TE, Kozloff KM, Ty JM, Ledgard F, Raggio CL, Gronowicz G, Goldstein SA, Marini JC. Alendronate Treatment of the Brtl Osteogenesis Imperfecta Mouse Improves Femoral Geometry and Load Response Before Fracture but Decreases Predicted Material Properties and Has Detrimental Effects on Osteoblasts and Bone Formation. Journal of Bone and Mineral Research 2009;24: 849-859.

[59] Boyde A, Travers R, Glorieux FH, Jones SJ. The mineralization density of iliac crest bone from children with osteogenesis imperfecta. Calcified Tissue International 1999;64: 185.
[60] Currey J. The effects of ageing and changes in mineral content in degrading the toughness of human femora. Journal of Biomechanics 1996;29: 257.
[61] Dong X, Guda T, Millwater H, Wang X. Probabilistic failure analysis of bone using a finite element model of mineral-collagen composites. Journal of Biomechanics 2009;42: 202.
[62] Burr D, Miller L, Grynpas M, Li J, Boyde A, Mashiba T, Hirano T, Johnston C. Tissue mineralization is increased following 1-year treatment with high doses of bisphosphonates in dogs. Bone 2003;33: 960.
[63] Ruppel M, Burr D, Miller L. Chemical makeup of microdamaged bone differs from undamaged bone. Bone 2006;39: 318.
[64] Timlin JA, Carden A, Morris MD, Rajachar RM, Kohn DH. Raman Spectroscopic Imaging Markers for Fatigue-Related Microdamage in Bovine Bone. Analytical Chemistry 2000;72: 2229-2236.
[65] Danova NA, Colopy SA, Radtke CL, Kalscheur VL, Markel MD, Vanderby R, McCabe RP, Escarcega AJ, Muir P. Degradation of bone structural properties by accumulation and coalescence of microcracks. Bone 2003;33: 197-205.
[66] Burr DB, Martin RB, Schaffler MB, Radin EL. Bone remodeling in response to in vivo fatigue microdamage. Journal of Biomechanics 1985;18: 189-200.
[67] Rodan GA, Martin TJ. Therapeutic approaches to bone diseases. Science 2000;289: 1508-14.
[68] Deftos LJ. Treatment of Paget's disease--taming the wild osteoclast. N Engl J Med 2005;353: 872-5.

[69] Glorieux FH, Bishop NJ, Plotkin H, Chabot G, Lanoue G, Travers R. Cyclic Administration of Pamidronate in Children with Severe Osteogenesis Imperfecta. New England Journal of Medicine 1998;339: 947-952.
[70] Forlino A, Cabral WA, Barnes AM, Marini JC. New perspectives on osteogenesis imperfecta. Nature Reviews Endocrinology 2011;7: 540-557.
[71] Brenner RE, Vetter U, Bollen A-M, Mörike M, Eyre DR. Bone resorption assessed by immunoassay of urinary cross-linked collagen peptides in patients with osteogenesis imperfecta. Journal of Bone and Mineral Research 1994;9: 993-997.
[72] Sato M, Grasser W, Endo N, Akins R, Simmons H, Thompson D, Golub E, Rodan G. Bisphosphonate action. Alendronate localization in rat bone and effects on osteoclast ultrastructure. Journal of Clinical Investigation 1991;88: 2095.
[73] Azuma Y, Sato H, Oue Y, Okabe K, Ohta T, Tsuchimoto M, Kiyoki M. Alendronate distributed on bone surfaces inhibits osteoclastic bone resorption< i> in vitro</i> and in experimental hypercalcemia models. Bone 1995;16: 235-245.
[74] Plotkin LW, Robert S; Parfitt, A. Michael; Roberson, Paula K.; Manolagas, Stavros C; Bellido, Teresita. Prevention of osteocyte and osteoblast apoptosis by bisphosphonates and calcitonin. Journal of Clinical Investigation 1999;104: 1363-1374.
[75] Gatti D, Antoniazzi F, Prizzi R, Braga V, Rossini M, Tatò L, Viapiana O, Adami S. Intravenous Neridronate in Children With Osteogenesis Imperfecta: A Randomized Controlled Study. Journal of Bone and Mineral Research 2005;20: 758-763.
[76] Seikaly MG, Kopanati S, Salhab N, Waber P, Patterson D, Browne R, Herring JA. Impact of alendronate on quality of life in children with osteogenesis imperfecta. Journal of Pediatric Orthopaedics 2005;25: 786-791.

[77] Letocha AD, Cintas HL, Troendle JF, Reynolds JC, Cann CE, Chernoff EJ, Hill SC, Gerber LH, Marini JC. Controlled Trial of Pamidronate in Children With Types III and IV Osteogenesis Imperfecta Confirms Vertebral Gains but Not Short-Term Functional Improvement. Journal of Bone and Mineral Research 2005;20: 977-986.
[78] Rauch F, Munns CF, Land C, Cheung M, Glorieux FH. Risedronate in the Treatment of Mild Pediatric Osteogenesis Imperfecta: A Randomized Placebo-Controlled Study. Journal of Bone and Mineral Research 2009;24: 1282-1289.
[79] Komatsubara S, Mori S, Mashiba T, Li J, Nonaka K, Kaji Y, Akiyama T, Miyamoto K, Cao Y, Kawanishi J. Suppressed Bone Turnover by Long-Term Bisphosphonate Treatment Accumulates Microdamage but Maintains Intrinsic Material Properties in Cortical Bone of Dog Rib. Journal of Bone and Mineral Research 2005;20: 2066-2073.
[80] Mashiba T, Turner C, Hirano T, Forwood M, Johnston C, Burr D. Effects of suppressed bone turnover by bisphosphonates on microdamage accumulation and biomechanical properties in clinically relevant skeletal sites in beagles. Bone 2001;28: 524-531.
[81] Mashiba T, Hirano T, Turner CH, Forwood MR, Johnston CC, Burr DB. Suppressed bone turnover by bisphosphonates increases microdamage accumulation and reduces some biomechanical properties in dog rib. Journal of Bone and Mineral Research 2000;15: 613-620.
[82] Allen MR, Reinwald S, Burr DB. Alendronate reduces bone toughness of ribs without significantly increasing microdamage accumulation in dogs following 3 years of daily treatment. Calcified Tissue International 2008;82: 354-360.
[83] Evans K, Lau S, Oberbauer A, Martin R. Alendronate affects long bone length and growth plate morphology in the< i> oim</i> mouse model for Osteogenesis Imperfecta. Bone 2003;32: 268-274.

[84] Misof BM, Roschger P, Baldini T, Raggio CL, Zraick V, Root L, Boskey AL, Klaushofer K, Fratzl P, Camacho NP. Differential effects of alendronate treatment on bone from growing osteogenesis imperfecta and wild-type mouse. Bone 2005;36: 150-158.
[85] Forlino A, Porter FD, Lee EJ, Westphal H, Marini JC. Use of the Cre/lox recombination system to develop a non-lethal knock-in murine model for osteogenesis imperfecta with an α1(I) G349C substitution. Variability in phenotype in BrtlIV mice. J Biol Chem 1999;274: 37923-31.
[86] Davis MS, Kovacic BL, Marini JC, Shih AJ, Kozloff KM. Increased susceptibility to microdamage in Brtl/+ mouse model for osteogenesis imperfecta. Bone 2012;50: 784-791.
[87] McCarthy EA, Raggio CL, Hossack MD, Miller EA, Jain S, Boskey AL, Camacho NP. Alendronate Treatment for Infants with Osteogenesis Imperfecta: Demonstration of Efficacy in a Mouse Model. Pediatr Res 2002;52: 660-670.
[88] Uveges T, Kozloff KM, Ty JM, Ledgard F, Raggio CL, Gronowicz G, Goldstein SA, Marini JC. Alendronate treatment of Brtl osteogenesis imperfecta mouse improves femoral geometry and load response before fracture but has detrimental effects on osteoblasts and bone formation and decreases predicted material properties. Journal of Bone and Mineral Research 2009;24: 849-859.
[89] Allen MR, Burr DB. Three years of alendronate treatment results in similar levels of vertebral microdamage as after one year of treatment. Journal of Bone and Mineral Research 2007;22: 1759-1765.
[90] Allen MR, Iwata K, Sato M, Burr DB. Raloxifene enhances vertebral mechanical properties independent of bone density. Bone 2006;39: 1130-1135.
[91] Allen M, Gineyts E, Leeming D, Burr D, Delmas P. Bisphosphonates alter trabecular bone collagen cross-linking and isomerization in beagle dog vertebra. Osteoporosis International 2008;19: 329-337.

[92] Viguet-Carrin S, Roux J, Arlot M, Merabet Z, Leeming D, Byrjalsen I, Delmas P, Bouxsein M. Contribution of the advanced glycation end product pentosidine and of maturation of type I collagen to compressive biomechanical properties of human lumbar vertebrae. Bone 2006;39: 1073-1079.
[93] Hernandez CJ, Tang SY, Baumbach BM, Hwu PB, Sakkee AN, van der Ham F, DeGroot J, Bank RA, Keaveny TM. Trabecular microfracture and the influence of pyridinium and non-enzymatic glycation-mediated collagen cross-links. Bone 2005;37: 825-832.
[94] Wang X, Shen X, Li X, Mauli Agrawal C. Age-related changes in the collagen network and toughness of bone. Bone 2002;31: 1-7.
[95] Boxberger J, Vashishth D. Nonenzymatic glycation affects bone fracture by modifying creep and inelastic properties of collagen. Trans Orthop Res Soc 2004;29.
[96] Tang SY, Zeenath U, Vashishth D. Effects of non-enzymatic glycation on cancellous bone fragility. Bone 2007;40: 1144-1151.
[97] Catanese J, Bank R, TeKoeppele J, Keaveny T. Increased cross-linking by non-enzymatic glycation reduces the ductility of bone and bone collagen. ASME-PUBLICATIONS-BED 1999;42: 267-268.
[98] Wu P, Koharski C, Nonnenmann H, Vashishth D. Loading on non-enzymatically glycated and damaged bone results in an instantaneous fracture. Trans Orthop Res Soc 2003;28: 404.
[99] Grissom LE, Harcke HT. Radiographic features of bisphosphonate therapy in pediatric patients. Pediatric radiology 2003;33: 226-229.
[100] van Persijn van Meerten EL, Kroon HM, Papapoulos SE. Epi- and metaphyseal changes in children caused by administration of bisphosphonates. Radiology 1992;184: 249-254.
[101] Åström E, Söderhäll S. Beneficial effect of long term intravenous bisphosphonate treatment of osteogenesis imperfecta. Archives of disease in childhood 2002;86: 356-364.

[102] Solomon CG. Bisphosphonates and osteoporosis. The New England journal of medicine 2002;346: 642.
[103] Rodan GA, Fleisch HA. Bisphosphonates: mechanisms of action. Journal of Clinical Investigation 1996;97: 2692.
[104] Marini JC. Do bisphosphonates make children's bones better or brittle? The New England journal of medicine 2003;349: 423.
[105] Laor T, Jaramillo D. Metaphyseal abnormalities in children: pathophysiology and radiologic appearance. AJR. American journal of roentgenology 1993;161: 1029-1036.
[106] Bikle DD, Morey-Holton ER, Doty SB, Currier PA, Tanner SJ, Halloran BP. Alendronate increases skeletal mass of growing rats during unloading by inhibiting resorption of calcified cartilage. Journal of Bone and Mineral Research 1994;9: 1777-1787.
[107] Camacho NP, Raggio CL, Doty SB, Root L, Zraick V, Ilg WA, Toledano TR, Boskey AL. A Controlled Study of the Effects of Alendronate in a Growing Mouse Model of Osteogenesis Imperfecta. Calcified Tissue International 2001;69: 94-101.
[108] Rubin C, Lanyon L. Regulation of bone mass by mechanical strain magnitude. Calcified Tissue International 1985;37: 411-417.
[109] Biewener AA. Musculoskeletal design in relation to body size. Journal of Biomechanics 1991;24, Supplement 1: 19-29.
[110] Marini JC. Should children with osteogenesis imperfecta be treated with bisphosphonates? Nature Clinical Practice Endocrinology & Metabolism 2006;2: 14+.
[111] Fielding JW. Subtrochanteric fractures. Clinical Orthopaedics and Related Research 1973;92: 86-99.
[112] Plotkin H, Rauch F, Bishop NJ, Montpetit K, Ruck-Gibis J, Travers R, Glorieux FH. Pamidronate treatment of severe osteogenesis imperfecta in children under 3 years of age. Journal of Clinical Endocrinology & Metabolism 2000;85: 1846-1850.

[113] Liberman UA, Weiss SR, Bröll J, Minne HW, Quan H, Bell NH, Rodriguez-Portales J, Downs RW, Dequeker J, Favus M, Seeman E, Recker RR, Capizzi T, Santora AC, Lombardi A, Shah RV, Hirsch LJ, Karpf DB. Effect of Oral Alendronate on Bone Mineral Density and the Incidence of Fractures in Postmenopausal Osteoporosis. New England Journal of Medicine 1995;333: 1437-1444.
[114] Cummings SR, Black DM, Thompson DE, Applegate WB, Barrett-Connor E, Musliner TA, Palermo L, Prineas R, Rubin SM, Scott JC. Effect of alendronate on risk of fracture in women with low bone density but without vertebral fractures. JAMA: The Journal of the American Medical Association 1998;280: 2077-2082.
[115] Komatsubara S, Mori S, Mashiba T, Li J, Nonaka K, Kaji Y, Akiyama T, Miyamoto K, Cao Y, Kawanishi J, Norimatsu H. Suppressed Bone Turnover by Long-Term Bisphosphonate Treatment Accumulates Microdamage but Maintains Intrinsic Material Properties in Cortical Bone of Dog Rib. Journal of Bone and Mineral Research 2005;20: 2066-2073.
[116] Mashiba T, Mori S, Komatsubara S, Cao Y, Manabe T, Norimatsu H, Burr DB. THe effects of suppressed bone remodeling by bisphosphonates on microdamage accumulation and degree of mineralization in the cortical bone of dog rib. Journal of Bone and Mineral Metabolism 2005;23: 36-42.
[117] Kwek EBK, Goh SK, Koh JSB, Png MA, Howe TS. An emerging pattern of subtrochanteric stress fractures: A long-term complication of alendronate therapy? Injury 2008;39: 224-231.
[118] Allen MR, Iwata K, Phipps R, Burr DB. Alterations in canine vertebral bone turnover, microdamage accumulation, and biomechanical properties following 1-year treatment with clinical treatment doses of risedronate or alendronate. Bone 2006;39: 872-879.
[119] Yamagami Y, Mashiba T, Iwata K, Tanaka M, Nozaki K, Yamamoto T. Effects of minodronic acid and alendronate on bone remodeling,

Microdamage accumulation, Degree of mineralization and bone mechanical properties in ovariectomized cynomolgus monkeys. Bone 2013;54: 1-7.
[120] Tang SY, Allen MR, Phipps R, Burr DB, Vashishth D. Changes in non-enzymatic glycation and its association with altered mechanical properties following 1-year treatment with risedronate or alendronate. Osteoporosis International 2009;20: 887-894.
[121] Glorieux FH, Bishop NJ, Plotkin H, Chabot G, Lanoue G, Travers R. Cyclic administration of pamidronate in children with severe osteogenesis imperfecta. N Engl J Med 1998;339: 947-52.
[122] Allen MR, Gineyts E, Leeming DJ, Burr DB, Delmas PD. Bisphosphonates alter trabecular bone collagen cross-linking and isomerization in beagle dog vertebra. Osteoporos Int 2008;19: 329-37.
[123] Tang SY, Allen MR, Phipps R, Burr DB, Vashishth D. Changes in non-enzymatic glycation and its association with altered mechanical properties following 1-year treatment with risedronate or alendronate. Osteoporos Int 2009;20: 887-94.
[124] Saito M, Mori S, Mashiba T, Komatsubara S, Marumo K. Collagen maturity, glycation induced-pentosidine, and mineralization are increased following 3-year treatment with incadronate in dogs. Osteoporos Int 2008;19: 1343-54.
[125] Boivin GY, Chavassieux PM, Santora AC, Yates J, Meunier PJ. Alendronate increases bone strength by increasing the mean degree of mineralization of bone tissue in osteoporotic women. Bone 2000;27: 687-94.
[126] Roschger P, Rinnerthaler S, Yates J, Rodan GA, Fratzl P, Klaushofer K. Alendronate increases degree and uniformity of mineralization in cancellous bone and decreases the porosity in cortical bone of osteoporotic women. Bone 2001;29: 185-191.
[127] O'Brien FJ, Taylor D, Lee TC. Microcrack accumulation at different intervals during fatigue testing of compact bone. J Biomech 2003;36: 973-80.

[128] O'Brien FJ, Taylor D, Clive Lee T. The effect of bone microstructure on the initiation and growth of microcracks. J Orthop Res 2005;23: 475-80.
[129] Verborgt O, Gibson GJ, Schaffler MB. Loss of Osteocyte Integrity in Association with Microdamage and Bone Remodeling After Fatigue In Vivo. Journal of Bone and Mineral Research 2000;15: 60-67.
[130] Verborgt O, Tatton NA, Majeska RJ, Schaffler MB. Spatial distribution of Bax and Bcl-2 in osteocytes after bone fatigue: complementary roles in bone remodeling regulation? J Bone Miner Res 2002;17: 907-14.
[131] Herman BC, Cardoso L, Majeska RJ, Jepsen KJ, Schaffler MB. Activation of bone remodeling after fatigue: differential response to linear microcracks and diffuse damage. Bone 2010;47: 766-72.
[132] Plotkin LI, Weinstein RS, Parfitt AM, Roberson PK, Manolagas SC, Bellido T. Prevention of osteocyte and osteoblast apoptosis by bisphosphonates and calcitonin. J Clin Invest 1999;104: 1363-74.
[133] Kennedy OD, Herman BC, Laudier DM, Majeska RJ, Sun HB, Schaffler MB. Activation of resorption in fatigue-loaded bone involves both apoptosis and active pro-osteoclastogenic signaling by distinct osteocyte populations. Bone 2012;50: 1115-22.
[134] Mulcahy LE, Taylor D, Lee TC, Duffy GP. RANKL and OPG activity is regulated by injury size in networks of osteocyte-like cells. Bone 2011;48: 182-8.
[135] Follet H, Li J, Phipps RJ, Hui S, Condon K, Burr DB. Risedronate and alendronate suppress osteocyte apoptosis following cyclic fatigue loading. Bone 2007;40: 1172-7.
[136] Plotkin LI, Manolagas SC, Bellido T. Dissociation of the pro-apoptotic effects of bisphosphonates on osteoclasts from their anti-apoptotic effects on osteoblasts/osteocytes with novel analogs. Bone 2006;39: 443-52.
[137] Plotkin LI, Lezcano V, Thostenson J, Weinstein RS, Manolagas SC, Bellido T. Connexin 43 is required for the anti-apoptotic effect of

bisphosphonates on osteocytes and osteoblasts in vivo. J Bone Miner Res 2008;23: 1712-21.
[138] Tami AE, Nasser P, Verborgt O, Schaffler MB, Knothe Tate ML. The role of interstitial fluid flow in the remodeling response to fatigue loading. J Bone Miner Res 2002;17: 2030-7.
[139] Muir P, Sample SJ, Barrett JG, McCarthy J, Vanderby R, Jr., Markel MD, Prokuski LJ, Kalscheur VL. Effect of fatigue loading and associated matrix microdamage on bone blood flow and interstitial fluid flow. Bone 2007;40: 948-56.
[140] Kozloff KM, Weissleder R, Mahmood U. Non-invasive optical detection of bone mineral. J Bone Miner Res 2007;22: 1208-16.
[141] Kozloff KM, Volakis LI, Marini JC, Caird MS. Near-infrared fluorescent probe traces bisphosphonate delivery and retention in vivo. J Bone Miner Res 2010;25: 1748-58.
[142] Li Y, Si R, Feng Y, Chen HH, Zou L, Wang E, Zhang M, Warren HS, Sosnovik DE, Chao W. Myocardial ischemia activates an injurious innate immune signaling via cardiac heat shock protein 60 and Toll-like receptor 4. Journal of Biological Chemistry 2011;286: 31308-31319.
[143] Smith BA, Gammon ST, Xiao S, Wang W, Chapman S, McDermott R, Suckow MA, Johnson JR, Piwnica-Worms D, Gokel GW. In Vivo Optical Imaging of Acute Cell Death Using a Near-Infrared Fluorescent Zinc− Dipicolylamine Probe. Molecular pharmaceutics 2011;8: 583-590.
[144] Chen R, Zheng X, Qian H, Wang X, Wang J, Jiang X. Combined near-IR photothermal therapy and chemotherapy using gold-nanorod/chitosan hybrid nanospheres to enhance the antitumor effect. Biomaterials Science 2013;1: 285-293.
[145] Verborgt O, Tatton NA, Majeska RJ, Schaffler MB. Spatial Distribution of Bax and Bcl-2 in Osteocytes After Bone Fatigue: Complementary Roles in Bone Remodeling Regulation? Journal of Bone and Mineral Research 2002;17: 907-914.

[146] Follet H, Li J, Phipps RJ, Hui S, Condon K, Burr DB. Risedronate and alendronate suppress osteocyte apoptosis following cyclic fatigue loading. Bone 2007;40: 1172-1177.
[147] Burger EH. Mechanotransduction in bone-role of the lacunocanalicular network. The FASEB journal 1999;13: 101.
[148] Tanaka K, Matsuo T, Ohta M, Sato T, Tezuka K, Nijweide P, Katoh Y, Hakeda Y, Kumegawa M. Time-lapse microcinematography of osteocytes. Mineral and electrolyte metabolism 1995;21: 189.
[149] Bronckers A, Goei W, Luo G, Karsenty G, D'souza R, Lyaruu D, Burger E. DNA fragmentation during bone formation in neonatal rodents assessed by transferase-mediated end labeling. Journal of Bone and Mineral Research 1996;11: 1281-1291.
[150] Gu G, Mulari M, Peng Z, Hentunen TA, Väänänen HK. Death of osteocytes turns off the inhibition of osteoclasts and triggers local bone resorption. Biochemical and biophysical research communications 2005;335: 1095-1101.
[151] Maejima-Ikeda A, Aoki M, Tsuritani K, Kamioka K, Hiura K, Miyoshi T, Hara H, Takano-Yamamoto T, Kumegawa M. Chick osteocyte-derived protein inhibits osteoclastic bone resorption. Biochem. J 1997;322: 245-250.
[152] Heino TJ, Hentunen TA, Väänänen HK. Osteocytes inhibit osteoclastic bone resorption through transforming growth factor-β: Enhancement by estrogen*. Journal of cellular biochemistry 2002;85: 185-197.
[153] Noble B, Stevens H, Loveridge N, Reeve J. Identification of apoptotic changes in osteocytes in normal and pathological human bone. Bone 1997;20: 273-282.
[154] Knothe Tate ML. In vivo demonstration of load-induced fluid flow in the rat tibia and its potential implications for processes associated with functional adaptation. Journal of experimental biology 2000;203: 2737-45.

[155] Turek J, Ebetino FH, Lundy M, Sun S, Kashemirov B, McKenna C, Gallant M, Plotkin L, Bellido T, Duan X, Triffitt J, Russell RG, Burr D, Allen M. Bisphosphonate Binding Affinity Affects Drug Distribution in Both Intracortical and Trabecular Bone of Rabbits. Calcified Tissue International 2012;90: 202-210.
[156] Roelofs AJ, Stewart CA, Sun S, Blazewska KM, Kashemirov BA, McKenna CE, Russell RG, Rogers MJ, Lundy MW, Ebetino FH, Coxon FP. Influence of bone affinity on the skeletal distribution of fluorescently labeled bisphosphonates in vivo. J Bone Miner Res 2012;27: 835-47.
[157] Roelofs AJ, Coxon FP, Ebetino FH, Lundy MW, Henneman ZJ, Nancollas GH, Sun S, Blazewska KM, Bala JL, Kashemirov BA, Khalid AB, McKenna CE, Rogers MJ. Fluorescent risedronate analogues reveal bisphosphonate uptake by bone marrow monocytes and localization around osteocytes in vivo. J Bone Miner Res 2010;25: 606-16.
[158] Noble BS, Peet N, Stevens HY, Brabbs A, Mosley JR, Reilly GC, Reeve J, Skerry TM, Lanyon LE. Mechanical loading: biphasic osteocyte survival and targeting of osteoclasts for bone destruction in rat cortical bone. American Journal of Physiology-Cell Physiology 2003;284: C934-C943.
[159] Wang Q, Marini JC. Antisense oligodeoxynucleotides selectively suppress expression of the mutant alpha 2 (I) collagen allele in type IV osteogenesis imperfecta fibroblasts. A molecular approach to therapeutics of dominant negative disorders. Journal of Clinical Investigation 1996;97: 448.
[160] Deyle DR, Khan IF, Ren G, Wang P-R, Kho J, Schwarze U, Russell DW. Normal collagen and bone production by gene-targeted human osteogenesis imperfecta iPSCs. Molecular Therapy 2011;20: 204-213.
[161] Vahle JL, Sato M, Long GG, Young JK, Francis PC, Engelhardt JA, Westmore MS, Ma YL, Nold JB. Skeletal changes in rats given daily subcutaneous injections of recombinant human parathyroid hormone (1-34) for 2 years and relevance to human safety. Toxicologic pathology 2002;30: 312-321.

[162] Bargman R, Posham R, Boskey A, DiCarlo E, Raggio C, Pleshko N. Comparable outcomes in fracture reduction and bone properties with RANKL inhibition and alendronate treatment in a mouse model of osteogenesis imperfecta. Osteoporosis International 2012;23: 1141-1150.
[163] Sinder BP, Eddy MM, Ominsky MS, Caird MS, Marini JC, Kozloff KM. Sclerostin antibody improves skeletal parameters in a Brtl/+ mouse model of osteogenesis imperfecta. Journal of Bone and Mineral Research 2013;28: 73-80.
[164] Kurata K, Heino TJ, Higaki H, Väänänen HK. Bone Marrow Cell Differentiation Induced by Mechanically Damaged Osteocytes in 3D Gel-Embedded Culture. Journal of Bone and Mineral Research 2006;21: 616-625.
[165] Löhler J, Timpl R, Jaenisch R. Embryonic lethal mutation in mouse collagen I gene causes rupture of blood vessels and is associated with erythropoietic and mesenchymal cell death. Cell 1984;38: 597-607.